INSIGHTS INTO CONVENTIONAL AND LOW TEMPERATURE DIESEL COMBUSTION USING COMBUSTION TRAJECTORY PREDICTION MODEL

A Dissertation

by

JOSHUA ANDREW BITTLE

Submitted to the Office of Graduate and Professional Studies of
Texas A&M University
in partial fulfillment of the requirements for the degree of

DOCTOR OF PHILOSOPHY

Chair of Committee,	Timothy Jacobs
Committee Members,	Jerald Caton
	Adonios Karpetis
	Michael Pate
Head of Department,	Andreas Polycarpou

May 2014

Major Subject: Mechanical Engineering

ABSTRACT

Attempting to bridge the gap between typical off-line engine simulations and on-line real-time control strategies a computationally efficient model has been created that predicts the combustion trajectory (path through the ϕ-T plane). To give an indication of time progression in the combustion event the results are first shown as a function of crank angle, but most discussion is focused on the behavior of the combustion trajectory on the ϕ-T plane. The conditions investigated here include injection timing sweeps between a conventional and late timing (8° and 0° before top dead center, or bTDC, respectively) as well as full exhaust gas recirculation (EGR) sweeps at both timings.

These test conditions highlight how EGR influences the combustion trajectory at different timings – i.e., showing the typical soot-NOx trade-off and the defeat of this trade-off when low temperature combustion (LTC) is obtained. The major insight gained from this modeling approach is how LTC trajectory is different from conventional case in the ϕ-T plane. Attempting to understand the differences and hypothesizing about the causes suggests that there is no specific region that is defined as LTC. In fact the LTC trajectory looks very similar to a conventional one with just subtle differences that keep it from moving into the soot formation region. Additionally, the traditional conceptual explanations for diesel combustion are explored relative to how they are illustrated in the combustion trajectory, especially the transition from pre-mixed to mixing controlled combustion. Understanding this behavior in this context aids in explaining the different observations for the LTC modes.

ACKNOWLEDGEMENTS

The guidance and assistance form my committee chair, Dr. Jacobs, has been invaluable and is gratefully acknowledged. Additionally, I would like to thank my other committee members, Dr. Caton, Dr. Karpetis, and Dr. Pate for their assistance and efforts in supporting this research.

I have had the opportunity to work with many fellow graduate students who have been a great source of help, motivation, and camaraderie. Additionally, the departmental staff has always been most helpful and I have enjoyed getting to know them all over the years.

Finally, thanks to my mother and father for their constant encouragement and to my wife for her patience and love especially as more time kept being tacked on the end – graduation always just over the horizon.

TABLE OF CONTENTS

Page

LIST OF FIGURES

Page

LIST OF TABLES

Page

1. INTRODUCTION

1.1 Motivation

The prevalence of internal combustion engines (both diesel and gasoline) in the world today is a strong indicator that despite growing global concern about the effect engine emissions are having on the environment, the global dependence on these engines will likely only continue to increase. In an effort to mitigate any potential negative side effects on the environment, the governing bodies of the United States and the European Union regulate the emissions being released into the atmosphere by the internal combustion engine. Every few years the EPA (in the United States) and EURO (in Europe) emissions standards are updated with more stringent requirements.

It has been typical for the past decades that the emissions from a gasoline engine are easier to control due to the use of the three-way-catalyst (which does not work for diesel engines due to lean operation). Diesel engines have coped with this setback by requiring substantial after-treatment systems be installed. With any future emissions regulations, however, it is getting close to the point where after-treatment is not enough to bring the diesel engine under the regulated emission levels. It is very likely that future diesel engines will be required to combine after-treatment systems with some very advanced diagnostic measurement techniques, control strategies, and performance prediction capability in order to reach the EPA and EURO emissions requirements.

The introductory material here starts by highlighting some of the areas of active research in combustion control and diagnostics. Based on a literature review (see Appendix) it is hypothesized that based on cylinder pressure data combined with other

"stock" engine sensors a prediction algorithm can be developed to control the engine to a low emissions operating condition. The work completed here includes the introduction and validation of a detailed, and yet simple, combustion modelling approach that seems to offer the possibility of implementation as a real-time engine controller as hypothesized.

1.2 Background – Current active research areas and progress

Many areas of research are being pursued in support of ultimately improving our ability to predict and control internal combustion engines. Advances in any one of these areas will potentially enable future engines to meet and exceed the emissions regulations. The areas focused on and summarized here include: chemical kinetics modeling of the combustion processes, on-board emissions measurement techniques, closed-loop feedback control of the engine based on various measurements, off- and on-line engine model simulations, and the design of consumer ready data acquisition and processing hardware to support these control and prediction techniques.

1.2.1 Chemical kinetics

Being able to predict steady-state engine operation based on current operating parameters is one of the hot topics in engine research. In particular, significant effort is being put into chemical kinetic modeling and CFD simulations techniques that may allow for real-time prediction of the combustion process. There are many researchers pursing this topic, but it remains a complicated and difficult task due to the complexity of fuel chemical kinetics.

One of the common areas of research is in the mapping of all possible chemical kinetic pathways that a hydrocarbon could follow during the combustion process. This would allow for very precise predictions of things like ignition delay, and coupled with CFD simulations would allow the prediction of the ignition equivalence ratio – very critical parameter in determining the exhaust species composition. One such effort by Westbrook et al. has compiled a detailed library of the chemical kinetic mechanisms for the n-alkane hydrocarbons from n-octane (C_8) to n-hexadecane (C_{16}) [1]. The problem is that standard diesel fuel is a varying mixture of hundreds or even thousands of long chain hydrocarbons – typically with carbon numbers between C_{10} and C_{24} [2].

The computation power required to track the chemical kinetics of every possible constituent in the diesel fuel is out of reach for current technology, but a potential remedy for this issue is to find a relatively simple surrogate fuel to represent typical diesel behavior. The simple surrogate fuel is chosen such that it very closely matches the experimental results of typical diesel fuel and is composed of only a few hydrocarbons that have established chemical kinetics databases. Pitz et al. have compiled a summary of the recent progresses in the development of candidate diesel surrogates [3].

A second approach to the modeling difficulties is to identify which reactions and species are the most important and perform a process called “mechanism reduction” to simplify the required calculations. Essentially the researcher starts with the full array of all possible reactions and intermediate species and then selectively removes various combinations and determines if the saved computation time is worth the potential increase in predictive error. There are numerous algorithms designed to make the

process of selection efficient and effective. For example, Lu and Law present their approach for mechanism reduction of the n-heptane chemical kinetics [4].

The work put into developing a diesel surrogates combined with strategies for chemical kinetic mechanism reduction so that ultimately more precise predictive combustion control may be implemented becomes even more daunting considering all the efforts being put into the development of renewable alternative fuels. Each fuel would have to be characterized and mapped and any controller would have to have built in databases to account for each fuel type as well as a way to detect the fuel being in the case of the proposed "drop-in" fuels.

1.2.2 On-board emissions measurements

Having real-time knowledge of the emissions being produced by the engine allows for closed-loop control techniques to help minimize the various regulated species. Typical research grade emissions measurement systems, however, are very expensive and take up quite a lot of space. Both characteristics make it impossible to reasonably expect these systems to be installed in production vehicles. There are a number of current production on-board exhaust emissions measurement devices which are installed to provide this feedback to the engine controller. Riegel et al. from Robert Bosch GmbH have assembled a very thorough summary of the various exhaust gas sensors including numerous types of oxygen sensors, NOx sensors, and hydrocarbon sensors current as of 2002 [5].

Gasoline engines have been utilizing narrow-band oxygen sensors for decades to give the engine tighter control over maintaining the desired stoichiometric air fuel

mixture. These sensors can only give an indication if there is too much, not enough, or just the right amount of air for the current fuel flow rate. More recent efforts have brought the wide-band oxygen sensor to production vehicles that allow for a quantitative measurement of the oxygen concentration over quite a large range.

Diesel engines have typically not needed an oxygen sensor because they don't use the three-way catalyst. However, with the addition of selective catalytic reduction (SCR) systems designed to reduce the NOx levels in the exhaust, new diesel engines are now being equipped with these oxygen sensors to provide feedback control over the SCR system.

The oxygen sensor gives an indication of the potential NOx concentrations that can be used for control purposes, but obviously a direct measurement of NOx in the exhaust would be preferred. There are many research groups and companies that are working toward developing a high accuracy sensor similar in packaging to the oxygen sensors.

The primary issue is that the most promising measurement technique for sensing NOx (mixed-potential) shows a cross sensitivity to oxygen [5]. This means that the signal conditioner or data processing algorithm must have some way to isolate the desired portion of the signal. Alternatively, the sensor could be installed behind another device that removes the oxygen from the stream thus allowing a non-contaminated measurement.

Another issue with the NOx sensors is the accuracy at low concentrations. With emissions regulations further restricting the allowable levels of NOx the limits of the

measurement devices are being pushed. For these low concentration measurements an alternative measurement technique has been investigated based on the limiting current principle described by Kato et al. [6]. Alternatively, Hasei et al. have presented a modified NOx sensor still utilizing the mixed potential method but better suited for the low concentration measurements [7].

In either case, the NOx sensor has not been established as an industry standard for production vehicles. The oxygen sensor has enabled gasoline engine emission control and more recently in diesel SCR systems. In much the same way, NOx and other species specific exhaust emissions detection devices may play a crucial role in enabling the attainment of the government regulated emission standards in the future.

1.2.3 Off-line engine modeling simulation and on-line intelligent driver style learning

Another approach to engine modeling that doesn't necessarily include the tracking of all of the various chemical reactions and species (as discussed in the 1.2.1

Chemical kinetics section above) uses various empirical based routines to predict the engine's behavior under a given set of conditions. These modeling efforts can range from the very simple (zero-dimensional) to incredibly complex (3-D computational fluid dynamics coupled with detailed chemistry tracking). These models are most useful in aiding engine calibration procedures by minimizing the on-line dynamometer engine test cell operation time. As engines are routinely equipped with more and more electronic actuators and setting, the calibration time is theoretically increased factorially. In other words for each speed and load to be calibrated, every possible combination of actuator positions needs to be tested to find the optimal settings. This effort can be minimized

somewhat by operator experience, but the time involved regardless is quite large. By employing off-line engine modeling simulations part of this work can be eliminated. Even better is the fact that most of the simulations can be run at a faster rate than they could be on the actual engine enabling reduced overall calibration time and substantially reduced calibration man hours.

Atkinson and Mott presented a good overview and more details about this rising complexity in engine calibration [8]. Their work also included an introduction to a promising engine modeling routine that has the potential to even further simplify the engine calibration burden. Utilizing a neural network that can learn the engine behavior simply by being "fed" actual engine data, the points in between can be satisfactorily interpolated by the simulation. Given that the emissions regulations are enforced over standardized drive cycles (for example, the FTP cycle in the United States) it is very beneficial to be able to predict the transient operation.

Rutland et al. [9] presented a couple of studies implementing a neural network simulation for diesel engines. First, a neural network was developed and trained based on inputs from KIVA based engine model with the conclusions showing good agreement at the validation conditions between the neural network and the KIVA model [9]. Secondly, the validated neural network was then used to optimize the controllable diesel engine operating parameters based on a weighted minimization function including predicted NOx, soot, fuel consumption, and error between the desired torque set point and the actual torque [10]. The results of both of these studies show promise for the application of the neural networks, but unfortunately neither show how the results

compare to an actual engine. Another group, Ismail et al. [11], using a different neural network did show validation of the predictions versus the real engine it was simulating with generally good agreement in emissions and combustion parameters except for hydrocarbons and the location of maximum heat release rate.

A mid-point compromise between neural networks, complex 3-D modeling, and zero dimensional modeling is found in the area of multi-zone models that utilized correlations for phenomena such as heat transfer, fuel mixing rates, and burn rates. Quite a few groups have investigated and created these models with success. A number of older simulations are based on various phenomenological diesel jet evolution descriptions, for example [12]. Recently models for diesel jet evolution have been improved based on laser diagnostic results. Xue and Caton demonstrated a relatively detailed six zone simulation based on this new diesel jet evolution that included sub-models for ignition delay, heat transfer and combustion rates [13]. Most of these model simulations are able to reasonably predict the behavior of whatever real engine they are calibrated and tuned against; however, their application to conditions for the engine which weren't calibrated and especially to other engines is very limited.

As was alluded to above, controlling an engine under steady operation is difficult, but minimizing penalties to emission production, fuel consumption, and thermal efficiency during transient operating is even harder. Add to the issue that engine transients are often caused by potentially random input by the vehicle driver. System modeling and control implementations have been shown to be effective at reducing the

penalties during transient engine operation in off-line (i.e. not while the actual engine is running), but their application is not yet as established in on-line operation.

One of the issues of transient operation is the interpolation that the engine controller must use when the current engine state is in between the tabulated calibration points. Malikopoulos et al. used a stochastic system model to implement an on-line (i.e. while the engine is running) self-learning control of the "optimal" injection timing [14-16]. Using engine simulation software, the engine behavior during a portion of the FTP-75 drive cycle was modeled. By adding the "real-time self-learning optimization" routine to the controller the study observed a decrease in predicted total fuel consumption of approximately 8% and a decrease (though hard to quantify) in predicted average NOx concentration among other conclusions.

This methodology is likely applicable to many different engine types with relatively less customization than the off-line simulation models. The drawback at this point is that the method referenced has not been implemented to control and physical engine, only a simulated one, so there may be as yet unseen issues to overcome.

1.2.4 Designing of advanced production engine control hardware

Most of the on-line/real-time control methods discussed to this point likely will require significant processing power and data throughput. Current consumer engine controller hardware is optimized for the typical static control lookup table operation. Therefore, a consumer ready implementation of any of these methods will require significant advances in engine controller computation power and signal processing as

currently the only systems capable of implementing these control strategies are quite expensive and generally large compared to typical engine controller hardware.

Schten et al. from Delphi Corporation have recently published the results of their efforts to produce a “automotive grade controller for in-cylinder pressure based engine control” [17]. They address and summarized the primary design issues related to the objective, such as the conversion from time based measurements to aligned crank angle measurements, and the intensive CPU burden for any processing of the crank angle resolved measurements (such as heat release calculations). The result of the study creates essentially a second engine control module (with similar packaging to the standard ECU modules) that incorporates data acquisition and processing hardware. The outputs of this module were then theoretically be fed to the standard ECU module for implementation. The results of the system were then compared with those from a typical research grade combustion analysis with good agreement. The data comparison included basic pressure analysis as well as heat release. This is very promising considering the strong likelihood that in-cylinder pressure diagnostics and feedback controls will likely be required in future engine packages.

1.2.5 Feedback control of various critical combustion parameters

A decade ago the emissions regulations and engine complexity were at levels such that the manufactures could meet the standards by using real-time on dyno calibration procedures. As discussed previously, with the increasing complexity of the engines, the man hours required for completing this calibration increases. Additionally, with the increasing strict emissions control regulations it is becoming difficult to attain

the desired levels with static control maps. This is even true when portions of the calibration are done using computer simulation techniques. The next step required in order to meet the tight control necessary to meet the emissions regulations is to implement real-time closed loop control over each of the engine actuators and settings. This control can account for engine manufacturing differences, engine wear, and varying ambient conditions that would otherwise cause deviation from the expected calibrated performance.

Closed loop control techniques were initially applied to what would now be relatively simple tasks such as using the exhaust oxygen sensor as a feedback to control the exhaust gas recirculation valve to maintain a desired air mass flow rate [18]. A simple feedback control loop is also now universally applied to the control of the high pressure common rail fuel pressure systems on diesel engines. Additionally, as tighter control over combustion phasing became a concern, the start of combustion location was indirectly measured by ionization sensing and used as a feedback control to adjust the start of injection timing [19].

Some of the more complex feedback control based methods require the acquisition and processing of crank angle resolved signals. The challenges associated with implementing these types of measurements and calculations in a consumer grade engine control unit were discussed above and in more detail in [17]. Regardless of the current end user hardware availability, the efforts in the area of closed loop engine feedback control are progressing on research grade hardware with hopes of aiding in the attainment of the regulated emissions requirements.

One of the most common research tools currently used to study engines is high fidelity piezoelectric cylinder pressure measurements. These measurements are a great tool that enables numerous combustion diagnostic calculations. This includes calculating the thermodynamic work done during each cycle, calculating the cylinder temperatures based on ideal gas assumptions, using energy balance calculations to model the fuel combustion process, and subsequently determining things such as start of combustion, and other combustion phasing parameters.

These calculations and potential for feedback control apply very well to an advanced combustion mode currently being investigated (and discussed in depth in the detailed literature review in the appendix) for its simultaneous reduction in NOx and soot, called low temperature combustion (LTC), but has some inherent side effects such as increased HC and CO emissions and larger cycle-to-cycle and cylinder-to-cylinder variations. These side effects might be mitigated to some extent by eliminating the combustion stability issues. Husted et al. implemented a cylinder pressure based control routine that would, in real-time, adjust the injection timing and duration to balance the combustion phasing and mean effective pressure (a measure of cylinder work), respectively with impressive results [20]. Secondly, the side effects are compounded by the potential for alternative fuels being used in the engine with varying cetane number. Hasegawa et al. implemented an ignition timing (which is very influential on the LTC performance) control that would adjust the start of injection or the EGR valve position (in conditions where injection timing control wasn't sufficient) to effectively minimize the influence of varying cetane number on the engine performance parameters [21].

The efforts in the area of cylinder pressure based feedback control will be the primary focus of this proposal, so a more exhaustive exploration of the current status of the literature in this area will be reserved for the appendix.

1.3 Objective

As previously mentioned, the focus of this dissertation work is motivated by the desire to enable closed-loop feedback control of the engine based on a combination of cylinder pressure and other typical stock engine sensors. As demonstrated in the previous sections there are numerous areas currently under study - all with the end goal of making the engine manufactures' job of meeting emissions regulation requirements feasible in the future. The decision to focus on cylinder pressure based methods for this work was made due to the potential for broad application (i.e. non-engine specific) and the fact that the hardware required for implementation is not out of reach. In fact Audi is already incorporating cylinder pressure transducers into the advanced TDI engines for cylinder balancing purposes [22]. Additionally, the advanced data acquisition and processing required is actively being pursued by Delphi [17] (and surely other OEM's) as described in the appendix.

In particular the advanced combustion mode typically called low temperature combustion (LTC) will be targeted for control using closed loop real-time methods. Low temperature combustion is very promising due to the substantially reduced NOx and soot emission levels [23]. It has not, however, been globally added to consumer engines as a ECU control mode do to the inherent side effects of increased CO and HC emissions [24] and combustion instabilities as well as limited load operating range. Additionally, a

full calibration of each engine model by the manufactures for both a conventional combustion mode as well as the LTC mode (where applicable) could potentially double the man hours required. Even when using computer simulation techniques (as described above) to minimize the man hours required for calibration, the complexity of the model must be increased to account for the LTC behavior making it more difficult to ensure an accurate calibration. Another notable issue with LTC operation is the stability issues when transitioning from conventional to LTC mode (due to temperature response) [25]. Also, the cylinder imbalance has been observed to increase during LTC operation due to the sensitivity if ignition timing to small differences in EGR distribution [25].

Cylinder pressure gives detailed information about the combustion process, but there are still significant gaps in the knowledge. Combining the cylinder pressure with other typically stock sensors (such as exhaust oxygen, intake pressure and temperature, and exhaust temperature and pressure) may provide a clear enough picture to implement a closed-loop control routine that would allow for operating in either a conventional mode (still using the static control maps or not) or a LTC mode with the virtual flip of a switch. Investigating the feasibility of, and methodology required to implement, this idea is the objective of this research.

More specifically, the objective is to implement a method using mostly stock sensors to estimate the local ignition equivalence ratio and thus estimate the likely combustion path and also the likely relative concentrations of NOx and soot emissions. The local equivalence ratio at ignition and the combustion path followed by the fuel air mixture directly influences the NOx and soot formation [26]. Therefore predicting this

path based on current engine conditions would allow for a minimization function to be implemented that would automatically adjust (though closed-loop control) the engine operating parameters to attain an LTC mode. This type of algorithm has the potential to be much less processing intensive (and thus less costly in hardware) than attempting to implement an on-line multi-zone model like those described above.

Developing new prediction and control methods for internal combustion engines is an active area. These two areas have traditionally been very separate efforts. Prediction models typically aim to match cylinder pressure and emission formation then expand to predict other performance characteristics at unknown operating conditions [27-30]. Real-time control methods have recently been focused on cylinder balancing (both start of combustion and mean effective pressure) and combustion phasing for optimal efficiency [19-21, 31-33]. Blending these two areas by creating a fast, yet detailed model that can be installed and utilized on a real-time engine controller was the motivation for this study.

While the initial goal of implementing a real-time engine control algorithm was not achieved, the model development that will be the major focus of the rest of this document shows at least initial promise for future controller application. In addition, the results presented here reveal interesting features about both general combustion events and how conventional combustion differs from low temperature combustion (LTC). By identifying these differences this model can be leveraged in the future to enable automatic engine control of LTC modes – eliminating the need for off-line calibration. Perhaps more importantly, the model was also designed from the beginning to be very

general (i.e. not specific to one engine). The work here will not focus on the future applications, but instead explore how the model has further validated traditional conceptual models of combustion processes as well as offering new ideas for how LTC is manifested differently from a conventional mode. All of the observations and analysis are done with the primary output of the model – the combustion trajectory through the local equivalence ratio and reaction temperature plane (ϕ-T plane). This shows how the combustion event may progresses through the soot and / or nitric oxide (NO) formation regions.

The interest in this type of modeling was inspired initially by the work of Kook, et al. [34] who used a postulated path and recognized how it illustrates the benefits of dilution in avoiding soot and NO formation. The foundation of the present model, however, was Gao and Wagner's [28] two zone model which was created in an attempt to simplify the calculation method (based on run-time minimization considerations) compared to Gao's original multi-zone model [27] while still retaining the ability to track equivalence ratio and reaction temperature – i.e. the combustion trajectory. Both of Gao's models take the standard simulation approach of predicting the cylinder pressure. The work presented here recognizes the growing trend of production-based in-cylinder pressure feedback [22]; thus, this study's approach relies on measured pressure (rather than predicted pressure) to save computational time.

To enable the proposed work, the new engine installation has been completed and verified as described above. While the real-time control applications have not been demonstrated, the literature review included a number of studies that used the same

engine and engine controller hardware that will serve as the testing platform for this work. The remainder of this document will include a detailed description of the developed model followed by validation results from a medium duty diesel engine under multiple operating conditions.

2. COMBUSTION TRAJECTORY MODEL DESCRIPTION

The following section describes the model and its solution method. Only critical equations will be shown here and sources for additional information will be referenced.

The model takes the following inputs:

- Engine speed
- Intake manifold temperature
- Exhaust gas recirculation (EGR) percent
- Rail pressure
- Fuel flow rate
- Injection timing parameters
- Cylinder pressure

The model is constructed as a spatially zero-dimensional model with two true zones – a reaction and unburned zone. By the nature of the fuel injection and entrainment sub-models there are additional sub-zones containing discrete amounts of fuel which can entrain air from the unburned/unmixed zone and also upon burning switch from the unburned to reaction zone. The time resolution of the model depends on the sampling resolution of the cylinder pressure and therefore, while in reality processes occur continuously, they are assumed to occur in a discrete step fashion; the result is only known at each time step.

The general steps of the model are illustrated in the flowchart of Figure 1. Each block will be described in detail to follow. The model was coded in LabVIEW to enable simple integration with the custom engine controller (also coded in LabVIEW) in the future.

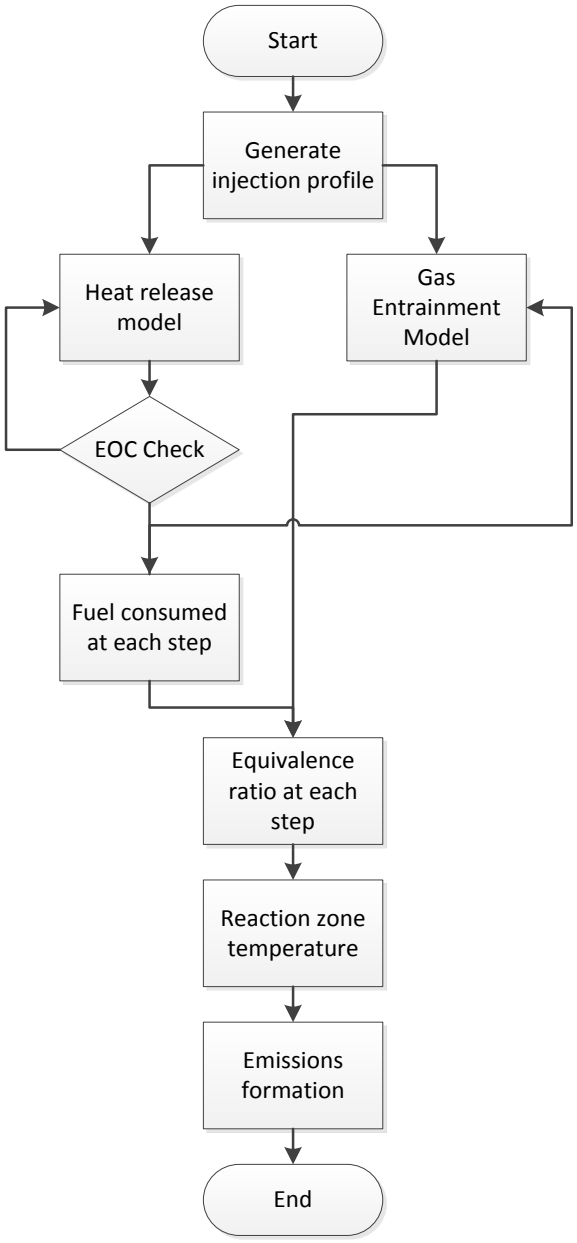

Figure 1 - Model flow chart

The general process of the model discretizes an assumed injection profile into individually trackable fuel packets. The discretization resolution equals the cylinder pressure resolution. Using single-zone heat release and gas entrainment models, the

amount of fuel / air burned is predicted at each calculation step in each discretized packet. The fuel is assumed to burn in a sequential fashion in the order of its timing of injection. Knowing the mixture composition at each step (i.e., exhaust gas recirculation, or EGR, rate and equivalence ratio) the reaction temperature is predicted as the local adiabatic flame temperature including compensation for changing initial temperature.

2.1 Injection profile

The initial step in the model solution is to generate an injection profile. If there is no change in the operating conditions, then this step need not be repeated on each subsequent function call to save time. Based on the total engine fuel flow rate (measured by positive displacement metering system), the commanded start of injection and injection duration, an assumed triangle injection rate pattern is generated. The amount of fuel injected at each calculation step is taken as a lumped fuel packet as the model moves forward. The integral over the entire injection profile must result in the total fuel per cycle per cylinder. In other words, the area of the triangle and the base (injection duration) are known. The unknown is the height or the peak injection rate. Once this is solved, the injection rate at each step in the ramp up and ramp down can be calculated. For high load conditions this would need to be modified to account for the time when the injector is completely open, but presently the model is only considered for low load conditions.

2.2 Heat release

Next, the heat release calculation is based on the overall theme of reducing computational complexity and thus uses a basic single zone model with a correlation for

the gas constant. A thorough description of this and other possible approaches is given by Depcik et al. [35]. The gas constant correlation developed by Brunt and Platts [36] is used. Based on the heating value of the fuel, the incremental fuel consumption rate can be determined and thus the heat release calculation can be halted once all of the fuel has been consumed. An internal consistency check must be done, however, as it would not be realistic for the heat release calculation to halt in the middle of the main heat release or conversely if it had not stopped when the valves open. A single tuning constant is introduced to avoid these inconsistencies. A multiplier on the calculated heat release value at each step is automatically, and iteratively adjusted (i.e. repeating the whole heat release calculation) until the heat release rate at the moment the fuel is completely consumed is less than 5% of the maximum value. The end of combustion location is noted and stored for the next time the code runs. When determining this balancing constant, there is also a built in check to make sure the fuel consumed never out paces the fuel injection for short ignition delay conditions. The tuning constant is fairly stable – always between 0.9 and 1.1 for the conditions evaluated in this study.

2.3 Gas entrainment (original)

Parallel to the heat release calculations (through dual core processor leverage) the fuel and air entrainment process is modeled by conservation of momentum between injected fuel packet and the unmixed gas zone. This makes use of the well-established injection spray penetration model by Hiroyasu et al. [37] The routine tracks the entrained air for each injected fuel packet. This allows for calculating the equivalence ratio of each

packet which effectively adds extra zones to the base two-zone model without adding any calculation complexity.

The gas entrainment prediction model calculation is one of the most computationally expensive portions of the code – roughly 60% of the total time with a 0.2 crank angle degree resolution. This is the reason for the parallel operation with the heat release portion. To save time, the entrainment model is only solved from start of injection through end of combustion. The end of combustion location is passed from the heat release model for processing the next cycle. The side effect of this parallel coding structure is that the first function call must use an assumed initialization value and therefore may create large initial error.

The major feature of the spray penetration model is that length increases initially proportionally to time. Once the main liquid core starts to break up the tip length then increases proportionally to the square root of time. This effect is captured with the parametric equations shown below.

Initially the penetration length is a function of only the liquid density, injection pressure gradient, and time as shown in Equation 1.

$$\boldsymbol{S = 0.39\sqrt{\frac{2\Delta P}{\rho_l}}\,t} \tag{1}$$

After the liquid core begins to break up, the penetration length becomes a function of the injection pressure gradient, cylinder gas density, nozzle diameter, and the square root of time as shown in Equation 2.

$$\boldsymbol{S = 3.07\left(\frac{\Delta P}{\rho_g}\right)^{0.25}(d_o t)^{0.5}} \tag{2}$$

Finally, the break up time is defined as an equation that is a function of the liquid density, cylinder gas density, nozzle diameter, and injection pressure gradient as shown in Equation 3.

$$t_b = 28.65 \frac{\rho_l d_o}{\sqrt{\rho_g \Delta P}} \tag{3}$$

The air entrainment process is simply modeled by considering conservation of momentum as the fuel is injected and moves into the cylinder as shown in Equation 4. This process is also described by Hiroyasu et al. [37]. It is important to remember there is no spatial resolution captured in this model, but by utilizing the spray penetration length model the spray velocity can be determined.

$$m_f U_o = \left(m_f + m_g\right) U \tag{4}$$

The initial momentum only includes the fuel as it is injected. The downstream momentum includes the entrained gas mixture which is balanced by the decreased spray velocity.

The initial injection velocity is simply a function of the injection pressure and liquid density as shown in Equation 5.

$$U_o = \sqrt{\frac{2\Delta P}{\rho_l}} \tag{5}$$

2.4 Gas entrainment (improvement)

The biggest improvement to existing sub-models that the work presented here offers is the modification of the coefficients used in Equation (1) and modifying the form of ideal injection velocity shown in Equation (5). The motivation for these changes was the observation that rail pressure essentially didn't change mixing model and

therefore sweeps of rail pressure were not suitably captured with the base model from Hiroyasu [37].

The ideal injection velocity in Equation (5) is derived from the isentropic flow equations for incompressible substances (i.e. the Bernoulli equation). The upstream velocity is assumed to be negligible and therefore the injection velocity is only a function of the pressure gradient across the injector nozzle (assumed to be change from rail pressure to cylinder, i.e. neglecting line losses). This value is the ideal/maximum velocity one could expect and yet it is used as the basis for the entrainment model. A higher initial momentum means more air must be entrained as the spray penetrates further into the cylinder (resulting in maximum entrainment for even low injection pressures). It seems likely that the initial injection velocity (and thus entrainment rate) should be lower than the absolute maximum.

The derivative of the spray penetration length (in Equation (1) and (2)) gives the velocity of the jet. The model by Hiroyasu uses a discharge coefficient of 0.39 for the initial penetration distance of Equation (1). Note that the time variable will drop out when taking the derivative. This means that the velocity of the fuel jet is constant until break up and is equal to 0.39 times the ideal injection velocity from Equation (5). This is already an inconsistency – how can the velocity decrease by 61% without entraining any air (note that the entrainment only occurs as the velocity changes)? Based on this observation the initial injection velocity was changed to be 0.39 multiplied by Equation (5) to eliminate the inconsistency. This change made improvements to some conditions, but still was not reliably predicting expected trends with rail pressure.

The final step that improved the predictive abilities of the model was making the discharge coefficient a function of injection pressure and duration – not just a constant. This was done by leveraging data determined as part of an injector calibration procedure. A 2D table was given showing injected volume per injection as a function of injection pressure and commanded duration. Starting with a simple volumetric flow equation ($\dot{V}_{avg} = AV_{avg}$) and assuming a constant area the average injection velocity can be determined after converting the volume flow per injection to volume flow rate using knowing injection time and area. Dividing this calculated injection velocity by the ideal velocity gives the final result – the discharge coefficient as a function of rail pressure and injection duration. These values were not tuned at all; they were just taken as whatever the calculation generated.

Examples of "before and after" are shown in the model validation section to follow.

2.5 Fuel consumption rate and burning order

The next step in the model solution is to take the overall fuel consumption rate (heat release rate normalized by heating value, i.e. mass fraction burned) and determine how much of each fuel packet burned at each calculation step. Based on the phenomenological construction of a fuel/air plume burning from the outside inward, it is assumed that the fuel burned at each step came from the earliest injected fuel packet until that packet is fully consumed. This means that the first fuel injected is the outer most layer of the fuel/air plume with a simple analogy to an onion for each subsequent

fuel packet being the next layer. This allows for tracking of the equivalence ratio of each packet as it burns.

For early stage reaction before the fuel plume has become well mixed Figure 2 represents the fuel packets and their distribution. The analogy to onion layers is clearly visualized in this way. The late stage of combustion when the fuel has become well mixed and has started to interact with the wall and lose its traditional plume structure is harder to model without considering spatial variations. However, Figure 3 gives a visual representation of how the packet burning order and outside inward burn pattern can still apply. After the end of injection the fuel plume will continue into the wall and start to deform some fuel/air mixture may even detach from the main plume.

While the nature of the cylinder processes are much more complex than can be illustrated by this simple graphic, the types of behavior shown in both Figure 2 and Figure 3 are well demonstrated in the optical studies of many researchers such as Musculus et al. [38].

Based on the calculated fuel consumed at each step, the unburned fuel that has been in the cylinder the longest (i.e. outer layer) will be decreased. The amount of fuel consumed is assumed to have burned at the instantaneous equivalence ratio based on the air entrainment process. At each step in the trajectory calculation the same percentage of fuel consumed from the packet is removed from the air calculations. The local equivalence ratio may increase if fuel is consumed faster than fresh air is entrained (results in richening trajectory path); the local equivalence ratio may continue to

decrease for low burn rates as air is mixed faster than it is consumed (results in a leaning trajectory path).

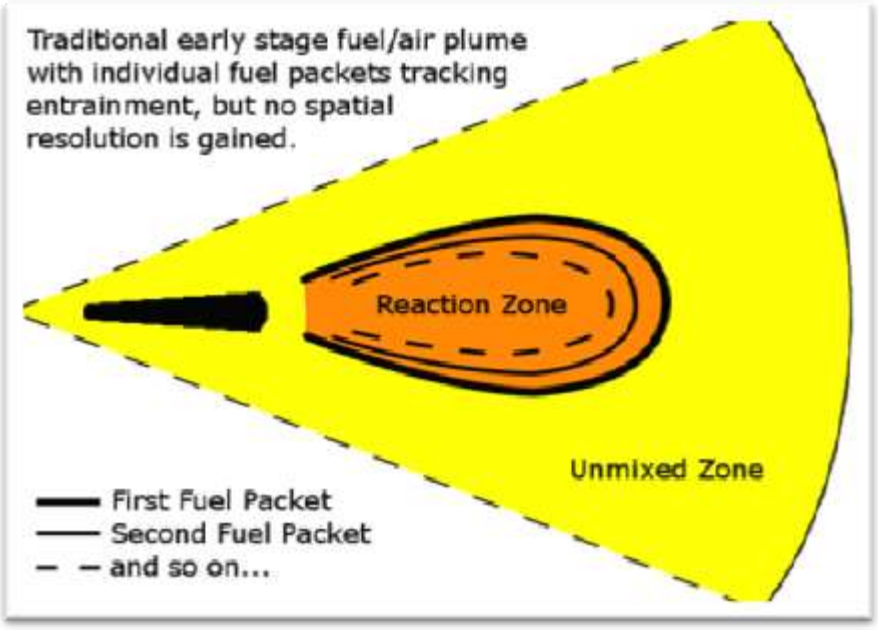

Figure 2 - Conceptual illustration of early stage entrainment process and fuel distribution. The assumed sequential burn pattern based on the order of the fuel packet injection creates an outward-in arrangement with on continuous fuel/air plume.

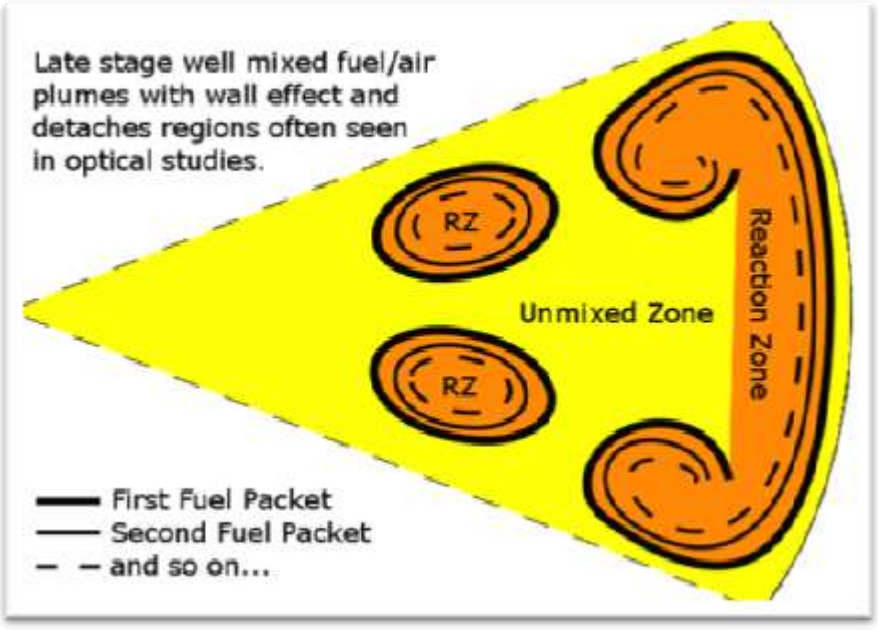

Figure 3 - Conceptual illustration of late stage well mixed entrainment process and fuel distribution. This shows how the sequential burn order does not contradict the well mixed state characteristic of low temperature combustion.

2.6 Reaction temperature

The next process is to calculate the burning temperature at each time step. Because of the speed of reaction (~23μs for each calculation step at 1400 RPM) and the small volume involved in the combustion of an individual fuel packet it is assumed that the combustion occurs adiabatically and thus occurs at the instantaneous local adiabatic flame temperature. A tradeoff between accuracy and calculation time was required for this portion of the code. The flame temperature, for a given fuel, is primarily a function of EGR, equivalence ratio, and initial temperature. Therefore these effects must be accounted for when predicting the flame temperature. Ideally, an equilibrium (rich and lean) solver would be used with property data included but this is computationally

expensive especially for rich mixtures due to iterative solution process. In fact, implementing only a single rich equilibrium mechanism (water gas shift) doubled the calculation time required for the whole solution.

The method that is utilized here is a 2-D look up table generated off-line using a full equilibrium solver. This includes effect of equivalence ratio and EGR on the flame temperature. This table was generated for a constant initial condition of 700 K. To compensate for a different initial condition a simple energy balance assuming constant specific heats offset is employed that introduces only a small error, as shown in Equation 6.

$$\boldsymbol{Tflame(Tinitial)} \cong \boldsymbol{Tflame(700\ K)} + \boldsymbol{(Tinitial - 700\ K)} \quad (6)$$

It was found that on average without EGR over a range of initial temperatures from 700 – 1000 K there was less than 4 K error the between the full solver calculated flame temperature and the simplified equation above. When adding EGR the error becomes non-linear and increases to 12 K at 50% EGR. The improved calculation time gained by using this method is deemed worth the trade off in flame temperature prediction accuracy. While NO formation is primarily a temperature driven mechanism, the conditions for which this model is being developed (LTC) will likely have low NO concentrations such that this small temperature error may be acceptable.

Of course, initial temperature of the fuel packet must now be predicted. This is calculated using another simple energy balance assuming constant specific heats of the cylinder contents, shown in Equation 7 where T_{bulk} is calculated based on the ideal gas law for the whole cylinder, M_{tot} is the total trapped mass in the cylinder, $T_{unbunred}$ is the

temperature of all the unreacted mix remaining in the cylinder, the summation of $M_{reaction,i}$ represents the amount of mass that has been reacted up until the current time step, and finally the summation of $M_{reaction,i}*T_{flame,i}$ represents accumulated reacted mass/temperature up until the current time step. The unburned mixture temperature is taken as the initial temperature when calculating the flame temperature. As a result of the bulk temperature being calculated based on the ideal gas law for the whole cylinder, the unburned mixture temperature (as expected) must be less than the bulk temperature. While this may not truly represent the unburned mixture temperature, it at least gives an estimate to use as the initial temperature for flame temperature calculation.

$$\boldsymbol{T_{bulk}M_{tot} = \left(M_{tot} - \sum M_{reaction,i}\right)T_{unburned} + \sum M_{reaction,i}T_{flame,i}} \quad (7)$$

The result of this calculation combined with the equivalence ratio data for each packet provides the main output of the model – the combustion trajectory of each injected fuel packet through the standard soot and NO formation islands in the equivalence ratio, reaction temperature plane (as described by Kamimoto and Bae [26]). This calculated trajectory will be the primary analysis tool in the later sections.

Due to the sequential nature of the packet burning the inherent 2-D arrays of unburned fuel (row index), entrained air (column index), and equivalence ratio (array value) for each fuel packet as a function of crank angle can be reduced to a 1-D array for faster processing when solving the emissions prediction sub-models. Note that the emissions formation models are described in the following section because of their complexity.

3. EMISSIONS PREDICTION MODELS AND CALIBRATION PROCEDURE

3.1 Nitric oxide formation estimation routine and calibration discussion

Nitric Oxide (NO) is formed from oxidation of atmospheric nitrogen (unless there is significant fuel bound nitrogen). The dominant mechanism for NO formation is called “Thermal NO” and is modeled using the Zeldovich mechanism – the reactions included in this mechanism are shown in Equation 8. Thermal NO formation primarily occurs in the flame front and post flame gases because of the high local temperatures. As a result of the flame front being so thin and residence time is short, the post flame gases formation is the dominant factor. This means combustion and NO formation can be treated separately and knowing the temperature of the reaction is sufficient to predict the formation process. The knowledge of the reaction temperature is the primary output of the combustion trajectory model.

$$\begin{aligned} \boldsymbol{O + N_2 \rightleftharpoons NO + N} \\ \boldsymbol{N + O_2 \rightleftharpoons NO + O} \\ \boldsymbol{N + OH \rightleftharpoons NO + H} \end{aligned} \tag{8}$$

This section will investigate two methods for predicting the engine out NO levels. The first method uses a simplified version of the Zeldovich Mechanism and a complex calibration factor equation to match the prediction with the experimental results. This method produces a slightly better statistical agreement between prediction and experiment, however it is a much more calculation intensive method. The second option utilizes the strong correlation between combustion temperature and NO formation as the only indicator for predicting the engine out NO formation levels. This only

requires averaging the temperatures output from the combustion trajectory model rather than employing additional sub-models.

3.1.1 NO prediction calibration – purely empirical method

To predict the NO formation in the post flame gases the first method discussed utilizes a very simplified version of the Zeldovich mechanism; the equation shown below as Equation 9, and its derivation is described by Heywood [39]. A simple numerical integration at each calculation step results in the final molar concentration of NO [mol/cm^3]. Based on the trapped mass in each cylinder this can be converted to a volume concentration [ppm] and compared to the experimental results.

$$\frac{d[NO]}{dt} = \frac{6x10^{16}}{T^{1/2}} exp\left(\frac{-69{,}090}{T}\right)[O_2]_e^{1/2}[N_2]_e \tag{9}$$

In this simplified form, the NO formation rate is only a function of the post flame gas temperature and the equilibrium concentrations of molecular oxygen and molecular nitrogen. The breakdown of molecular nitrogen and oxygen that drives thermal NO formation is primarily driven by temperature, so it makes sense that the formation rate is only a function of these things. The simplified nature of the model however results in a large bias error causing large over prediction in total NO at high levels (the error is relatively smaller at lower levels because of the scaling of the bias factor). Some interesting trends were found when investigating the relationship between predicted NO and the experimental values as seen in Figure 4. There was a clear opportunity to implement a calibration factor of the form in Equation 10.

$$NO(ppm) = \frac{NO_{raw}}{Calibration\ Factor} \tag{10}$$

This calibration factor is used to convert from the raw model output to experimental equivalent results. This parameter is not constant and calculating the specific value can be approached two ways. The first is a purely empirical formulation that takes into account potential influence of injection timing, EGR levels, and injection rail pressure. A power relation to account for EGR effect was found to be best. There was a clear difference in EGR influence for different injection timings. Therefore, different coefficients in the power relation are used for different injection timings to capture the injection timing effect. An additional linear multiplier was used to account for the rail pressure effect (i.e. more rail pressure gives more NO). The overall equation is shown below in Equation 11. Note that the values for "A" and "B" in Equation 11 are determined as a linear interpolation on injection timing between the coefficients for the power fits shown in Figure 4. The rail pressure multiplier was adjusted to maximize the R^2 value for the experimental NO versus corrected predict NO shown in Figure 5 (discussed in the next paragraph). Finally, the general multiplier was adjusted to bring the slope of the regression line in Figure 5 as close to 1.0 as possible (i.e. predicted = measured).

$$\boldsymbol{Cal.Factor = Gen.Multiplier} * \frac{\boldsymbol{A}*[\boldsymbol{NO_{raw}}]^{\boldsymbol{B}}}{\left[\boldsymbol{RP_{multiplier}}\frac{(\boldsymbol{RP}-\mathbf{500})}{\mathbf{500}}+\mathbf{1}\right]} \tag{11}$$

The development of this empirical result shows in quite a good agreement when comparing predicted NO versus experimental NO values as shown below in Figure 5. At low formation levels the model under-predicts and at higher levels it over-predicts. The R^2 value shown in Figure 5 suggests a strong agreement in the predicted and experimental results.

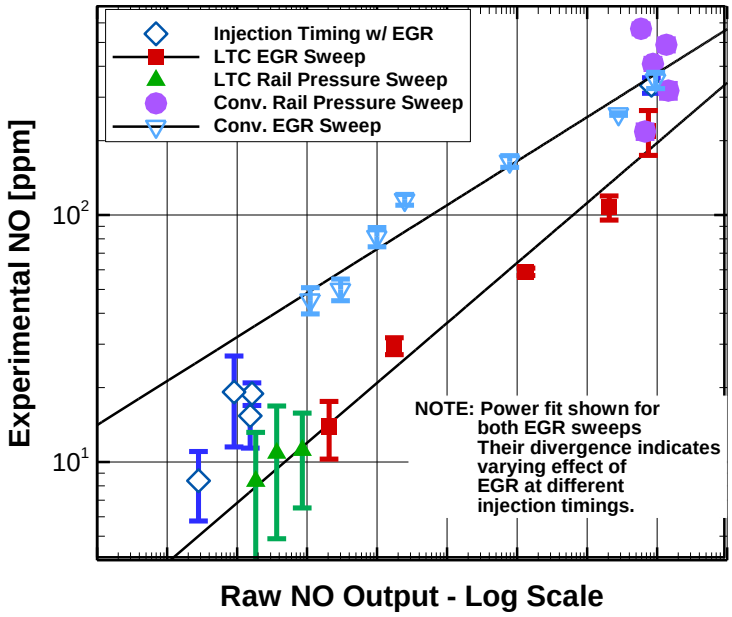

Figure 4 - Experimental NO versus raw NO output from the combustion model.

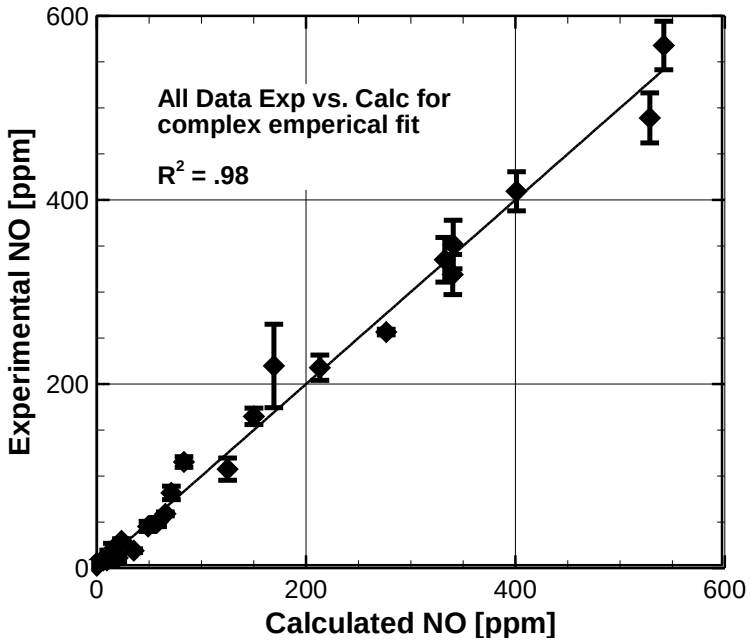

Figure 5 - Experimental NO versus the results of corrected predicted NO formation based on complex calibration factor in Equation 11.

3.1.2 NO prediction calibration – inverse average combustion temperature method

Alternatively, as is often the case with chemical kinetic formation rates, the experimental NO results correlate quite well with the predicted average combustion temperature. The correlation is easiest to see, and is shown in Figure 6, as a function of 1000/T such that higher numbers correspond to lower temperatures. Note the vertical axis (NO) is plotted on a log scale, while the horizontal axis (inverse temperature) is a normal scale. The linearity of the data set in this orientation suggests a strong exponential dependence on the average combustion temperature. This result is somewhat expected based on the formation rate equation shown in Equation 9. Using an Arrhenius style formulation, Equation 12 is used with constants based on the exponential fit of the data in Figure 6 to give a rough fix on the "A" and "B" constants. In the same way as the previous method, the exponential factor is adjusted to maximize the R^2 value for the experimental NO versus corrected predict NO shown in Figure 7 (discussed in the next paragraph). Finally, the general multiplier was adjusted to bring the slope of the regression line in Figure 7 as close to 1.0 as possible (i.e. predicted = measured).

$$\boldsymbol{NO_{predicted} = Gen.Multiplier * A * exp\left(B * \frac{1000}{T_{avg}}\right)} \quad (12)$$

This alternative method also shows a reasonable agreement when comparing predicted NO versus experimental NO values as shown below in Figure 7. At ultra-low formation levels the model under-predicts, but over a range from 100-500 ppm there is a moderate agreement (some above, some below). In some cases there is up to a factor of two error. The R^2 value shown in Figure 7 supports the moderate agreement in the predicted and experimental results though not as high as the first method.

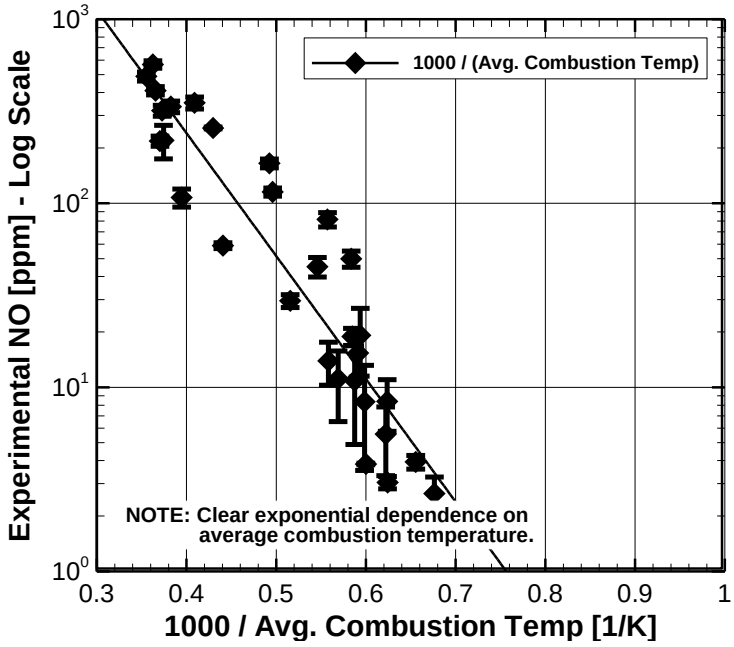

Figure 6 - Experimental NO versus inverse average combustion temperature.

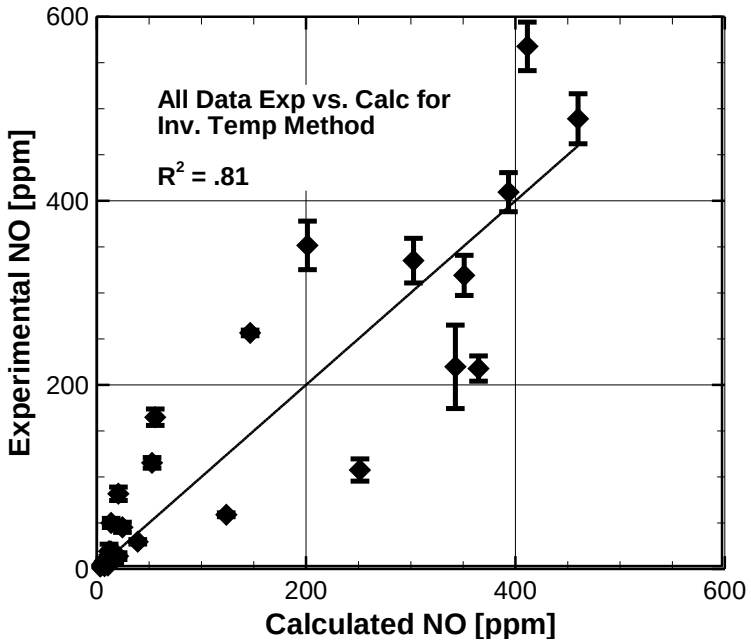

Figure 7 - Experimental NO versus the results of corrected predicted NO formation based on simple calibration factor in Equation 12.

3.1.3 Which NO calibration method to use? Accuracy vs. time considerations

The overarching factor for the entire model development has been calculation time. When choosing which NO calibration model to use the choice comes down to time versus accuracy. The required calculation time for both methods was determined on a desktop computer running Windows 7, a 1st Generation Intel Core Duo i3 processor and LabVIEW 2010. To start both methods at the same condition, the inputs were limited to the complete combustion trajectory temperature output as well as the operating conditions (i.e. rail pressure, EGR, injection timing).

The first method, based on the simplified Zeldovich mechanism and using the complex calibration constant resulted in an average calculation time of 24.4 µs. Because the calculation is so fast, this procedure was placed inside a loop that executed one million times then the average calculation time as determined from the total calculation time. To ensure that there was not some optimization routine in LabVIEW to detect repeated calculations a small random number was added to the temperature array each time the loop was ran – this added 0.3 µs to the overall calculation time.

For the second method, based purely on the average temperature, Equation 12 was used after first isolating the combustion temperature portion of the trajectory and averaging the result. This method turned out to take a significantly shorter time (at least relatively) of 2.5 µs. The same methods (one million times, and random addition) were utilized to ensure the same baseline conditions.

Both of the calculations time are clearly quite short, but it must be compared to the total calculation time for the model to determine if that small difference is

significant. Currently the average total time for the model is 11 milliseconds. Using both of the described methods in the whole model (as opposed to the isolated method used to get the individual calculation time) resulted in overall variation in the average calculation time of between 10-20 µs which matches well with the 21.9 µs. The difference is because the isolated methods used the same basic input (besides random addition) while the 10-20 µs variation was for many different engine operating conditions. A shorter, or longer, combustion event will obviously change the total calculation time because more calculation iterations are required.

In conclusion, a 20 µs difference in overall calculation time is a 1.8% difference in the total current calculation time. This isn't large, but it is not negligible either. As mentioned at the beginning, this case is a choice between accuracy and time. When the project starts to implement the model on an actual real-time controller where 20 µs (1.8%) might be the difference between completing the calculations in the available time or not, a more detailed decision matrix will need to be utilized to determine which model to use.

3.2 Soot formation estimation routine and calibration discussion

There are two primary pathways for soot formation under diesel engine conditions. One method for soot formation is the fragmentation of long chain fuel molecules once the available activation energy drops below the threshold to continue oxidation (i.e. splitting C-H bonds into CO and OH bonds – eventually forming CO_2 and H_2O). These fuel radicals can bond with each other and slowly conglomerate into a soot particle. This method is relatively slow compared to the second formation pathway but is

more active at higher reaction temperatures due to tendency to break carbon-carbon bonds.

Alternatively, at lower temperatures the bond structures of aromatic hydrocarbons are very prone to combining together. The relatively large size of these molecules and their resistance to oxidation (the ring structure requires more activation energy to oxidize than a straight chain) make for a fast soot formation and growth processes. As soon as the outer ring of hydrogen has been removed (or even partially removed) the aromatic hydrocarbon has a desirable bond spot for attaching to another carbon (think of pure a carbon structure with single bonds). The structure is not completely enclosed however, so often times soot is more precisely characterized as particular matter when it exits the engine because it may contain trapped/condensed unburned fuel, or other compounds.

After the soot is formed during the high temperature and pressure environment of combustion it is possible for the soot to be oxidized in the cylinder (i.e. the engine out soot can be much lower than the peak soot levels during combustion). This is a result of the continued mixing process – the soot forms in one region and then is transported to a region that favors oxidation and thus gets reduced. Two primary methods for oxidation are considered: continued oxidation by O_2 attack or OH attack. Both methods are dependent on the rate of diffusion into the soot conglomerate. A smaller particle will be reduced faster than a large particle simply because of surface area considerations.

The soot formation and oxidation model utilized are shown below. An Arrhenius formation mechanism is used to model the soot formation process (accounting for

pressure and temperature) with empirically determined activation energies and pre-exponential factor – see Equation 13. The variables are defined as follows: M_{sf} – soot formed, M_{fv} - fuel vapor mass, A_f - pre-exponential constant, P - Pressure, E_f - Activation energy, R - gas constant, T – Temperature.

$$\frac{dM_{sf}}{dt} = K_f M_{fv} \ with \ K_f = A_f P^{0.5} exp\left(-E_f/RT\right) \tag{13}$$

The Nagle and Strickland-Constable oxidation model is used to model the oxidation process. This model includes two pathways for oxidation and is primarily a function of the O_2 concentration and an estimated ratio between fast and slow reaction sites – see Equation 14. The variables are defined as follows: M_{so} - soot oxidized, MW_c - carbon molecular weight, ρ_s - soot density, D_s – soot diameter, M_s – current soot mass, and R_{Total} is a function of the predicted available reaction rates and reaction sites.

$$\frac{dM_{so}}{dt} = \frac{6MW_c}{\rho_s D_s} M_s R_{Total} \tag{14}$$

Both models combine to result in the net formation (it may be negative) of soot as the difference in formation and oxidation – see Equation 15. The variables are defined as follows: M_s - total soot, M_{sf} - soot formed, and M_{so} - soot oxidized.

$$\frac{dM_s}{dt} = \frac{dM_{sf}}{dt} - \frac{dM_{so}}{dt} \tag{15}$$

The soot formation model is solved numerically at each step along the combustion trajectory resulting in the final soot mass at the end of combustion. This value is converted to mass concentration [kg/cm^3] as is typically reported in particulate matter measurements. In the lab facility used here the primary indicator for soot levels is the smoke meter. This reports soot levels in filter smoke number (FSN) – an indication

of the opaqueness of a filter paper after an exhaust sample is passed through it. This is not a direct mass measurement. A number of studies have investigated correlating soot to FSN. These methods however are always empirically determined and thus are not likely to directly apply to the engine used here. For the purposes of model validation a custom empirical model was created. The methodologies and results will be described in the following sections.

3.2.1 Soot prediction calibration

The calibration factor the soot formation model is formed in the same manner as the NO factor; a single factor is used to convert the raw soot output from the model to match the experimental FSN value – see Equation 16. To begin developing an equation to predict this calibration factor the exact calibration factors for converting the raw soot output to match the experimental FSN values was plotted in Figure 8. There is quite a lot of trends happening in this figure – especially if all of the data was considered as a single set. By looking at the results for each actuator sweep (EGR, rail pressure, injection) it is clear that the trends among each of these is consistent.

$$\boldsymbol{Smoke\ Number\ [FSN]} = \frac{\boldsymbol{Soot_{raw}}}{\boldsymbol{Calibration\ Factor}} \tag{16}$$

To isolate the effect of each actuator change the data in Figure 8 is plotted again as a function of EGR, rail pressure, and injection timing in Figure 9 - Figure 11, respectively. First, in Figure 9, the effect of EGR is investigated. For the cases with roughly constant EGR level the data is shown, but not analyzed (points on left and right). The primary interest in this figure is the EGR sweep at the LTC timing (filled red squares) and the EGR sweep at the conventional timing (un-filled blue inverted

triangles). The roughly parallel linear trends for both injection timings suggests that the effect of EGR on FSN is constant regardless of injection timing. In other words, the effect of EGR can be treated separately from the other actuators.

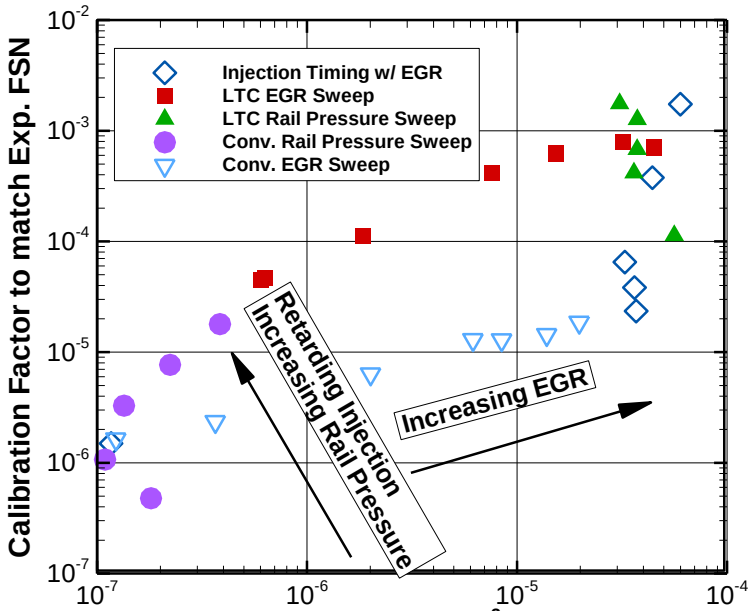

Figure 8 - Calibration factor required to exactly match the experimental FSN based on the output of the soot formation model. Calibration factor is of the form shown in Equation 16.

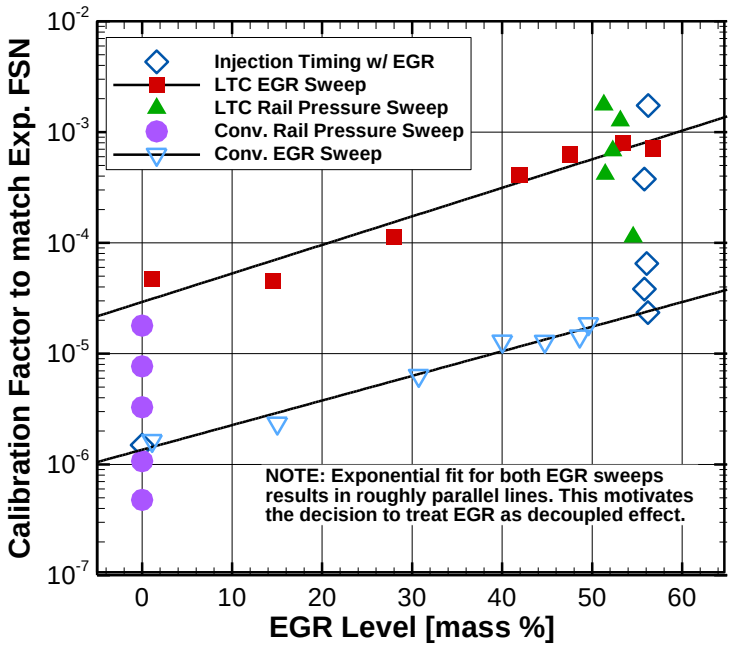

Figure 9 - Calibration factor as a function of EGR level [mass %]. The exponential curve fits illustrates the effect of EGR for use in empirical relation to predict the calibration factor.

Figure 10 shows the isolated effect of rail pressure on the calibration factor required to match the experimental FSN measurement. As with the EGR effect, the effect of rail pressure seems to be decoupled from the other actuators as the roughly parallel trend lines indicate. The behavior of the calibration factor as a function of injection timing is not as simple as can be seen in Figure 11. There is not a single trend line that captures the effect across the whole range of injection timings used in the validation data set. Because the goal of this empirical calibration equation is to achieve the best fit possible a two section trend was used to account for the influence of injection timing.

Because only one injection timing sweep was performed there is no way to determine if its influence is isolated from the other actuators. For the purpose of generating the calibration factor calculation equation it must be assumed to be decoupled. Bringing the three effects together into one equation was only possible because of the assumed decoupled nature of each actuator. The final equation, shown as Equation 17, includes separate factors for each actuator. The formulation is based on the assumption that the increase in the calibration factor from some baseline (i.e. the bottom left point in Figure 9) is just a combination of the various multipliers. If the rail pressure is equal to the rail pressure of the baseline condition then it doesn't change the calibration factor (i.e. the net rail pressure multiplier is one because it has a rail pressure of 500 bar). The same logic applies for the effect of EGR.

$$\boldsymbol{Cal.Factor} = \frac{\boldsymbol{Base\ Value}}{\boldsymbol{Gen.Multi.}}\left[\boldsymbol{RP_{multi.}}\frac{(\boldsymbol{RP-500})}{\boldsymbol{500}}+\boldsymbol{1}\right]\left[\boldsymbol{EGR_{multi.}}\frac{\boldsymbol{EGR}}{\boldsymbol{30}}+\boldsymbol{1}\right][\boldsymbol{Inj.Factor}] \quad (17)$$

The handling of the injection timing effect is a bit more complicated as indicated in the discussion of Figure 11. Because there is not just one trend for injection timing the influence of injection timing is split into a parametric equation, see Equation 18. It is suspected that this split behavior is caused by the combustion mode transitioning to LTC, though this is not confirmed.

$$\boldsymbol{Inj.Factor} = \begin{cases}\left[\boldsymbol{Inj_{multi.\#1}}\frac{(\boldsymbol{Inj.+8})}{\boldsymbol{4}}+\boldsymbol{1}\right] & \boldsymbol{if\ Inj.\leq 4°bTDC}\\ \left[\boldsymbol{Inj_{multi.\#2}}\frac{(\boldsymbol{Inj.+4})}{\boldsymbol{4}}+\boldsymbol{1}\right] & \boldsymbol{if\ Inj.> 4°bTDC}\end{cases} \quad (18)$$

Now that the calibration factor prediction equation has been developed Figure 12 shows the results. Ideally this figure would look just like Figure 8 if the matching was perfect. Obviously this is not the case.

The rail pressure and EGR sweep trends are quite accurately reproduced (although the conv. rail pressure sweep is slightly off in magnitude). For example, compare the solid purple circles (conv. rail pressure sweep) in both Figure 12 and Figure 8 as well as the solid green triangles (LTC rail pressure sweep). The trend of injection timing is also well reproduced – the unfilled blue diamonds in both Figure 12 and Figure 8.

While not perfect, the ability to reproduce most of the trends in Figure 8 indicates a good probability that the actuators are actually roughly decoupled (or at least can be treated that way in across the operating regimes investigated here). The calibration constants were manually adjusted until the highest R^2 correlation was achieved with the results shown in Figure 12.

To wrap up the discussion of the soot model calibration effort, see Figure 13 for the final results comparing the experimental FSN measurements with the calculated FSN values. Note the high R^2 correlation value. The model under predicts soot at the low levels, but overall does a generally good job – note the log scales (large geometric error on left of the figure isn't same as on the right).

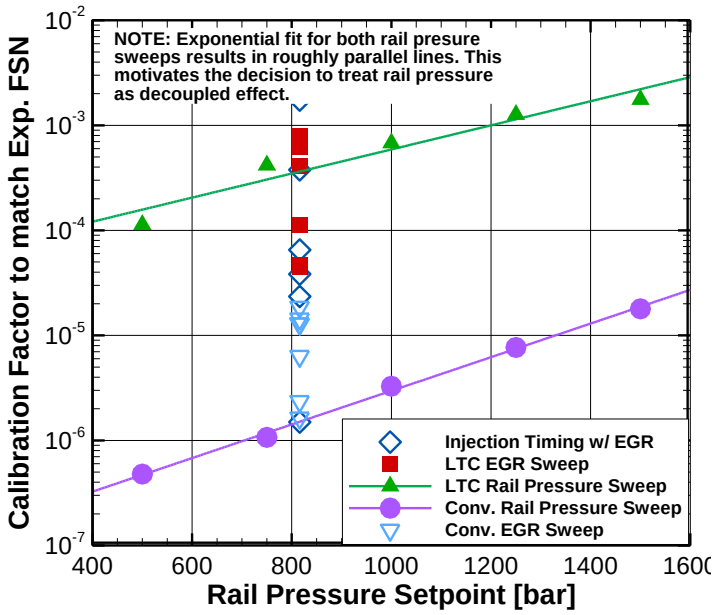

Figure 10 - Calibration factor as a function of Rail Pressure [bar]. The exponential curve fits illustrates the effect of rail pressure for use in empirical relation to predict the calibration factor.

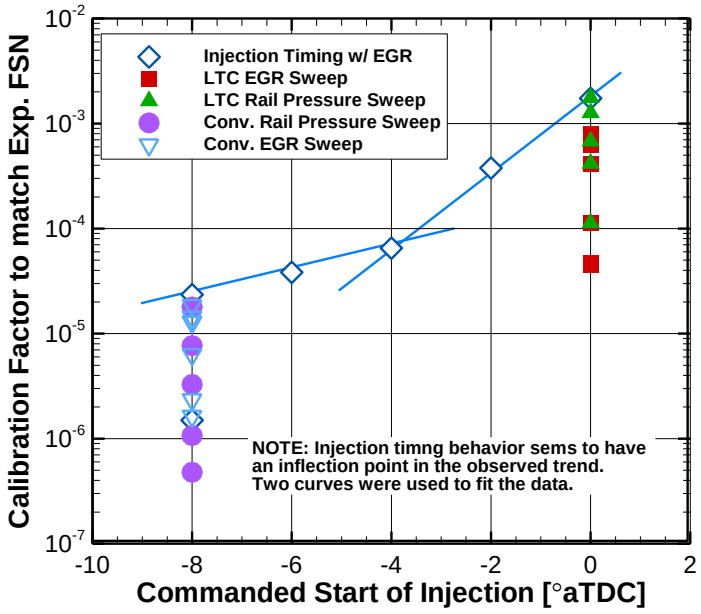

Figure 11 - Calibration factor as a function of commanded injection timing [°aTDC]. The exponential curve fits illustrates the effect of injection timing for use in empirical relation to predict the calibration factor.

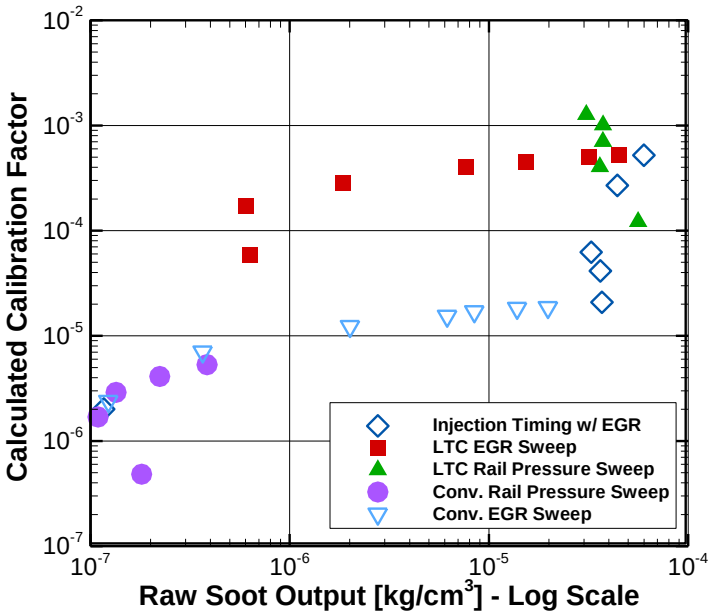

Figure 12 - Calculated calibration factor based on the empirical equation shown in Equation 17. Note that best R^2 value was achieved with a zero multiplier for the EGR effect (see Figure 13).

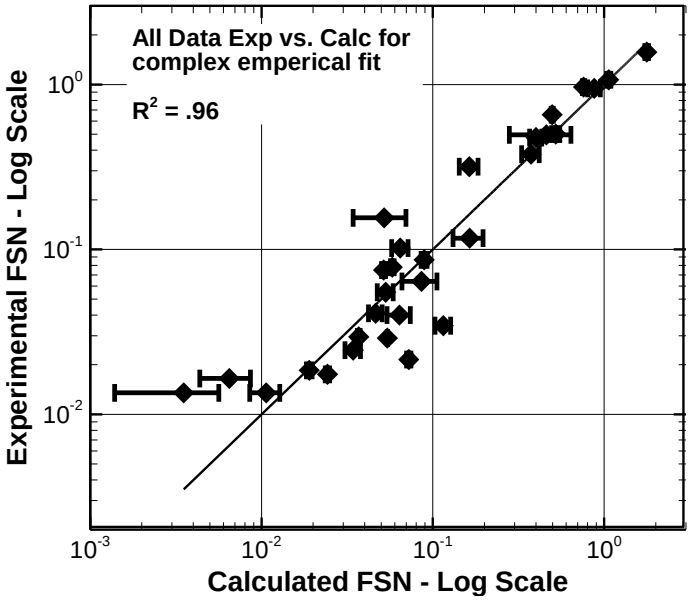

Figure 13 - Experimental FSN compared to the calculated FSN. The regression R^2 value is quite good – suggesting a good agreement despite using an empirically derived calibration constant.

3.2.2 Soot model computational time

As with the NO model calibration discussion the required calculation time to implement this whole procedure will be discussed. In this case there is no decision to be made between to competing methods, but knowledge of the computational time for each portion of the model will be crucial to help target optimization efforts in the future if needed. Because the soot prediction model includes many more layers to the equation (i.e R_{total} in Equation 14 is a function of other variables, which are also functions of other variables) the overall calculation time is significantly longer than the NO model at 80 µs. The code was ran in a loop one million times with a random value added to the temperature area to avoid any optimization routines in LabVIEW. The average calculation time was determined from the total time. If the code needs to be shortened for operation in a real-time controller application the soot model will be targeted before the NO model simply because it takes longer to process.

4. INITIAL MODEL VALIDATION AGAINST MEDIUM-DUTY DIESEL ENGINE

This section will present the major results of this study; the combustion trajectories computed for a number of different experimental test conditions. The most interesting data are the trajectories through the ϕ-T plane relative to the soot and NO formation regions. That type of presentation, however, doesn't show the time progression of the combustion process, so the initial results will be shown for an example conditions showing the results versus crank angle. After this orientation the main results will focus on the way the trajectory falls on the soot and NO formation maps, but the same time progression features are present in each trajectory.

4.1 Combustion mode transition trajectory analysis

The following sub-section will present a thorough analysis of a single predicted combustion trajectory when plotted on a time (crank angle) basis. Then an expanded set of data showing the engine transitioning from conventional combustion to LTC will be shown overlaid on the soot and NO formation regions showing the mode transitioning from conventional to LTC.

4.1.1 Trajectories plotted vs. crank angle to show time progression

Figure 14 shows the first results of the study – specifically the trajectory of the baseline conventional combustion case as a function of crank angle (CA). The engine is operated with no EGR, a standard injection timing of 8° before TDC (bTDC), 1400 revolutions per minute (RPM), a nominal load of 2 bar brake mean effective pressure (BMEP) with an rail pressure of 816 bar (stock OEM set point for this speed load). All

test data presented in this study are at the same nominal conditions except as noted. Heat release is shown (without an axis) to give orientation to the local equivalence ratio and reaction temperature as functions of crank angle.

In Figure 14 start of combustion can be seen to occur right before TDC. The jump in reaction zone temperature matches this timing (prior to ignition the reaction zone temperature is the same as the non-reacting zone). A sharp rise in equivalence ratio is seen as the rapid combustion progresses faster than the mixing rate (i.e., premixed burning). During this rise in equivalence ratio there is a corresponding slight drop in the reaction temperature. This matches the trend of adiabatic flame temperature versus equivalence ratio which has a maximum near stoichiometric and decreases to either side. From the point of maximum heat release the equivalence ratio starts to decrease towards stoichiometric as mixing starts to control combustion (i.e., mixing controlled, or diffusion, burning). The reaction zone temperature starts to decrease once again following the typical flame temperature versus equivalence ratio trend. In some other cases (shown in the following section, but not versus CA), the reaction temperature decreases counter to the expected trend in the late combustion stages. This likely a result of the energy added from combustion being overcome by the energy removed due to expansion.

A few subtle features of each trajectory are discussed. First, recall that the combustion model assumes that each fuel packet burns sequentially (i.e., only one at a time). The result of this approach is that the overall combustion trajectory can be plotted vs. time (or crank angle) simply by combining the reaction trajectory (mixing trajectory

is not shown) of each packet as it burns end to end. When observing the trajectories in Figure 14 this concatenation gives the illusion that there is only one continuous trajectory when this isn't the case. Looking closely small jagged "stair-stepping" edges can be seen (not the single large discontinuity, which will be discussed below); this is most noticeable towards the end of combustion in Figure 14. These edges result from one packet being consumed and the next packet starting to burn. The smoothness early in combustion results from the fuel that burns next having nearly the same time to mix and therefore nearly the same equivalence ratio as the previously burned packet. Later in combustion the fuel packets take more time to burn, so the edges are more noticeable. With each packet taking longer to burn, a lower equivalence ratio would be expected; however, note the slight increase in equivalence ratio near the end of combustion. This is a result of the entrainment model which is not only a function of time, but also injected fuel mass. The last few fuel packets injected contain very little mass, so even with large amounts of time to mix the actual equivalence ratio slightly increases.

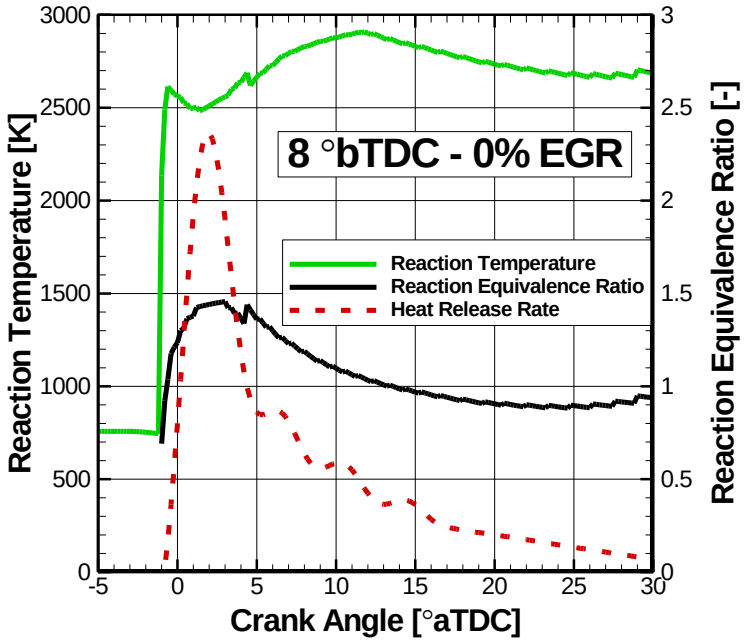

Figure 14 - Combustion trajectory shown versus crank angle for conventional combustion case. Nominal engine operating conditions: 1400 RPM, 2 bar BMEP, 816 bar rail pressure.

The large discontinuity observed in both equivalence ratio and temperature (e.g., the jump that occurs at approximately 4° after TDC in Figure 14) is a consequence of the assumed injection profile being triangular (linear rise with a sharp vertex and linear decrease). Interestingly this also serves as a marker for 50% mass fraction burned. Up until this point each successive fuel packet had linearly more fuel than the last which results in slightly faster entrainment (see detailed model description for reasoning) and therefore follows a similar trajectory as the previous fuel packet by "catching up". This is the same reason for the smooth nature of the combined trajectory discussed above. After mid-point this relation is broken for one step as the linear relation between the previous and next fuel packet shifts form a positive slope to a negative one.

Mathematically, the discontinuous derivative of the injected fuel amount causes a discontinuity in the mixing rate prediction.

4.1.2 Trajectories plotted on equivalence ratio vs. temperature plot

To show the differences in combustion phasing (the primary driver for varying combustion modes) and also relative intensities of the combustion event, observe the heat release profiles of four test conditions overlaid on top of each other in Figure 15. These conditions illustrate the transition from conventional combustion to LTC (i.e. adding EGR and retarding injection). Note the shifting combustion phasing as EGR is added at the conventional injection timing (solid black to dashed red). Combustion phasing correspondingly retards as injection timing retards. Initially the peak heat release rate increases slightly as longer mixing times occur in the lengthening ignition delay period (revealing, also, the occurrence of low temperature heat release). Very late phasing limits combustion intensity as piston expansion reduces in-cylinder temperatures and pressure. For Figure 15 and all future apparent heat release figures in this validation section the vertical axis will be the same scale to make easy visual comparisons for the combustion intensity between conditions. In other words the reader needs only to see that the one conditions is physically taller compared to another to know that it has a higher combustion intensity rather than looking at the axis values.

Figure 16 shows the combustion trajectories of the four conditions shown in Figure 15 on the ϕ-T plane overlaid on emissions data from [15]. Because the conventional no-EGR case (solid black squares) is the most isolated its general features will be highlighted. The first fuel to be injected has the longest time to mix, thus has a

low ignition equivalence ratio of around 0.6. This is immediately (only two steps/squares at the low equivalence ratio) followed by an increase in equivalence ratio and corresponding increase in temperature as the reaction follows the flame temperature limit towards stoichiometric. As the burning packets become rich (as combustion rate outpaces mixing rate) the temperature starts to decrease slightly. Soon, enough energy is released to increase the ambient mixture temperature (or the pre-ignition temperature of the subsequent fuel packets). At the same time for this case the mixing rate overtakes the burning rate (transitioning to a diffusion burning regime), further causing the reaction temperature to increase as the mixture leans. Eventually the reaction temperature decreases again as the equivalence ratio becomes slightly lean. The general clockwise rotation of the reaction pathway is common between all of the combustion trajectories shown in all future plots as the reaction progression will be similar in most cases. Some differences (as expected) are seen between conventional and LTC modes, but these will be described below.

Now compare the black solid squares (conventional no-EGR) to the red hollow circles (conventional with EGR) in Figure 16. The shifting to higher equivalence ratios and lower temperatures that is intuitively expected based on the soot-NOx tradeoff is indeed captured by the model. However, this shift may be counter intuitive as the general effect of EGR on combustion phasing is to allow more mixing time, so one might expect to see lower equivalence ratios as EGR is added. However because the EGR displaces fresh air mixture it takes a larger mixed volume to reach the same equivalence ratio.

The trajectory with high EGR has a slightly different shape because it is always rich, but the clockwise rotation is present. Going from red hollow circles, to green solid triangles, to pink hollow squares is the injection timing sweep with high EGR. The effect isn't very pronounced at the midpoint injection timing (4 °bTDC), but the longer combustion duration and decreased intensity is very apparent in the pink hollow squares trajectory, i.e. the late timing of 0 °bTDC. Notice that the clockwise rotation is almost not present. There is only a slight shifting to high reaction temperatures compared to that seen in the 4 and 8 °bTDC injection timing trajectories. This prediction corresponds well with the late phasing shown in the heat release profile. As described, the reaction temperature is calculated as the instantaneous flame temperature and a higher initial mixture temperature partially causes the higher reaction temperature as the trajectory rotates clockwise. Low intensity combustion and piston expansion appear to be balanced such that the ambient temperature of the cylinder mixture doesn't change significantly. This ultimately causes LTC manifestation with high EGR and late injection. A very important thing to note is that the LTC mode (pink hollow squares) is not dramatically far away from the soot formation region. While the soot formation contours in the figure stop at 1%, it is understood that soot formation will still be present at other points in the graph – just at lower concentrations. So while the LTC mode isn't in some specifically prescribed region (bottom left) of the figure it does not move to a higher formation contour as combustion progresses as the other high EGR operating points show. This is one of the important contributions this combustion trajectory prediction model makes – giving some visual qualification for what LTC means in terms of combustion trajectory.

LTC shouldn't be defined as a rectangular region, or any specific region on the ϕ-T plane. Low temperature combustion is characterized by simply staying slightly further away from the center of the soot formation region than conventional combustion. The trajectories shown in Figure 16 illustrate this point.

It is encouraging that the trajectories visually appear to agree with expected trends. The conventional timing, no EGR case (black solid squares) in the Figure 16 is predominately in the NO formation region and not in the soot region. The three cases with EGR have shifted away from the NO region and into the soot formation region. The case that can be classified as LTC (pink hollow squares) is further from the center of the soot formation region and critically does not move towards the center of the soot region as combustion progresses – both features suggest lower soot relative to the other conditions.

The conventional definition of LTC is that the soot concentrations remain at conventional combustion levels and the NO is dramatically reduced (i.e. defeating the soot-NOx tradeoff). By this definition, and verified by the experimental emission measurements (not shown, but see [40]), the conventional no EGR (black solid squares) case should, and does experimentally, have approximately the same soot concentrations as the LTC case (pink hollow squares). By a simple visual inspection it appears that the LTC case is much closer to the soot formation region than the conventional case – suggesting a discrepancy from the experimental results. This will be addressed first, before showing the predicted emissions values, because as with all emission predictions models there is significant opportunity for tuning and forcing a match to any

experimental data as is shown in the emissions modeling section. This can be deceptive and give an unwarranted sense of confidence in the results. To address this apparent discrepancy, first consider that soot formation and oxidation models are both heavily temperature dependent. It is understood that at higher temperatures more soot will be formed, but the oxidation kinetics are also accelerated resulting in low engine out soot. Taking this into consideration it follows that even though the oxidation is accelerated it is unlikely that all of the soot will be eliminated. This is contrary to lower temperature reactions were the dominate factor in determining engine out soot is the formation kinetics. Both mechanisms (high oxidation, or low formation) result in low engine out soot, but the authors postulate that the fact that a significant amount of soot is formed under conventional conditions (and then oxidized) may result in higher concentrations than the LTC condition were very little soot is formed in the first place. This hypothesis is given some credence from observations that the soot formation contours are significantly skewed to the high temperature region for very small soot formation concentrations (i.e., much less than the 1% shown in the figures). Lastly, a feature not captured by the models is the possibility that during late stage oxidation processes the stratification of diesel combustion may result in trapped soot that would have otherwise been oxidized if it were in the presence of oxygen. This would not be an issue at the LTC condition, again, because the formation kinetics is the limiting factor not the oxidation. All these thought experiments suggest that the gradient of soot concentration is not uniform in all directions and is likely steeper towards lower temperatures.

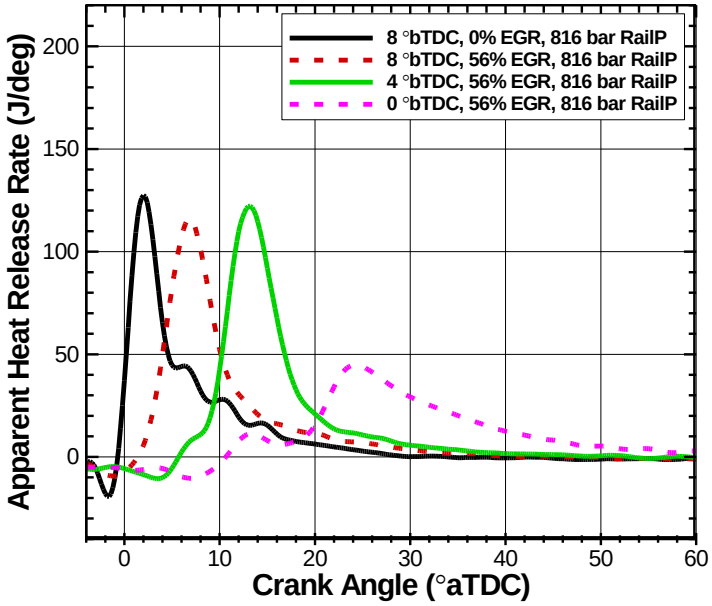

Figure 15 - Apparent heat release rate profiles for an injection timing sweep starting with no EGR and then adding maximum EGR at the same nominal engine conditions.

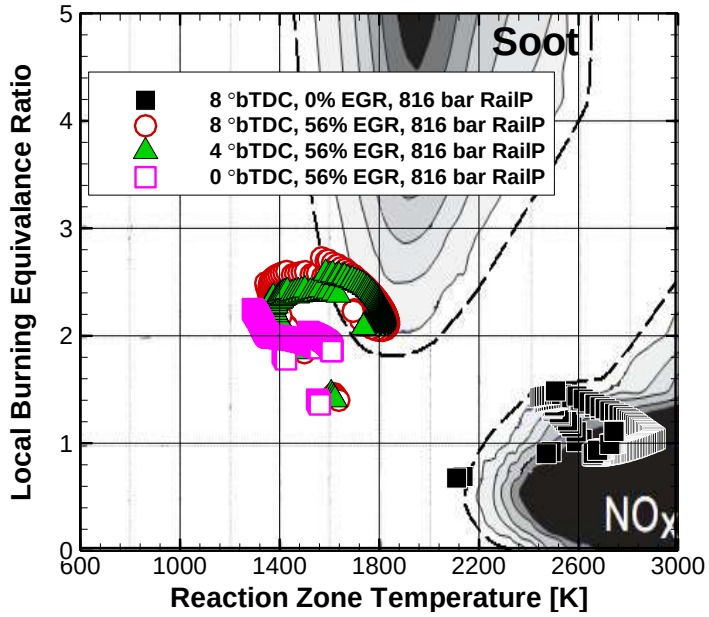

Figure 16 - Select combustion trajectories for an injection timing sweep starting with no EGR and then adding maximum EGR at the same nominal engine conditions.

The following figures, Figure 17 and Figure 18, show the emissions results for the full injection timing sweep at high EGR. More timings were tested than shown in Figure 16, but were omitted for clarity as they followed the same trends. Figure 17 shows the NO concentrations as a function of injection timing. The experimental results and the results from both methods for predicting NO concentration are shown. The expected trends based on the combustion trajectories match the experimental results and generally the predictions track well with the experimental results. For this particular control sweep the simpler inverse temperature method, "CallcNOinvT" in the figure, for prediction does a better job. However, recall from the emissions predictions calibration section that the complex method, "CalcNO" in the figure, did a better job (higher correlation) over the whole data set. The calibrated FSN prediction does an excellent job of tracking with the experimental results – seen in Figure 18.

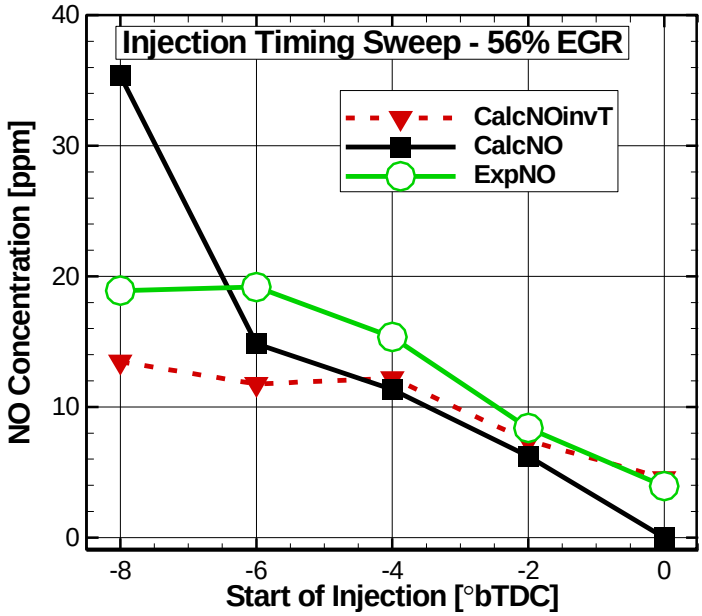

Figure 17 - Nitric oxide emission prediction comparison to experimental results for an injection timing sweep with a high EGR level. NOTE: This does not include the 0% EGR results from Figure 16.

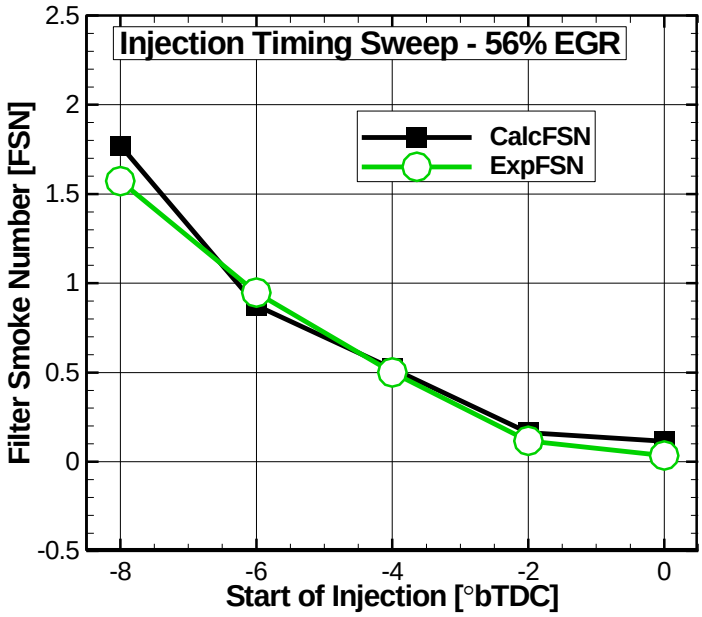

Figure 18 - Filter smoke number prediction comparison to experimental results for an injection timing sweep with a high EGR level. NOTE: This does not include the 0% EGR results from Figure 16.

4.2 Conventional combustion trajectory analysis

The model was further validated against rail pressure and EGR sweeps at both conventional and late injection timings. This section will first present the rail pressure sweep and then the EGR sweep at the conventional timing. The next section will show the same for the late injection timing. Less detail about the combustion trajectories shapes will be given as the same features described above are still applicable. Most focus will be on the general regions occupied by the combustion trajectories for the various set points as this is the primary visual indicator for emissions formation.

4.2.1 Rail pressure sweep

This section will show the combustion trajectory results and emissions prediction for a rail pressure sweep at a conventional combustion timing with no EGR while holding fueling rate constant (increased injection duration for decreased rail pressure). To first illustrate the effect on combustion phasing and intensity see Figure 19 which shows the heat release profiles for three of the tested rail pressures (min, mid, and max). Remember that the injection timing is constant, so as expected an increased rail pressure promotes better mixing and thus a higher peak heat release rate (more premixed mixture at ignition). The ignition timing can also be seen to advance with increasing rail pressure – likely the smaller droplets at higher injection pressures are vaporized more rapidly and therefore reach ignition quicker. Because the fuel is igniting around TDC it is a reasonable assumption that the ignition event is vaporization, not kinetically, limited.

This actuator sweep shows the least variation in the combustion trajectories – seen in Figure 20. Flame temperature is not directly influenced by rail pressure like it is

by EGR in the previous section; however, it is affected indirectly by the mixing rates and resulting equivalence ratio during combustion the temperature can be changed. Because of the effect of advancing ignition coupled with presumably better mixing at higher rail pressures the end result is a generally similar trajectory. The higher rail pressure mixes better, but has less time to do so and therefore the trajectory looks similar to a lower rail pressure which doesn't mix as well but has more time. The slight differences in trajectory (and also emissions) are attributed to the varying peak combustion intensity seen in the heat release profiles in Figure 19. The same clockwise rotation discussed previously is observed here, with the shifting to higher pre-ignition temperatures for each subsequent fuel packet starts to occur as the mixing rate starts to outpace the combustion rate. Because of the higher intensity reaction associated with the larger pre-mixed fraction at higher rail pressures the increased pre-ignition temperature for each fuel packet causes a higher peak reaction temperature of nearly 3000 K compared to 2800 K for the high and low rail pressures respectively.

The relative proximity of the trajectories in Figure 20 to the NO formation region suggests they will all have high NO concentrations with the higher peak temperatures generating more NO (i.e. higher rail pressure corresponds to higher NO in this case). Also, while not actually "in" the soot formation regions, recall that the edges of the contours are arbitrary and formation occurs in all regions (just at lower rates). Therefore the closer to the soot region the trajectory is the more soot is likely to be formed. Based on this general trend, the higher rail pressure that creates more NO by moving to higher temperatures also will create less soot because it moves away from the soot formation

region. Note however that the higher rail pressure conditions are essentially right on top of each other except at the peak reaction temperature locations.

Comparing these expected trends to the actual experimental and predicted emissions results show good agreement. The NO levels in Figure 21, while always relatively high, do increase with increasing rail pressure as expected. The complex NO model does a great job tracking the experimental results while the simple inverse temperature method does a poor job, and is deemed unacceptable in this case for magnitude, but the rough trend is still captured. The FSN results in Figure 22 once again match the expected trend - a sharp drop off for the first rail pressure step (from 500 to 750 bar) and then relatively steady (near zero) levels after that. This matches the minimal visible difference in the 1000 and 1500 bar trajectories shown in Figure 20, while the 500 bar case (black solid squares) is a bit more distinct.

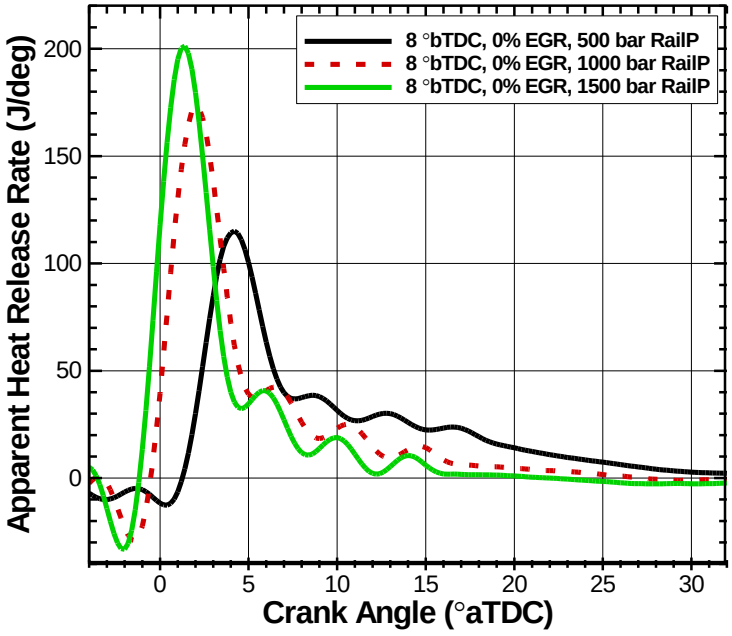

Figure 19 - Apparent heat release profiles for a rail pressure sweep at conventional combustion timing.

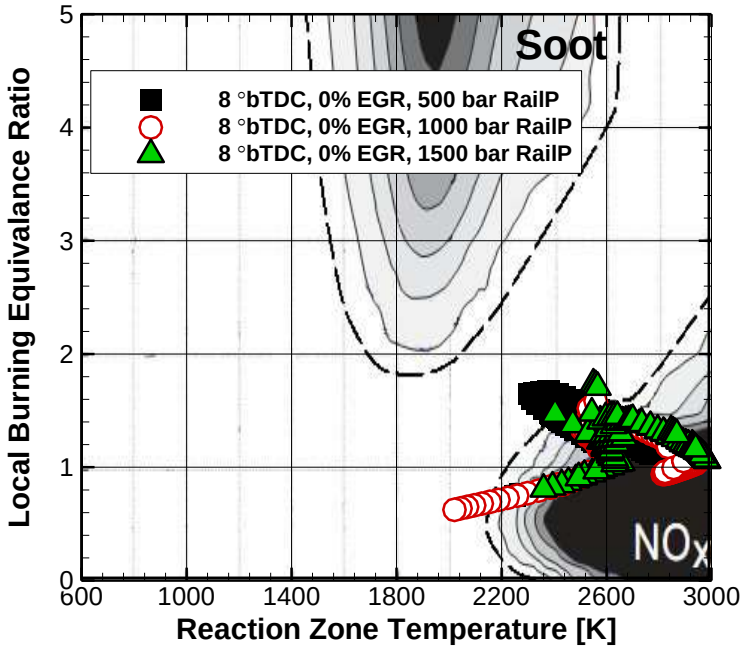

Figure 20 - Select combustion trajectories for a rail pressure sweep at conventional combustion timing.

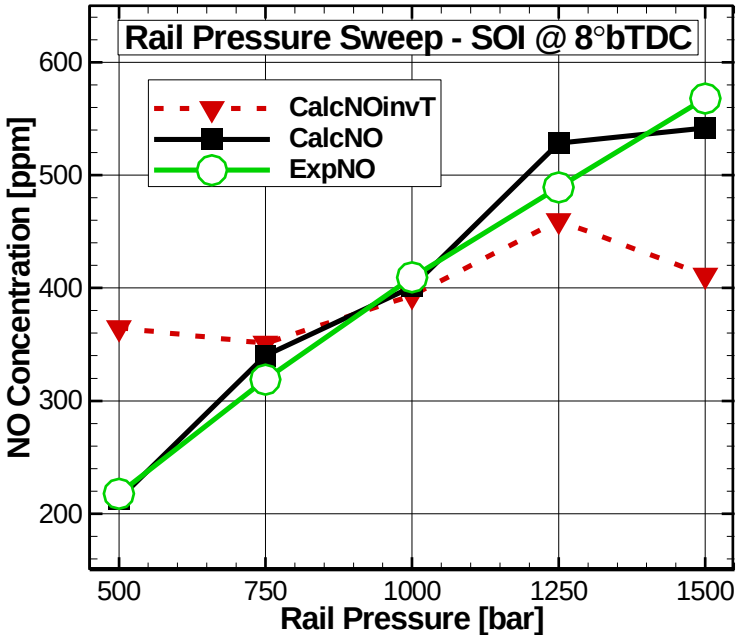

Figure 21 - Nitric oxide emission prediction comparison to experimental results for a rail pressure sweep at conventional combustion timing.

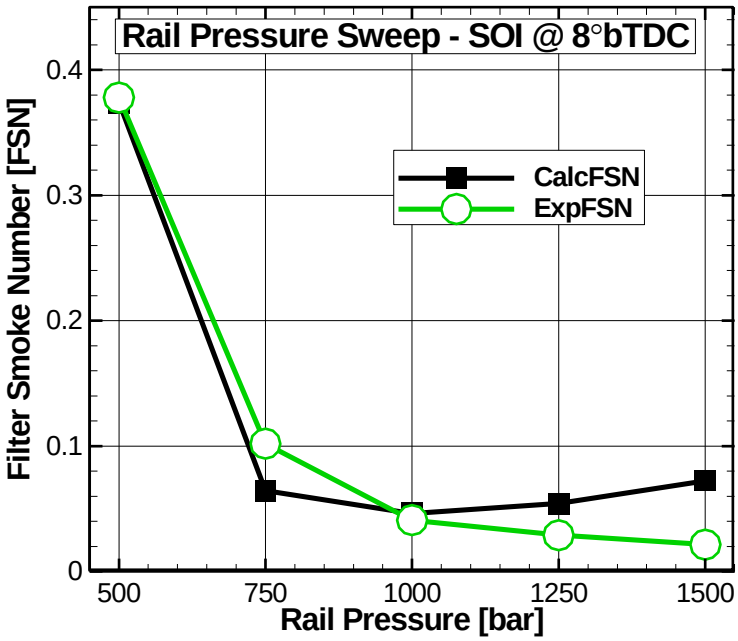

Figure 22 - Filter smoke number prediction comparison to experimental results for a rail pressure sweep at conventional combustion timing.

4.2.2 Exhaust gas recirculation sweep

The conventional diesel combustion event has been investigated using many techniques by other researchers, so it is interesting to see how these trajectory predictions compare with classical phenomenological models. At constant conventional injection timing the EGR level is swept from 0% to maximum while maintaining rail pressure. By observing the heat release profiles in Figure 23, notice that peak heat release rate is almost unaffected by the added EGR – likely because of the close proximity to TDC where the compression peak pressure and temperature are still high at ignition. Although the ignition event is delayed it only affects start of combustion and not combustion duration. Recall that while the extra mixing time afforded by the longer ignition delay would suggest lower equivalence ratio, the required volume of entrained gas to reach the same equivalence ratio increases because of the displaced fresh mixture resulting in a higher equivalence ratio for higher EGR. In general, the calculated trajectories agree with conceptual models regarding EGR-level soot / NO tradeoff behavior.

The trajectories in Figure 24 show the same clockwise trend as before. With more EGR, the ignition equivalence ratio increases and the initial flame temperature is also reduced directly. A very interesting feature that is present in previous data (refer to Figure 14 to help visualize) but is most obvious in the combustion trajectories now is the difference in behavior between what is traditionally called the pre-mixed and diffusion portions of the heat release profiles. The premixed portion is the large peak at the beginning and the diffusion portion is the typically lower rate and longer duration burn.

There is not an absolute transition point but generally it is somewhere after a first peak heat release location – sometimes identified by the inflection point in the heat release profile after a first peak heat release rate. Although pre-mixed combustion can be very intense (i.e., high heat release rate), it may only have a small effect on ambient mixture temperature (relative to diffusion burning) because of its short duration. The changing ambient mixture temperature is manifested in the model prediction by the changing reaction temperature in directions other than along the very well-defined equivalence ratio limit for a constant initial temperature. In other words a higher initial temperature allows for a higher peak reaction temperature. This effect will be visualized by observations in Figure 24. In addition to the clockwise progression, note the general "U" shape of each trajectory – this is clearest for the highest EGR case (pink hollow squares) and becomes more compressed for the zero EGR case (black solid squares). As EGR is added without increasing the peak heat release rate (see Figure 23) the difference in reaction temperatures at the late stages of combustion relative to the initial stages becomes more pronounced – the "U" becomes wider or better defined. This means that the later stages of combustion (the diffusion reaction) control the ambient fuel mixture temperature. This matches well with the typical flame structure models. Once a standing flame (or flame front) is established that is reacting slowly, the fuel burned next will have a higher initial temperature. To further illustrate how the trajectory visualizes the different phases of combustion (discussed above) note that the indication for transition from pre-mixed to diffusion combustion is the point in the trajectory where the equivalence ratio starts to level off and then decrease (or the turnaround point of the

"U"). This is the point where the reaction rate has slowed enough that the mixing is occurring faster than combustion and therefore the equivalence ratio decreases.

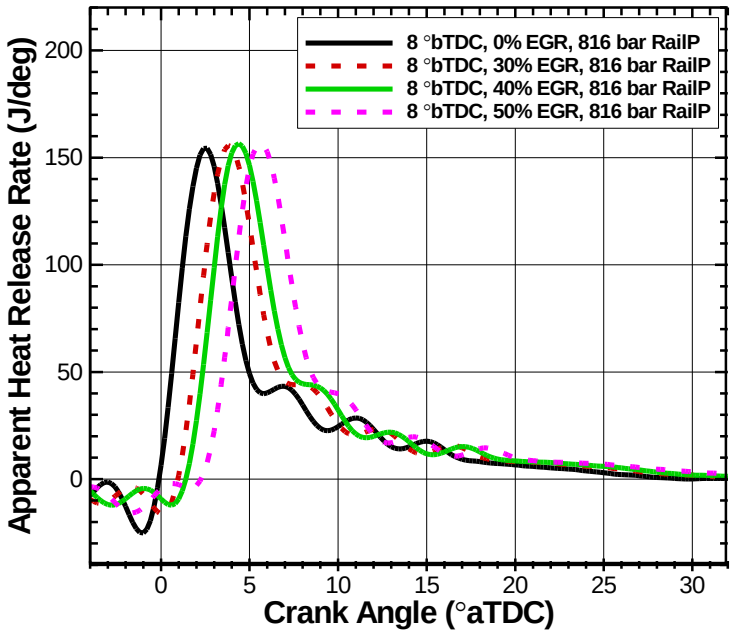

Figure 23 - Apparent heat release rate profiles for an EGR sweep at conventional combustion timing at the same nominal engine conditions.

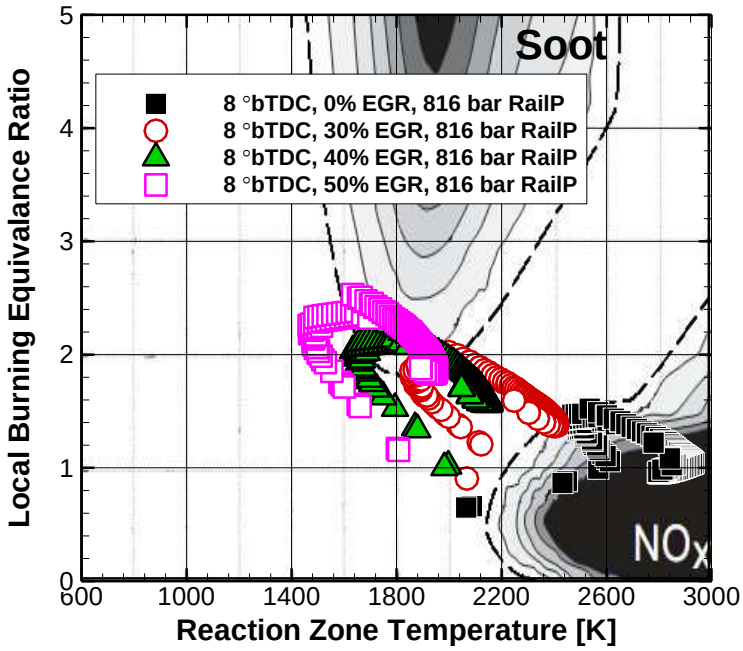

Figure 24 - Select combustion trajectories for an EGR sweep at conventional combustion timing at the same nominal engine conditions.

Observe the relative proximities of each trajectory in Figure 24. As expected from the soot-NOx tradeoff, with added EGR the trajectories move from the NO to soot formation region. Experimentally, the measured smoke and NO emissions do indeed behave inversely as seen in Figure 25 and Figure 26. There is still significant NO being formed even at 50% EGR, and the smoke has gone from effectively zero to above 1.0. The effect of increasing EGR on the limiting peak flame temperature causes a nearly linear decrease in NO emission, while the resulting increased equivalence ratio causes a localized exponential increase in FSN. From the perspective of the trajectories this is apparent as the late stages of combustion (the mixing controlled phase), or the right side of the "U"-shape described previously, occur in close proximity to the soot formation region. This is most apparent for the maximum EGR case (hollow pink squares), and this

corresponds well with the conceptual sooting flame models described by other researches (Dec [41] for example). As with the previous results, the model predictions for NO and FSN agree quite well using the complex methods for calculating the calibration factors. The simpler NO prediction method doesn't capture the magnitudes, but it does a good job with the trends.

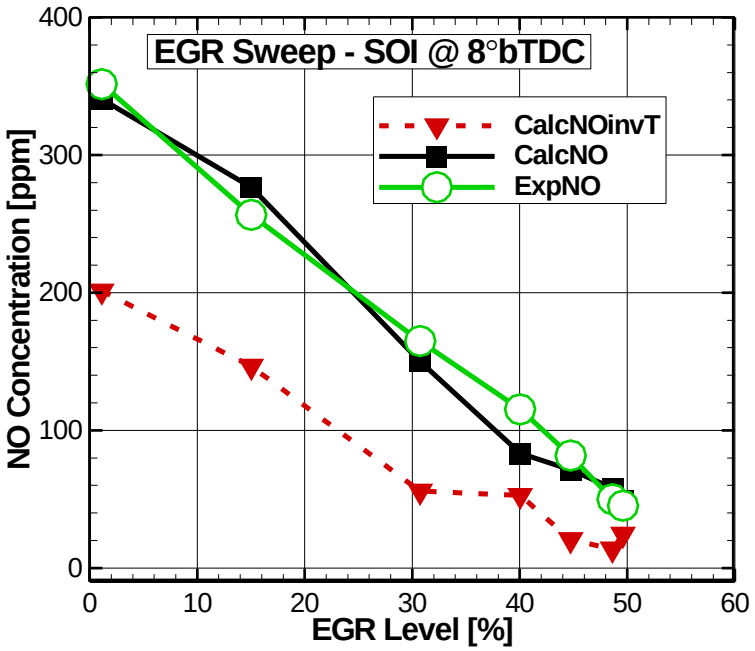

Figure 25 - Nitric oxide emission prediction comparison to experimental results for an EGR sweep at conventional combustion timing.

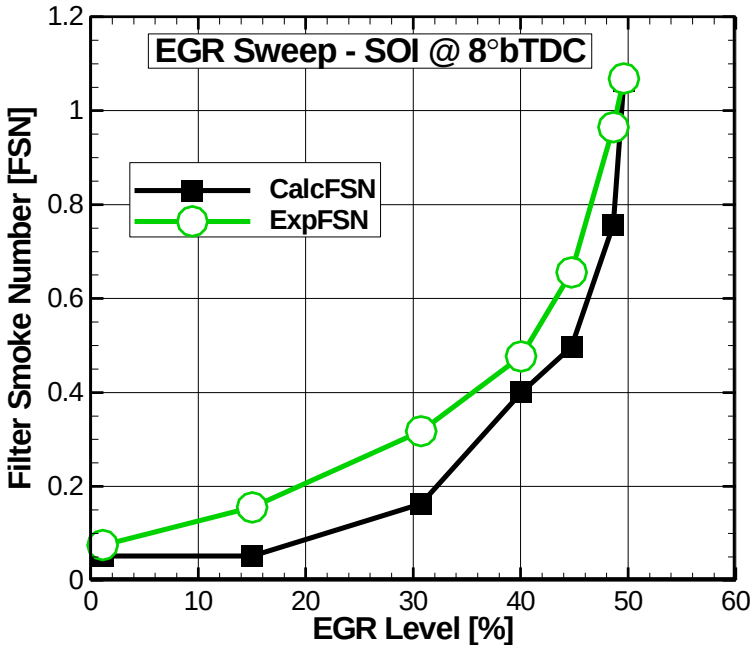

Figure 26 - Filter smoke number prediction comparison to experimental results for an EGR sweep at conventional combustion timing.

4.3 Low temperature combustion trajectory analysis

This section will present the rail pressure sweep and then the EGR sweep at the late timing. Again, less detail about the combustion trajectories shapes will be given as the same features described previously are still applicable. Most focus will be on the general regions occupied by the combustion trajectories for the various set points as this is the primary visual indicator for emissions formation

4.3.1 Rail pressure sweep

As with the rail pressure sweep at the conventional timing, the same sweep was performed at the late injection timing with maximum EGR. Note that five difference pressures were tested, but only three combustion trajectories are shown while all the data is included in the emission results.

Comparing the heat release profiles for the late timing (Figure 27) to those of the conventional timing (Figure 19) there is first an obvious combustion phasing shift caused directly by the injection timing change, but also a substantial decrease in the combustion intensity. Recall that the vertical axis scale in both figures is the same. Because combustion is less intense, the duration is increased accordingly because each condition has the same amount of total fuel being injected. This decreased intensity is attributed to the lower ambient temperatures at ignition due to piston expansion as well as the EGR limited reaction temperature. The EGR limits the reaction temperature both directly (heat capacity) and indirectly (mixing requirements). The end result is that the kinetically driven high intensity pre-mixed reaction is slowed because of the inverse relationship between temperature and reaction rate.

One would expect an advanced ignition and more intense reaction (due to better mixing and vaporization) at higher rail pressures. This was observed for the conventional injection timing, but isn't completely followed here. Specifically, increasing from 500 to 1000 bar (solid black to dashed red) the combustion event is delayed and has a lower peak intensity. This is not completely understood, but the result is a more apparent low temperature heat release (LTHR) prior to the start of the high temperature heat release (HRHR). The lower intensity is likely a result of the retarded combustion phasing, but the reason for the increased delay before HTHR is unclear. Likely there is some combination of mixing and kinetics that isn't evident at this point. As this path of study (or others) progress in the future to further understand the separation of LTHR and

HTHR this behavior may be clarified. Regardless, the final rail pressure does have a higher intensity and advanced phasing while still having a noticeable LTHR portion.

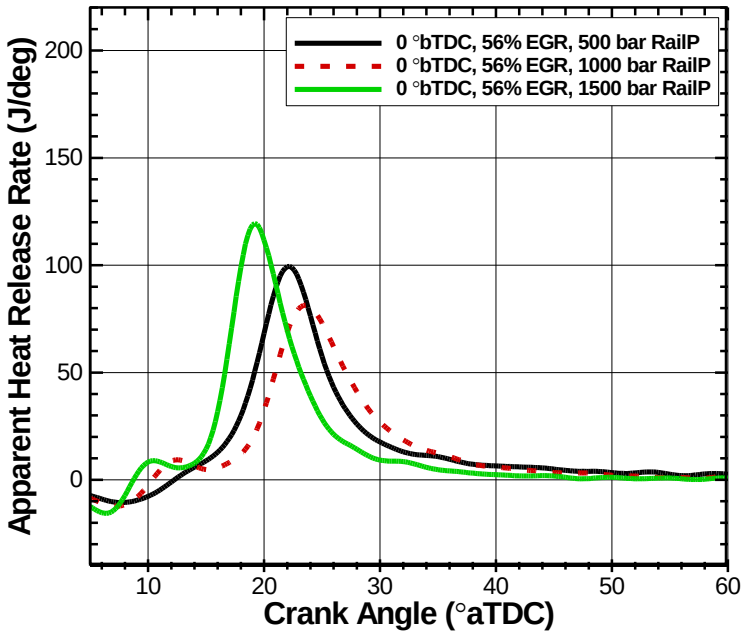

Figure 27 - Apparent heat release profiles for a rail pressure sweep at LTC combustion timing.

The combustion trajectories of the conventional timing rail pressure sweep did not sure much difference (Figure 20), and the trajectories of the late timing rail pressure sweep are not much different with a few exceptions. In Figure 28, the low injection pressure (solid black squares) has a very high average equivalence ratio compared to the other conditions. This illustrates the effect rail pressure has on the mixing process – especially when there is substantial EGR present in the cylinder. For the higher rail pressures, there is a diminishing effect the shortened ignition delay counters the improved mixing resulting in a similar ignition equivalence ratio. Once again, the

counter clock wise rotation is present with the higher rail pressures becoming more compact – a feature that may be indicative of LTC modes and will be discussed more in the following section.

Comparing the 1000 bar (hollow red circles) to the 1500 bar (solid green triangles) case there is still a slight difference in the trajectories. As expected a higher injection pressure results in a lower equivalence ratio (better mixing). From the heat release profiles in Figure 27 the advanced phasing of the 1500 bar case combines with the improved mixing to result in slightly higher peak reaction temperatures as seen in Figure 28. Recall the influence of the ambient temperature on the flame temperature. As combustion progresses the piston expansion will tend to decrease the bulk temperature in the cylinder. This means that a combustion event phased closer to TDC creates higher ambient temperatures.

Based on the trajectories very little NO should be expected, but a general increase with rail pressure is present as the proximity to the NO region increases (recall that the formation regions don't simply stop, the contours are just not continued). The soot results are not quite as clear. Based on proximity, they are all about the same distance from the soot region. Figure 29 and Figure 30 show the predicted and experimental results of the NO and smoke respectively. First, note the experimental trend for the NO matches what is expected – i.e. a slight increase but still generally very low levels. As with the trajectories, the FSN data is a bit harder to describe. The 500 bar (solid black squares) condition has a very high smoke number and yet isn't visually any closer to the soot formation region than the other conditions. Conceptually this makes

sense as a poorly mixed cylinder will form soot without having the adequate oxygen to oxidize it, but how this is manifested in the trajectories isn't obvious. The primary limitation of the trajectory visualization is that time isn't apparent, however, observe again the same trajectories Figure 28 shown in Figure 31 with only every 50^{th} symbol plotted. This corresponds to a symbol every 10 crank angle degrees. Note that the 500 bar rail pressure condition spends nearly 50 degrees (or five symbols) near the soot formation region. The emissions formation contours are plotted assuming the same residence time at each condition, but as may then be expected with the highly time dependent soot formation mechanisms a longer residence time at the 500 bar condition results in a higher smoke number compared to the other conditions.

Once again, the emissions prediction models match well with the experimental results. In this case the simple inverse temperature method for the NO prediction reasonably reproduces the magnitudes and trends. As a result of assuming a activation temperature of 1700 K for the thermal NO mechanisms the complex NO method shows zero formation for the lowest two rail pressures because the reaction temperature did not rise above this threshold.

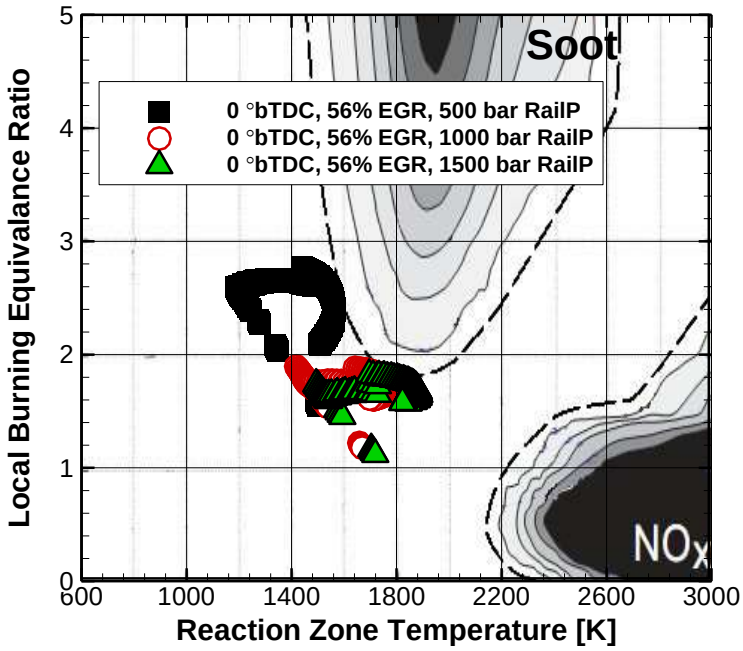

Figure 28 - Select combustion trajectories for a rail pressure sweep at LTC combustion timing.

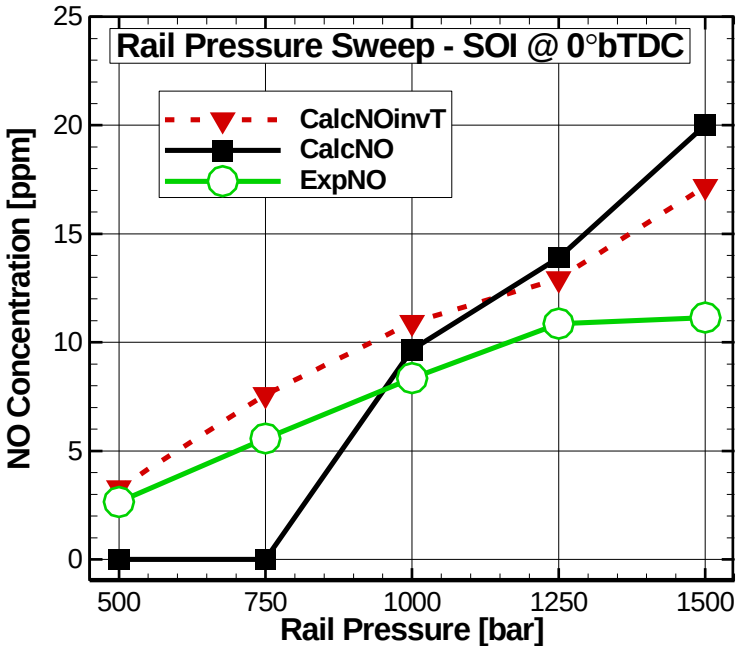

Figure 29 - Nitric oxide emission prediction comparison to experimental results for a rail pressure sweep at LTC combustion timing.

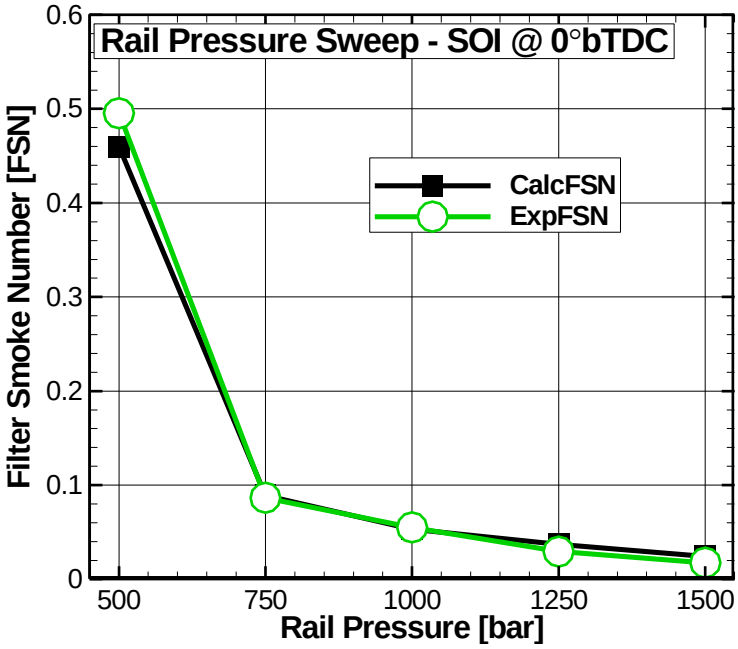

Figure 30 - Filter smoke number prediction comparison to experimental results for a rail pressure sweep at LTC combustion timing.

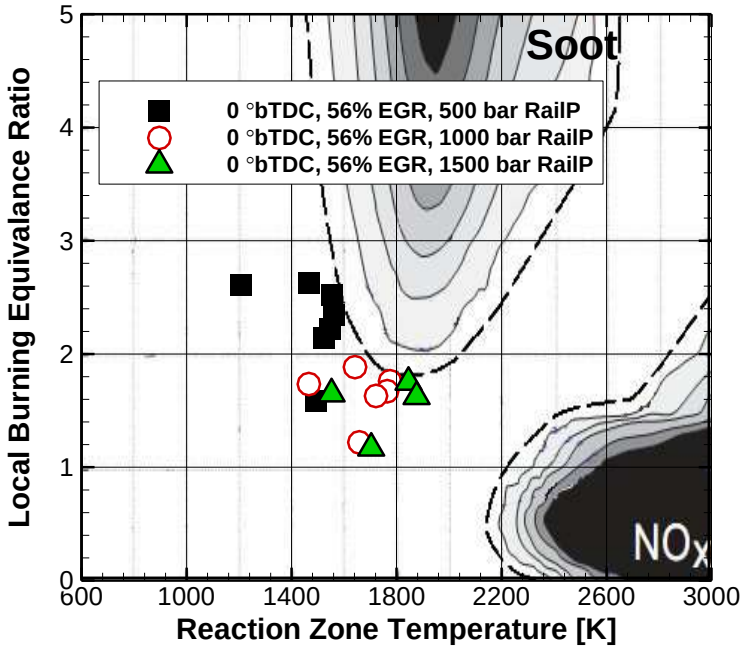

Figure 31 - Combustion trajectories for rail pressure sweep at LTC combustion timing with symbols plotted every 10 crank angle degrees.

4.3.2 Exhaust gas recirculation sweep

Another EGR sweep was performed while maintaining constant rail pressure and injection timing to explore the trajectories at late (LTC) injection timing. Comparing this to the EGR sweep at the conventional timing shows how EGR influences combustion differently when the combustion phasing is directly altered by the injection timing. Figure 32 shows the heat release profiles for a number of different EGR levels. As expected, EGR delays combustion phasing. The shifted combustion phasing (and longer mixing time) increases combustion duration two ways. First, the longer mixing time allows the fuel to become more distributed throughout the cylinder. Once ignition occurs the amount of fuel in the proximity of the initial ignition is lower and so does not burn as intensely (less fuel burning in a localized region). Second, the piston expansion serves to cool the chamber, thereby further tempering the reaction. The same amount of fuel is injected, but it burns relatively slower (than conventional combustion) consequently taking longer to complete. Comparing Figure 33 and Figure 24 it is evident (and expected) that with more time for mixing the average equivalence ratio for each trajectory is lower than that of a similar condition in the conventional combustion EGR sweep. This is the general idea for how this LTC strategy attains low emissions; the more interesting differences between the conventional and LTC modes are the shapes of the trajectories.

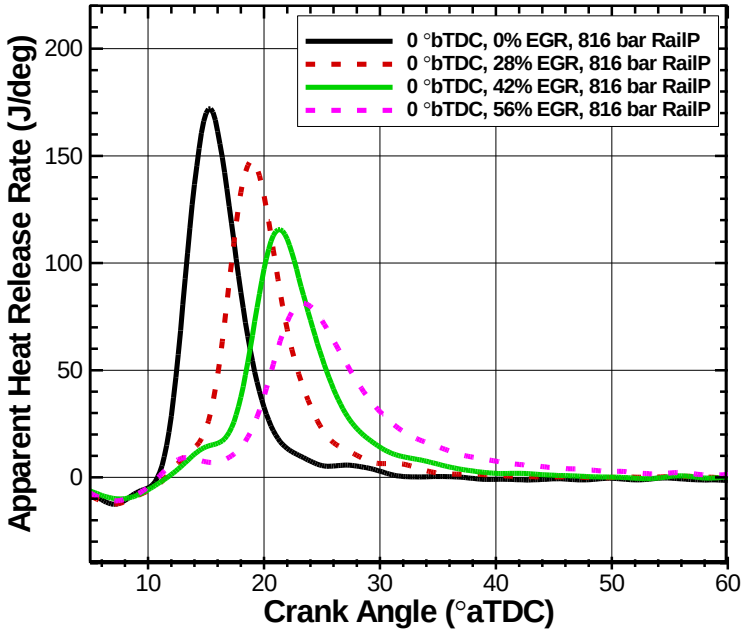

Figure 32 - Apparent heat release profiles for an EGR sweep at LTC combustion timing at the same nominal engine conditions.

Despite having longer combustion durations for the LTC mode, the combustion trajectories can generally be described as more compact. In general the majority of the combustion event for all of the late timing cases (even with low EGR levels) occurs in a narrow band of equivalence ratio. This feature is a bit unexpected as this seems to match with what would be expected for a higher load, long injection, standing flame diffusion burn (as described by Dec [17]) where the mixing process prior to burning is roughly the same for each portion of the continuing injection and the flame front has stabilized. The temperature would increase, but the equivalence ratio would stay generally the same. However the cases here are all low load (2 bar BMEP) and the injection event (not shown) is nearly complete at start of combustion and is completely finished by the peak heat release location – well before any transition to a standing diffusion flame could take

place. This behavior does coincide, however, with the premise of the combustion model assumption; i.e., sequential burning of each fuel packet leads to an outward-in burn patter. This is effectively the same construction as Dec's description, but instead of a standing flame front, the flame front moves inward as it collapses toward the middle. Physically if the flame front speed in this construction is balanced by the mixing "velocity" then this nearly constant equivalence ratio combustion event is possible. In a conventional combustion case the fuel is moving towards the flame, while the LTC case has the flame moving towards the fuel as well – again because the lower intensity reaction is balanced (or overcome) by the mixing rate.

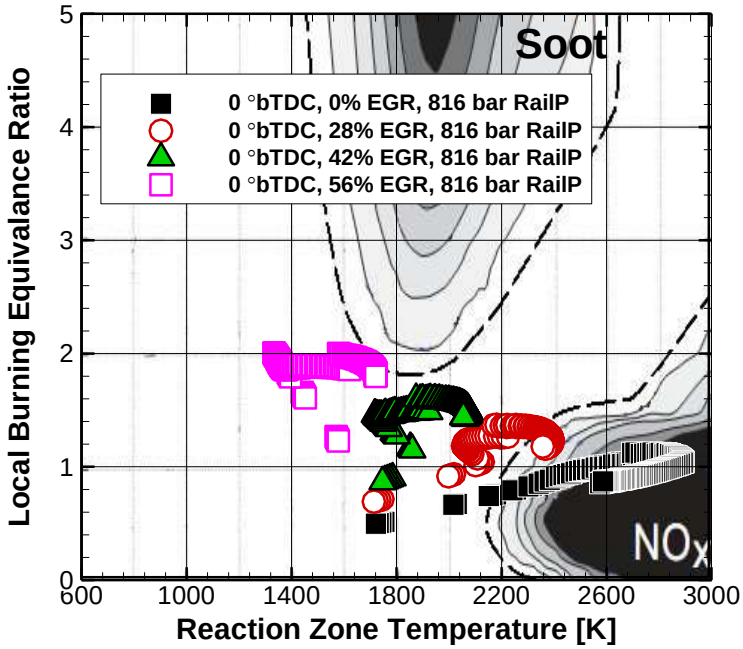

Figure 33 - Select combustion trajectories for an EGR sweep at LTC combustion timing at the same nominal engine conditions.

As mentioned before, as EGR is added at the late injection timing the shift in proximity from the NO to the soot formation region is observed just like it is at the conventional injection timing. However because of the extra mixing time at the late injection timing the equivalence ratio doesn't increase as much as it did at the conventional timing when the EGR is added. This means that a similar reduction in NO might be expected without as much of an increase in smoke. These expectations are indeed observed experimentally for both the NO and FSN as seen in Figure 34and Figure 35, respectively.

The reduction in NO for the late timing is even more pronounced due to the late phasing maintaining a lower bulk temperature and thus limiting the peak reaction temperature even further (compare the maximum EGR cases, hollow pink squares, in Figure 33 to those in Figure 24). Additionally, the FSN does indeed increase as EGR is added, but not nearly to the extent that it does for the conventional injection timing. The complex model predictions do a reasonable job once again at matching the experimental results for both NO and smoke number. The simple inverse temperature method for NO also does a good job with the observed trend, but over predicts the NO by more than 200% in some cases.

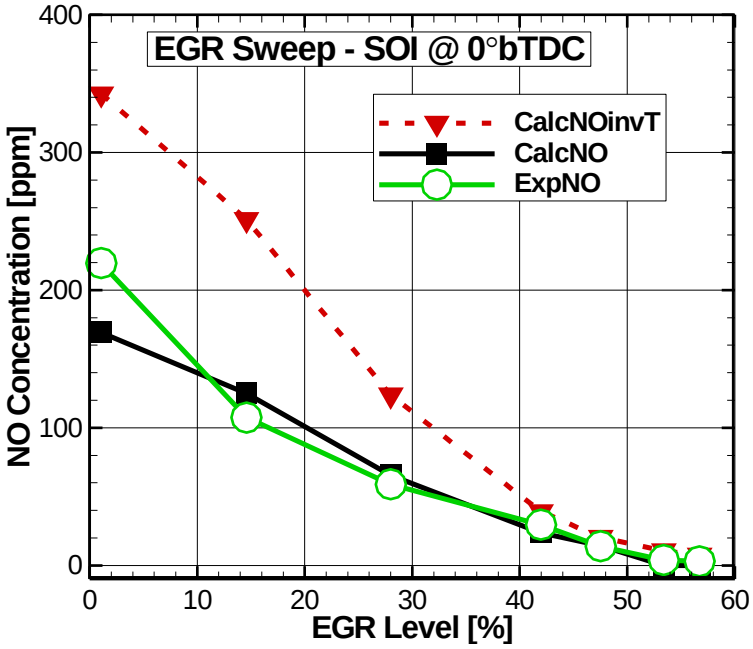

Figure 34 - Nitric oxide emission prediction comparison to experimental results for an EGR sweep at LTC combustion timing.

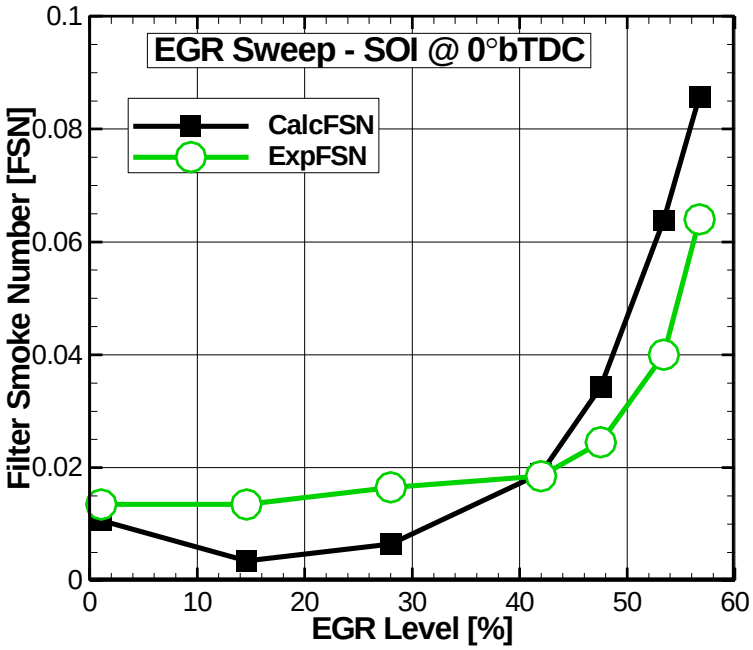

Figure 35 - Filter smoke number prediction comparison to experimental results for an EGR sweep at LTC combustion timing.

4.4 Trajectory sensitivity analysis

Accounting for uncertainty due to assumptions made in the development of the model is not possible, but a sensitivity analysis of a number of the primary inputs will give an indication of the influence each in the trajectory due to measurements. The parameters investigated are cylinder pressure, total fuel mass, intake temperature, start of injection, engine speed, rail pressure, exhaust gas recirculation, and the mixing model constant. Start of injection is adjusted plus/minus one degree. All of the other parameters are adjusted plus/minus five percent.

The combustion trajectory seems to be quite insensitivity to the magnitude of the cylinder pressure or total fuel mass as seen in Figure 36. Three test conditions are shown: conventional timing no EGR, conventional timing with maximum EGR, and late timing with maximum EGR (or LTC). The baseline case is shown in red squares with larger symbols underneath the sensitivity tested results. The green circles represent the trajectory if the parameter shown is actually 5% higher, while the blue gradients represent a 5% lower value. A trend that will be seen for most of the parameters shows that understanding the effect on the entrained air determines how it effects the trajectory. The cylinder pressure has a small effect on all stages of the trajectory. A higher cylinder pressure will decrease the pressure difference across the injector and therefore slightly decrease the injection velocity. At the same time, the higher cylinder pressure will result in a higher gas density which also will tend to decrease the injection velocity. In both cases a decreased injection velocity means more air has been entrained (the fuel slows down as it entrains air) so a lower equivalence ratio would be expected. Because the

difference between the rail pressure and the cylinder pressure is so larger, the change in the fuel spray velocity is less than 0.1%. The density effect is more significant, but only results in a combined change in fuel spray velocity of 1.3% which matches well with the slight changes in local equivalence ratio in the trajectories in the left frame of Figure 36. The effect is more visible for the high EGR cases because 1% of two is twice as larger as 1% of one (i.e. the average equivalence ratio of the high EGR cases compared to the no EGR case).

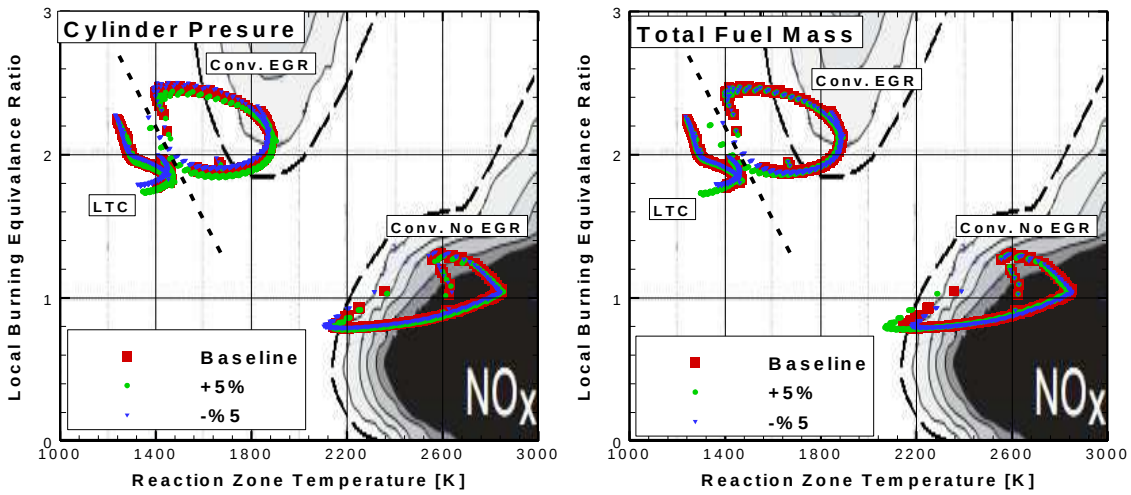

Figure 36 - Parameters showing low sensitivity on the predicted combustion trajectory.

The effect of total fuel mass is even less visible than the cylinder pressure in the right frame of Figure 36. One might have expected a higher (or lower) cylinder pressure would have a more significant effect on the trajectory as it is the primary determining factor for the heat release calculation. However this is not the case for the same reason that the total fuel mass is not a significant input parameter. That is it is only the

combustion phasing and relative intensities of the burn rate that determine the trajectory. For the cylinder pressure the magnitude does not change the phasing of the heat release and therefore the mixing time isn't effected significantly as previously discussed. While the total fuel mass affects the magnitude of the heat release profile (and can change the later stages due to end of combustion determination logic as seen in the figure) if less fuel is injected, then slightly less is burned at each step but that fuel packet has the same proportional amount of fuel regardless, so the fractional amount of fuel consumed is relatively unchanged. Because a higher total fuel mass will have higher heat release rates overall, the end of combustion determination will allow combustion to continue longer. So the late stage of combustion may last longer which is what is seen at the tail end of the trajectories in the right frame of Figure 36.

Figure 37 shows a number of parameters that have a significant impact on the predicted trajectory. Most of the parameters shown affect the entrainment predictions (and thus the equivalence ratio), but the intake temperature primarily affects the reaction temperature. The intake temperature affects the air density slightly (by changing the trapped mass) and therefore affects equivalence ratio, but that influence is small compared to the impact on reaction temperature as seen the top left frame of Figure 37. While it is interesting that this is the only parameter to effect temperature without changing the mixing process the explanation for the observed changes is quite simple. A higher initial reaction temperature will directly causes a higher reaction temperature. The percentage change in peak reaction temperature is roughly paralleled by the imposed change on intake temperature.

The sensitivity of the trajectory to the rest of the parameters shown in Figure 37 is primarily caused by their influence on the mixing process. The combustion phasing is unchanged and so given more time for mixing, or more efficient mixing, the equivalence ratio will decrease while less time/efficiency will increase the equivalence ratio. An extra one degree of time (slightly advanced timing) for mixing will mean a lower equivalence ratio during combustion and the opposite for less time (slightly delayed timing) – both of which can be seen in the top right frame of Figure 37. Engine speed has a slightly more significant effect because the change in engine speed affects the mixing time by multiplication (i.e. every degree is longer) compared to start of injection which only adds or subtracts once. Based on simple calculations the change in mixing time prior to ignition for the engine speed is about half that of the start of injection change, but over the course of the entire combustion process the engine speed gives nearly three times the change in mixing time. This more significant effect can be seen in the middle left frame of Figure 37.

The mixing model constant (the leading 3.07 of Equation (2) in Section 2.3) and rail pressure both directly affect the mixing prediction equations. A higher rail pressure would indicate better atomization and therefore quicker vaporization and mixing (or the opposite for a lower rail pressure). Mathematically a higher rail pressure also increases the spray velocity in the same Equation (2) referenced above. However it also decreases the time until spray break up as shown in Equation (3) thereby giving more time for mixing. A higher mixing constant actually predicts a higher spray velocity which means less air entrained and therefore a higher equivalence ratio. The sensitivity to both of

these parameters can be seen in the middle right, and bottom left frames of Figure 37. They both have a comparable magnitude effect to that of the start of injection results.

The last parameter to discuss in the sensitivity to EGR rate as seen in the bottom right frame of Figure 37. Its influence has been discussed in the previous sections but from the perspective of a controlled change in EGR rate not measurement error. Since the EGR is assumed to be a non-reactive part of the cylinder mixture to get the same amount of available oxygen a larger volume of gas must be entrained into the fuel. So higher EGR means high equivalence ratio given the same amount of mixing time. A 5% error in EGR measurement is a 2.8% absolute error for the cases shown which have a baseline EGR rate of 56%. Of all of the example parameters shown, the EGR rate is perhaps the most difficult to measure – especially without a full emissions bench as would be the case if implemented as a real-time engine controller. Besides engine speed (which would be unlikely to have a 5% error in measurement) the EGR rate shows the strongest influence on the combustion trajectory. Additionally, since EGR is one of the primary control parameters for enabling low temperature combustion understanding its influence is critical.

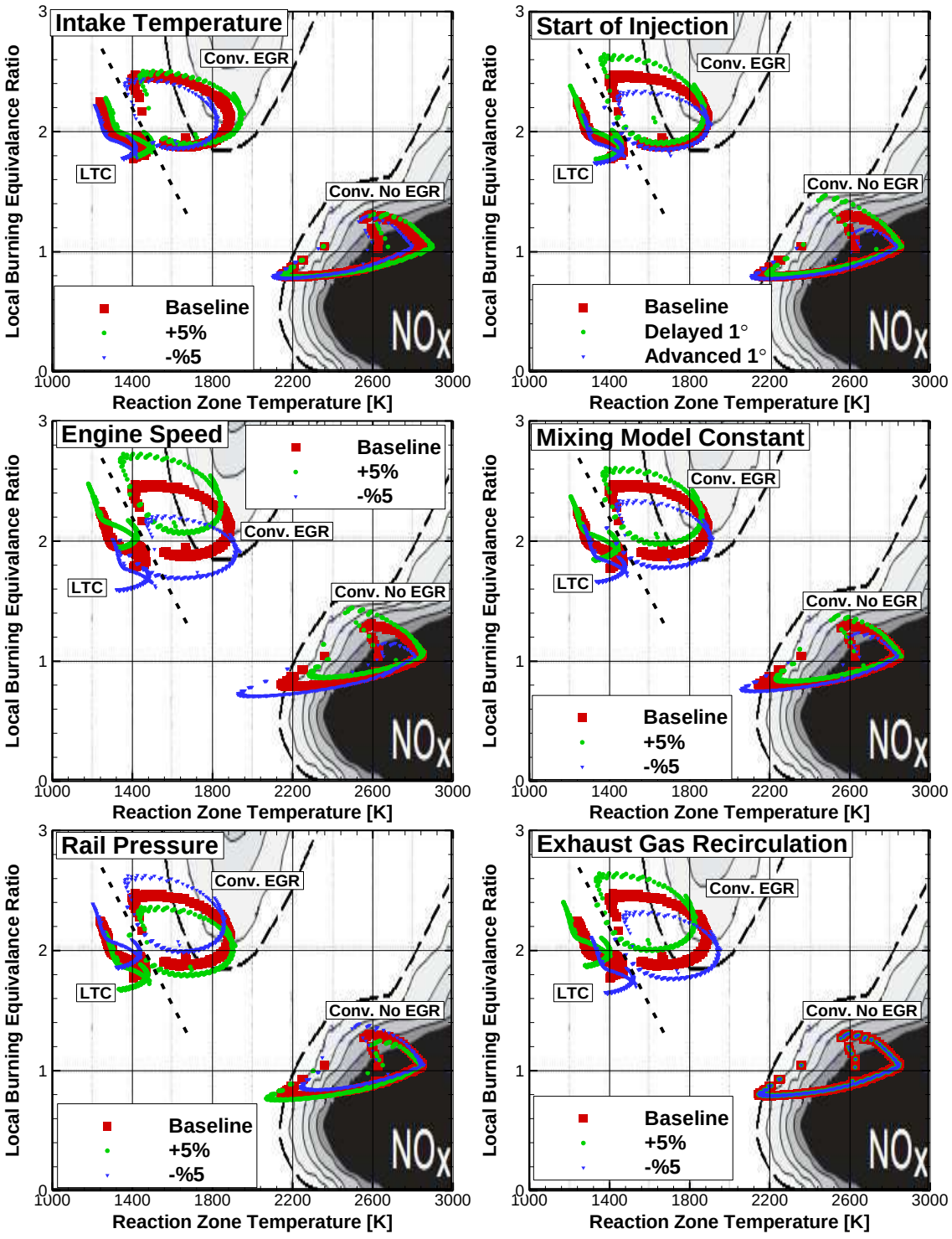

Figure 37 - Parameters showing high sensitivity on the predicted combustion trajectory.

4.5 Demonstration of the entrainment model improvement

The last topic to discuss in validating the trajectory prediction model is the improvement resulting from the implementation of the empirically determined injection discharge coefficient described in the model description section. It is not appropriate to use the same discharge coefficient for every injection event as the pressure and duration influence this behavior. Figure 38 shows a comparison for the same rail pressure sweep at the late injection timing using both the constant coefficient from Hiroyasu et al. [37] on the bottom and the empirically determined values on the top. A higher discharge coefficient results in a higher predicted mixing rate (in addition to the direct effect rail pressure has on the mixing model). For example, the three cases shown here have discharge coefficients ranging from 0.535 to 0.6, higher than the 0.39 proposed by Hiroyasu though some cases have lower values.

Visually the effect the modified coefficient has on the trajectory is not just a lower equivalence ratio due to higher predicted mixing rates, but also higher reaction temperatures as the reaction follows the local adiabatic flame temperature limit imposed the current equivalence ratio and EGR rate. The trajectory shape is generally remains the same as the calculated heat release rate (which dictates fuel consumption) is unaffected by the mixing prediction.

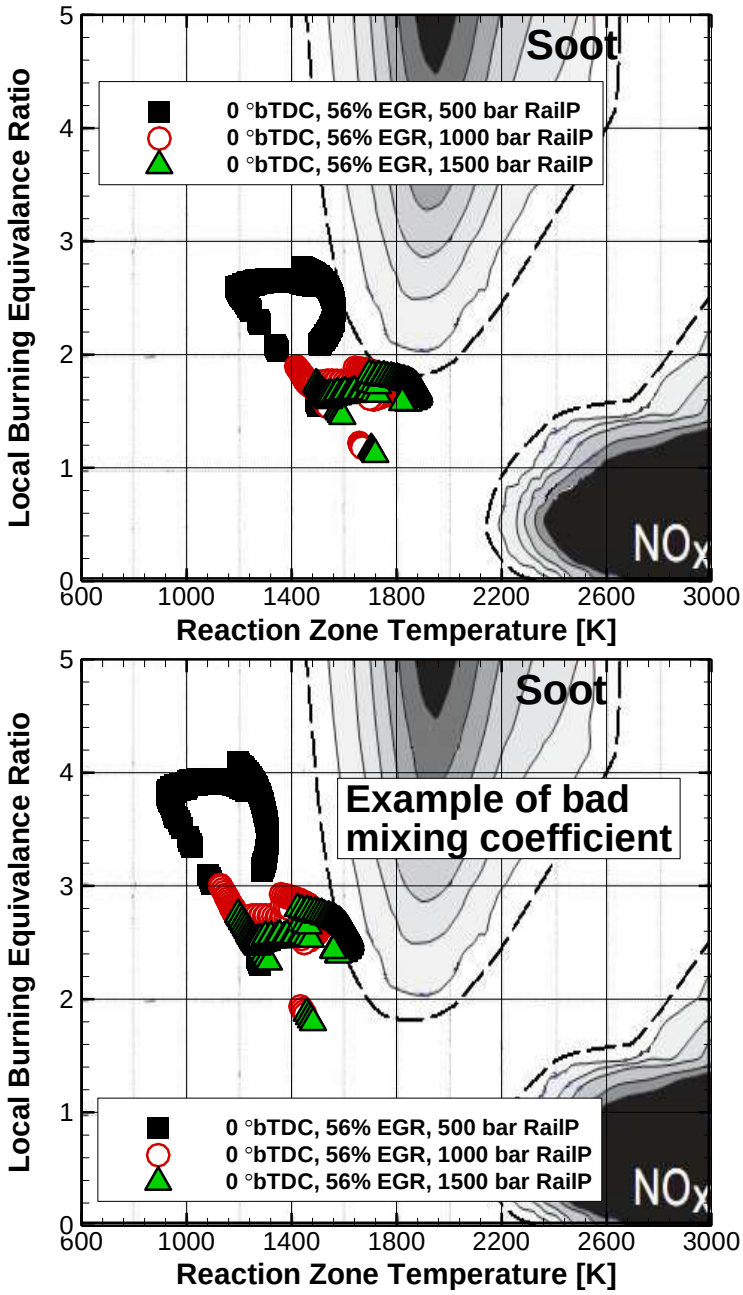

Figure 38 - Example of the effect of the improved entrainment model coefficient based on injector calibration (top) compared to the single value used by Hiroyasu et al. [37] (bottom).

5. SUMMARY AND CONCLUSIONS

The model created for this study is targeted for future use in real-time engine control to enable improved engine emissions and efficiency. To achieve this, a fast and suitably detailed model is created. The results presented here show some interesting insights into the way both conventional and low temperature combustion modes are manifested in the ϕ-T plane based on the model construction. A few observations confirm expected behaviors, albeit from a different perspective, and offer different ways to perceive both conventional and advanced modes of combustion.

This study shows diesel combustion (conventional and LTC) follows this general pattern: initial ignition at relatively low equivalence ratio is followed by clock wise progression to higher equivalence ratios as fast burn rates consume fuel faster than fuel mixing, after which transitioning to mixing controlled combustion increases local temperatures, increasing mixing rate, and thus causing the mixture equivalence ratio to move toward stoichiometric at end of combustion. While targeted at enabling LTC prediction, the model revealed some interesting parallels with other phenomenological models describing conventional combustion. Specifically transition from premixed to mixing controlled combustion becomes clearly apparent for conventional combustion trajectories.

Only subtle differences were observed when comparing conventional high EGR condition and the LTC mode. The two trajectories actually overlap significantly and only deviate during the later stages of the combustion event due to the lower intensity reaction (a result of combustion phasing). The conventional case illustrates significant

temperature rise into the soot formation region while the LTC case does not – thereby avoiding the high soot formation.

The optimizations made to reduce computational time of this model may not be capturing all of the complex cylinder behavior or phenomenological aspects of combustion (particularly the sequential burning assumption). However, the fact that the model predicts trajectories that are seemingly consistent with the expected behavior based on the experimental test conditions suggests continued effort towards development as a real-time controller input is warranted.

REFERENCES

1. Westbrook, C.K., et al., *A comprehensive detailed chemical kinetic reaction mechanism for combustion of n-alkane hydrocarbons from n-octane to n-hexadecane.* Combustion and Flame, 2009. **156**(1): p. 181-199.

2. Farrell, J., et al., *Development of an experimental database and kinetic models for surrogate diesel fuels.* Development, 2007. **1**: p. 0201.

3. Pitz, W.J. and C.J. Mueller, *Recent progress in the development of diesel surrogate fuels.* Progress in Energy and Combustion Science, 2010(doi: 10.1016/j.pecs.2010.06.004).

4. Lu, T. and C.K. Law, *Strategies for mechanism reduction for large hydrocarbons: n-heptane*. Combustion and Flame, 2008. **154**(1-2): p. 153 - 163.

5. Riegel, J., H. Neumann, and H.M. Wiedenmann, *Exhaust gas sensors for automotive emission control.* Solid State Ionics, 2002. **152–153**(0): p. 783-800.

6. Kato, N., et al., *Long Term Stable NOx Sensor with Integrated In-Connector Control Electronics*. 1999, SAE International.

7. Hasei, M., et al., *Sensing Performance for Low NOx in Exhausts with NOx Sensor Based on Mixed Potential*. 2000, SAE International.

8. Atkinson, C. and G. Mott, *Dynamic model-based calibration optimization: An introduction and application to diesel engines.* SAE paper, 2005: p. 01-0026.

9. He, Y. and C.J. Rutland, *Modeling of a Turbocharged DI Diesel Engine Using Artificial Neural Networks*. 2002, SAE International.

10. Brahma, I. and C.J. Rutland, *Optimization of Diesel Engine Operating Parameters Using Neural Networks*. 2003, SAE International.

11. Mohamed Ismail, H., et al., *Artificial neural networks modelling of engine-out responses for a light-duty diesel engine fuelled with biodiesel blends.* Applied Energy, 2012. **92**(0): p. 769-777.

12. Arsie, I., et al., *Multi-Zone Predictive Modeling of Common Rail Multi-Injection Diesel Engines*. 2006, SAE International.

13. Xue, X. and J.A. Caton, *Detailed multi-zone thermodynamic simulation for direct-injection diesel engine combustion.* International Journal of Engine Research, 2012. **13**(4): p. 340-356.

14. Malikopoulos, A.A., D.N. Assanis, and P.Y. Papalambros, *Optimal Engine Calibration for Individual Driving Styles*. 2008, SAE International.

15. Malikopoulos, A.A., D.N. Assanis, and P.Y. Papalambros, *Real-time self-learning optimization of diesel engine calibration.* Journal of Engineering for Gas Turbines and Power, 2009. **131**: p. 022803.

16. Malikopoulos, A.A., P.Y. Papalambros, and D.N. Assanis, *Online Identification and Stochastic Control for Autonomous Internal Combustion Engines.* Journal of dynamic systems, measurement, and control, 2010. **132**: p. 024504.

17. Schten, K., et al., *Design of an Automotive Grade Controller for In-Cylinder Pressure Based Engine Control Development*, in *SAE World Congress*. 2007, SAE International: Detroit, MI. p. SAE paper no. 2007-01-0774.

18. Amstutz, A. and L.R. Del Re, *EGO sensor based robust output control of EGR in diesel engines.* Control Systems Technology, IEEE Transactions on, 1995. **3**(1): p. 39-48.

19. Glavmo, M., P. Spadafora, and R. Bosch, *Closed Loop Start of Combustion Control Utilizing Ionization Sensing in a Diesel Engine*. 1999, SAE International. p. SAE paper no. 1999-01-0549.

20. Husted, H., et al., *Cylinder Pressure-Based Control of Pre-Mixed Diesel Combustion*, in *SAE World Congress*. 2007, SAE International: Detroit, MI. p. SAE paper no. 2007-01-0773.

21. Hasegawa, M., et al., *Study on Ignition Timing Control for Diesel Engines Using In-Cylinder Pressure Sensor*. 2006, SAE International. p. SAE Paper no. 2006-01-0180.

22. Birch, S., *Audi diesel targets bin 5, euro 6*, in *Automotive Engineering Internation*. 2008. p. 24-25.

23. Jacobs, T., et al., *Lean and rich premixed compression ignition combustion in a light-duty diesel engine.* SAE Transactions - Journal of Engines, 2005. **114**(SAE Paper No. 2005-01-0166): p. 382-393.

24. Ojeda, W., et al., *Development of a Fuel Injection Strategy for Diesel*, in *SAE World Congress*. 2008: Detroit, Michigan USA. p. SAE Paper No. 2008-01-0057.

25. Bittle, J., et al., *Cylinder-to-cylinder variation sources in diesel low temperature combustion and the influence they have on emissions.* Spring Technical Meeting of the Central States Section of the Combustion Institute, 2012.

26. Kamimoto, T. and M. Bae, *High Combustion Temperature for the Reduction of Particulate in Diesel Engines.* SAE Transactions – Journal of Engines, 1988. **97**(SAE Paper No. 880423).

27. Gao, Z. and W. Schreiber, *A phenomenologically based computer model to predict soot and NO x emission in a direct injection diesel engine.* International Journal of Engine Research, 2001. **2**(3): p. 177-188.

28. Gao, Z., et al., *Using a phenomenological computer model to investigate advanced combustion trajectories in a CIDI engine.* Fuel, 2011. **90**(5): p. 1907-1918.

29. Johri, R., A. Salvi, and Z. Filipi. *Real-Time Transient Soot and NOx Virtual Sensors for Diesel Engine using Neuro-Fuzzy Model Tree and Orthogonal Least Squares*. 2011: ASME 2011 Internal Combustion Engine Division Fall Technical Conference.

30. Gao, Z., et al., *A proposed methodology for estimating transient engine-out temperature and emissions from steady-state maps.* International Journal of Engine Research, 2010. **11**(2): p. 137-151.

31. Beasley, M., et al., *Reducing Diesel Emissions Dispersion by Coordinated Combustion Feedback Control*. 2006, SAE International. p. SAE Paper no. 2006-01-0186.

32. Quillen, K.P. and M. Viele. *An Analysis of Next Cycle Control Based on Cylinder Pressure Derived Calculations*. in *ASME Internal Combustion Engine Division Fall Technical Conference*. 2009. Lucerne, Switzerland.

33. Quillen, K.P., M. Viele, and S.A. Ciatti. *Next-Cycle and Same-Cycle Cylinder Pressure Based Control of Internal Combustion Engines*. in *ASME Internal Combustion Engine Division Fall Technical Conference*. 2010. San Antonio, TX.

34. Kook, S., et al., *The influence of charge dilution and injection timing on low-temperature diesel combustion and emissions*, in *SAE Powertrain & Fluid Systems Conference*. 2005: San Antonio, Texas USA. p. SAE paper no. 2005-01-3837.

35. Depcik, C., et al., *Instructional use of a single-zone, premixed charge, spark-ignition engine heat release simulation.* International Journal of Mechanical Engineering Education, 2007. **35**(1): p. 1-31.

36. Brunt, M.F.J. and A.L. Emtage, *Evaluation of IMEP routines and analysis errors*, in *SAE International Congress and Exposition*. 1996, SAE International: Detroit, Michigan.

37. Hiroyasu, H., T. Kadota, and M. Arai, *Development and use of a spray combustion modeling to predict diesel engine efficiency and pollutant emissions: Part 1 combustion modeling.* Bulletin of JSME, 1983. **26**(214): p. 569-575.

38. Musculus, M.P.B., P.C. Miles, and L.M. Pickett, *Conceptual models for partially premixed low-temperature diesel combustion.* Progress in energy and combustion science, 2013. **39**(2–3): p. 246-283.

39. Heywood, J.B., *Internal Combustion Engine Fundamentals*. 1988: McGraw-Hill, Inc.

40. Bittle, J., B. Knight, and T. Jacobs, *Two-stage ignition as an indicator of low temperature diesel combustion.* Combustion Science & Technology, 2011. **183**(9): p. 947-966.

41. Dec, J., *A Conceptual Model of DI Diesel Combustion Based on Laser-Sheet Imaging.* SAE Transactions - Journal of Engines, 1997. **106**(SAE paper No. 970873): p. 1319-1348.

42. Szymkowicz, P., *Discussion about Laminar Flow Element measurement accuracy at low flow rates with Jacobs, T.* 2012.

43. Payri, F., et al., *Digital signal processing of in-cylinder pressure for combustion diagnosis of internal combustion engines.* Mechanical Systems and Signal Processing, 2010. **24**(6): p. 1767-1784.

APPENDIX – LITERATURE REVIEW

The focus of this proposal is the idea that a method can be developed that will allow for real-time automatic feedback control of the combustion process such that the engine out emissions are minimized (based on nitrogen oxides and particulate matter). This could be implemented on top of normal engine calibration procedures and would be "turned on" during engine operation based on current operating condition (i.e. accelerating, highway cruising, idling, or coasting). This literature review will be split into two focus areas: past and current efforts to implement real-time combustion control and secondly, potential diagnostic methods for determining the likely emissions production without direct measurement. The potential for real-time control will be shown to be well spread and quite effective in the areas it has been applied to date. Engine emissions formation measurements and models are also well established. Some of these may be useful for real-time implementations, but may not be practical in a consumer friendly form (cost wise). The major effort of this study will be modifying/developing a prediction model that can then be programed to calculate efficiently (within one engine cycle) as to be used as an input to the real-time next cycle engine controller.

7.1 Past and current real-time combustion control efforts

The following section will contain descriptions and summaries of various studies with the main effort being to implement some form of real-time combustion control. This is certainly not all inclusive as this type of effort has been pursued by many groups,

but it does contain a good representation of the various focus areas (such as cylinder balancing, combustion phasing control, or fine tuning load control).

7.1.1 Glavmo, Spadafora, and Bosch (1999)

The study by Glavmo et al. [19] presents the authors efforts to close the control loop of ignition timing by utilizing a ionization sensor to detect the start of combustion with the goal of using this to automatically adjust the start of injection timing. In addition to the obvious efficiency improvement potential (due to increased control over combustion phasing), the method also enables for compensation for drop in fuels that may have significantly different ignition/injection properties.

The use of an ionization detector as opposed to cylinder pressure transducers is proposed by the authors for its ability to more accurately detect pilot ignition events. Due to the small amount of fuel typically used in pilot injections it can be difficult to detect when ignition occurs using only a cylinder pressure transducer. Additionally, the ionization detector is relatively a lower cost sensor compared to the cylinder pressure transducer.

The study shows good agreement between calculated heat release (from a cylinder pressure transducer) and the ionization sensor output. Suggesting that it is suitable as an ignition detector for both pilot and main injections as anticipated. Additionally, the authors suggest that by including this detector in the glow plug packaging, the sensor would be ideally placed as well as giving it the ability to self-cleaning function to remove soot coating from the sensor.

The work did not actually implement the start of combustion control routine, but it did present a control methodology. The demonstrated ability to sense the start of combustion location means that it likely would serve as a viable real-time controller input, however, as has been discussed, future emissions regulations will likely require real-time control over many more factors beyond simply the ignition timing.

7.1.2 Beasley, Cornwell, Fussey, King, Nobel, Salamon, and Truscott (2006)

The study by Beasley et al. [31] presents an interesting approach to the issue of reducing engine emissions production by combustion feedback control. Their efforts target a method for compensating for production tolerances and component ageing which ultimately aims to reduce size of the emissions dispersion cloud. While the emission regulation targets are often achievable when a specific engine is tuned, the same calibration will not produce exactly the same result on a different engine (due to production differences) and a given engine will perform differently over time due to component ageing. This paper may provide great opportunity for comparison as the engine used by Beasley et al. is identical to the one that will be used for the research being presented in this proposal.

The work presents a very thorough sensitivity analysis of the effects each setting has on the size and distribution of the emissions dispersion cloud (including every input actuator and every output parameter of interest). Once this analysis was completed and the primary control factors identified, a survey of the available sensor technologies was performed to identify what type was most appropriate for the control strategy methodology being used. The authors concluded that piezo-based cylinder pressure

transducer will likely be required as other methods do not offer enough fidelity in the measurements.

The real-time control methods studied in this paper include combustion phasing control (by 50% burned mass location set point), peak pressure control, and also a combustion stability control. Both the 50% burned mass location and peak pressure set point control methods are clearly shown to be quite effective even in an on/off testing (i.e. control was off, then turned on, and then turned back off) where the control response was very nearly instant.

Perhaps the most interesting part of the study was the combustion stability control method. This control strategy is designed to maintain stability "in response to forced instabilities" such as a sudden change in injection timing while at high EGR levels. The controller immediately advanced the targeted 50% burned mass location and then a subsequent increase in the target mass air flow rate (i.e. decrease in EGR level). This is a very important achievement as it is going to be quite common for sudden "forced instabilities" to occur when the engine is being driven down the road.

7.1.3 Hasegawa, Shimasaki, Yamaguchi, Kobayashi, Sakamoto, Kitayama, and Kanda (2006)

Hasegawa et al. [21] implemented a similar control method to Beasley et al. [31] for ignition timing control that adjusted the start of injection or the EGR valve position (in conditions where injection timing control wasn't sufficient) to effectively minimize the influence of varying cetane number on the engine performance parameters.

Hasegawa et al. specifically studied the use of real-time control methods during low temperature combustion events (the focus of this proposal) as a way of compensating for differences in fuel cetane number. Without real-time control the results show the expected increase in cycle-to-cycle variation, and increase in HC and CO emissions as the cetane number is decreased (causing the combustion phasing to be delayed). When the control is enabled, this penalty is decreased substantially. Additionally, the authors' efforts to compensate for ignitability issues under high EGR conditions also proved even more successful. By actively controlling the EGR ratio in addition to the injection timing the penalty in cycle-to-cycle variation and HC and CO emissions is all but eliminated as the fuel cetane number is changed.

This paper successfully demonstrated that by employing some type of real-time control under low temperature combustion can successfully compensate for a range of fuel cetane numbers. Furthermore, at a given cetane number this real-time control method is even able to bring the HC and CO emissions to levels below that of the comparable conventional combustion mode. This is also manifested as an improvement in fuel consumption all while maintaining the reduced soot and NOx emissions.

7.1.4 Husted, Kruger, Fattic, Ripley, and Kelly (2007)

The study by Husted et al. [20] utilized a cylinder pressure based control routine that would, in real-time, adjust the injection timing and duration to balance the combustion phasing and mean effective pressure respectively between each of the engine's cylinders with good success. Husted et al. were also investigating the potential for real-time control of diesel low temperature combustion (like Hasegawa et al. [21],

and what is being pursued in this research proposal). The study by Husted et al. takes an additional step of investigating the potential of real-time control during transient operation – a typically challenging pursuit.

For steady state operation, the experimental results shows a marked improvement in the cylinder-to-cylinder variation of both IMEP and the 50% burned mass location, though a significant cycle to cycle variation is still observed. The cylinder-to-cylinder variation of 50% burned mass location was reduced by almost 99% on a cycle by cycle standard deviation between each cylinder basis. The reduction in BMEP COV was reduced from 3.6% to 0.73% with the balancing control enabled.

The transient control method was tested at a constant engine speed while the load set point was immediately changed form 1.0 bar BMEP to 5.0 bar BMEP and back again after roughly 70 engine cycles. With control disabled there is an apparent unintended retarding of combustion phasing as the control must transition between combustion modes (50% burned mass location shifts almost 15 crank angle degrees) and a large variation in cylinder BMEP as the transition is made. With real-time control enabled, there is a slight change in combustion phasing that is quickly damped out with a maximum deviation of roughly five crank angle degrees. The BMEP change is much smoother and the cylinder balance is maintained even under the transient operation.

7.1.5 Quillen and Viele (2009)

In the study published by Quillen and Viele [32] the functional hardware requirements of implementing a cylinder pressure based next-cycle control strategy is investigated. The benefits of having next-cycle control ability are numerous – from

precise cylinder balancing and combustion phasing control to very fast transient response capability, and to nearly instant fault detection. The work presented by Quillen and Viele can actually be viewed as a system validation test for the engine controller that will be used for this proposed research as it is identical hardware and software. Quillen and Viele are from the company that the engine controller to be used was purchased, so it is appropriate to investigate the various literatures that have already been published utilizing the same system.

Due to the calculation timing requirements for next cycle control the calculation time of each subroutine becomes very important. The study presents analysis of each of the subroutines used to identify the most time consuming portions. One important trade-off that is immediately apparent is that calculating the heat release using single zone model with heat transfer correlations and correlations for specific heats requires 10x more processing time than simply a single zone with constant specific heats and no heat transfer. In fact, using the relatively complex heat release routine takes more time itself than is available for a 4 stroke, V-8 engine operating at 6000 RPM when using a 0.1 degree crank angle resolution.

Balancing the desired detail with the hardware limitations will be a key aspect in this proposed research, and using some of the information and methodology described by Quillen and Viele will likely be very helpful.

7.1.6 Quillen, Viele, and Ciatti (2010)

A second study by Quillen, Viele, and Ciatti [33], utilized the previously mentioned functional hardware requirements discussion in [32] and applied them to an

experimental test engine for validation. Their study is once again performed using the same controller hardware that will be utilized for this proposed research. Additionally, the engine used is also the same GM 1.9L model that will be used in this proposed research.

The study by Quillen et al. [33] demonstrated both a next-cycle control method (similar to those discussed and implemented by others above) and a same cycle control method. The next cycle control method showed good results and was able to control the 50% burned mass location for all four engine cylinders simultaneously to the same location. The same cycle control method was primarily a proof of concept as opposed to a demonstration of any improved combustion behavior. The method utilized three injection events where each subsequent injection was not triggered until the heat release rate of the previous injection had come down below some threshold level.

Most relevant for the research proposed here is that the next cycle control method is practical on the available hardware. Before moving on to the specific work of this work, the results found by Quillen et al. will be replicated to ensure that the facilities are fully operational.

7.2 Emissions prediction diagnostics efforts

The following section will contain descriptions and summaries of a number of studies that focus primarily on emissions formation prediction models and methods. As with the previous section, this is certainly not an exhaustive effort, but also attempts to give a representative view on the many approaches researchers have taken in this area. The papers are discussed in chronological order.

7.2.1 Gao and Schreiber (2001)

The phenomenologically based model for soot and NOx prediction assembled by Gao and Schreiber [27] uses a multi-zone model to track fuel spray and local combustion behavior in diesel engines. This type of model gives considerably more information than standard single zone models while being computationally fast relative to more complex 3-D CFD type models. In order for this type of model to work it must use phenomenological based sub models for predicting things like injection penetration length and air entrainment processes. The model is composed of two major regions – the surrounding unmixed gas (largest zone) and then the fuel/air mixture region. The fuel/air mixture region is broken up into many small zones in both an axial direction and radial direction relative to the fuel injector nozzle tip.

As with any model of this type significant tuning with constants is required, but ultimately good agreement with the reference engine results was achieved. The model was able to capture the soot-NOx tradeoff for various levels of dilution (EGR) as well as across an injection timing sweep with expected results. Also, because of the large number of zones in and around the fuel spray jet, interesting contour maps were able to be analyzed for things like equivalence ratio, NOx, and soot concentrations.

This type of model provides good agreement with experiments, but only after significant tuning and also at a relatively high computational cost compared to simple single zone models. The ability to implement next cycle control (as desired in this research proposal) is unlikely to be feasible with a model of the type utilized by Gao and Schreiber here.

7.2.2 Gao, Conklin, Daw, and Chakrevarthy (2010)

The study by Gao et al. [30] presents the authors efforts to account for difference between steady-state and transient engine operation by generating a method to predict the transient response from the steady-state calibration maps. This methodology is perhaps quite promising due to the potential for general application to many different engines. All engines undergo steady-state calibration and thus have the available maps that are used as input for the methodology presented by Gao et al. in this work.

A significant portion of the difference between steady operation and transient response is due to relatively slow temperature changes compared to the speed at which an actuator set point can be modified. The authors attempt to predict this delay in response by adding a first order time lag effect for the temperature change. This allows the prediction model to more precisely interpolate between calibrated operating conditions. Applying the effect of this temperature lag prediction also allows for the prediction of the lag in response of both fuel consumption and engine out emissions production.

The methodology is shown to accurately predict the trends of multiple engine sizes and fuels for engine out emissions, exhaust temperature, and fuel consumption during realistic drive cycles that include cold and warm starts.

7.2.3 Johri, Salvi, and Filipi (2011)

The study by Johri et al. [29] presents the authors' efforts to address the difficulty in transient emissions prediction (similar motivation to [30] discussed above, but different approach). Traditional steady emissions prediction methods are typically able

to match experimental emissions levels after the typical calibration efforts. This article incorporates some alternative modeling methods ("neuro-fuzzy model tree") combined with real-time engine emission analyzers as calibration input to enable accurate tracking of the transient emissions formation differences.

The authors discuss the necessary complexities required to track transient emissions production using a single model approach. The model solution methods as well as the training procedure both pose difficult numerical challenges (non-linear, complex structure, and very high order equations). The authors propose the break these complex processes down into multiple models for each engine section (spatially). This approach allows for each section to be linear (and thus computationally easier to solve).

The model does a good job at tracking both the engine out soot and NOx over a long drive cycle with numerous transitions between low and high load operating conditions (such as might cause significant transient emissions response). The model does a better job at tracking the NOx than the soot (though both are much better than the steady state predictions).

This approach does a good job of enabling real-time transient emissions prediction and might be able to be implemented as a real-time controller input. The major drawback as is relevant to this research proposal is that the model presented by Johri et al. [29] is based much more heavily on mathematical modeling techniques rather than fundamental combustion phenomenon.

7.2.4 Gao, Wagner, Sluder, Daw, and Green Jr. (2011)

Gao et al. [28] present a two-zone model that attempts to capture the spatial homogeneity of diesel combustion and allows for NOx and soot prediction in the high temperature fuel rich region. The model is able to accurately predict engine behavior under conventional, high-dilution, and low temperature combustion modes. The model incorporates multiple phenomenological based sub-models to capture the mixing, ignition, heat release, and emissions formation behavior. As with all models, this requires specific tuning of model constants to match the experimental engine results.

The most interesting part of the work, as is relevant to the proposed research here, is the resulting prediction of the combustion trajectory. It is well established that the concentrations of soot and NOx are strong functions of the local equivalence ratio and temperature in the cylinder [26]. If the equivalence ratio and temperature are known as a function of crank angle then the trajectory of the combustion event through the soot and NOx formation regions can be plotted. A large number of combustion diagnostic techniques attempt to quantify this combustion trajectory and prediction of the path opens the door to very interesting control techniques. The study by Gao et al. [28] serves as the foundation for this research presented

7.3 Literature review summary

This brief look at some of the available literature focused on real-time combustion control and emissions prediction diagnostic techniques shows an active research field. The standard real-time control strategies focus on using cylinder pressure based calculations as the control parameter (such as start of combustion, combustion

phasing, or cylinder balancing). The emissions prediction methods and models are always aimed at providing high levels of combustion behavior detail or enabling off-line simulation capability. Many models mention and discuss the potential of using the prediction results as input to an engine controller, but none that have been found here actually implement the prediction results on a real engine. With this literature review complete it is clear that bridging this gap will provide a significant contribution to the engine research community and has the potential for future consumer grade implementation to aid in maintaining compliance with the increasingly strict emissions regulations.

APPENDIX – NEW ENGINE PRELIMINARY DATA AND OBSERVATIONS

A significant effort prior to starting work on this proposed study has been installing and commissioning a new engine and test cell. This included starting from an empty test bed and eventually getting a fully operational test facility with state-of-the-art engine control hardware and data acquisition systems. The following sub-sections will describe the installation as well as present some initial data.

8.1 Engine test cell configuration

8.1.1 General engine information

The experimental testing to be done as part of this work will be performed on production model year 2007 GM 1.9L engine (Model Number Z19DTH). Besides additional sensors and measurement devices, the engine is completely stock (except for the exhaust gas recirculation path, discussed later) and will provide a great platform for testing the effects of any number of control strategies (or other experimental work) versus baseline data for this specific engine. This section will provide a description of the installation including pictures and graphics to describe the important design choices made during the installation process. Figure 39 shows the engine from the exhaust side as well as the radiator (left), intercooler (top), and the exhaust pipe (at the bottom edge). Some basic engine specifications are listed in Table 1.

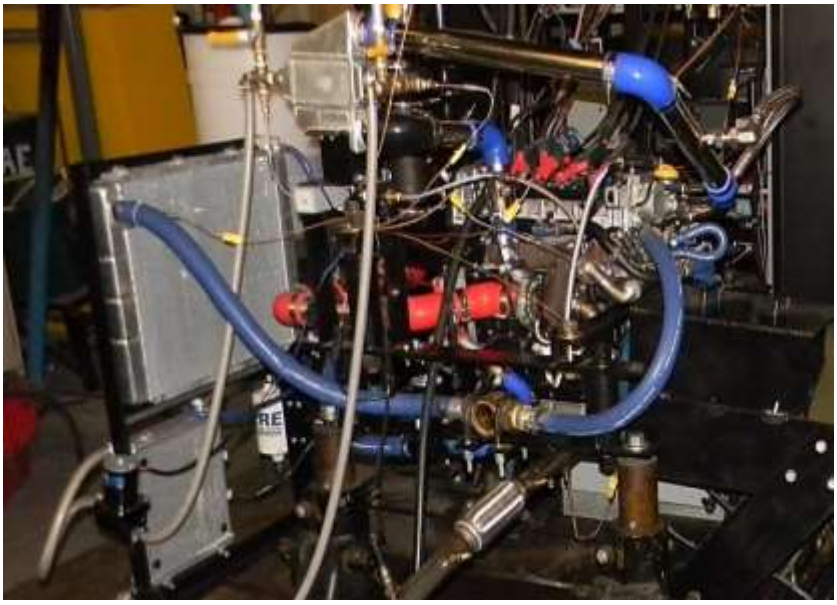

Figure 39 - Engine pictured from the exhaust side. Also includes the radiator and intercooler and other smaller components.

8.1.2 Engine air path and components

The air flow path is shown in Figure 40. The fresh air is filtered and then the flow rate is taken twice – once using a laminar flow element (LFE) and then using the stock mass air flow sensor (MAF). The air then is compressed by the turbocharger and then cooled in the liquid-to-air intercooler. The liquid-to-air intercooler was chosen to give a large potential cooling capacity and more flexible opportunity to implement a feedback control option on the post intercooler temperature. The intercooler is pictured in Figure 41.

The engine is equipped with a higher pressure exhaust gas recirculation system (EGR) – i.e. it transfers the exhaust from before the turbine to the intake air after it has gone through the compressor. The now cooled and pressurized intake air is then mixed

with EGR. The mixing location for the EGR addition has been modified from the stock setup to be much further upstream from the intake manifold. The new configuration can be seen in Figure 42. The fresh air and EGR mixture is then distributed between the four cylinders. The combustion products exit the cylinder and a portion is passed through the EGR cooler to be recycled while the majority goes through the turbine side of the turbocharger. Finally the air is passed outside the building and vent on the roof.

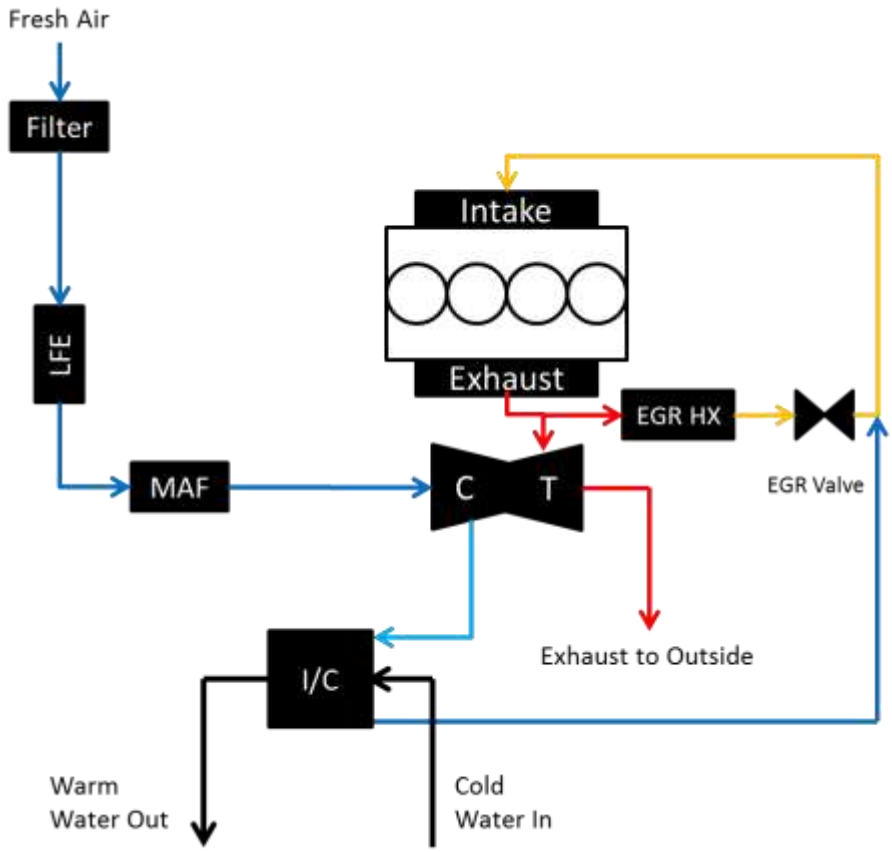

Figure 40 - Air path through engine (color indicates relative temperature) including major components such as the Laminar Flow Element, Mass Air flow sensor, Turbocharger, EGR cooler, and EGR valve.

Table 1 - General Engine Specifications

Manufacturer/Model	General Motors / Z19DTH
Cylinders/Layout	4 in line, 16 valves
Bore	82 mm
Stroke	90.4 mm
Displacement	1.91 L
Rated Power	110 kW at 3250 rev/min
Rated Torque	315 Nm from 200-2750 RPM
Compression Ratio	18.0 : 1
Ignition	Compression
Fuel System	Electronic common rail, direct injection
Air System	Variable geometry turbocharger with EGR

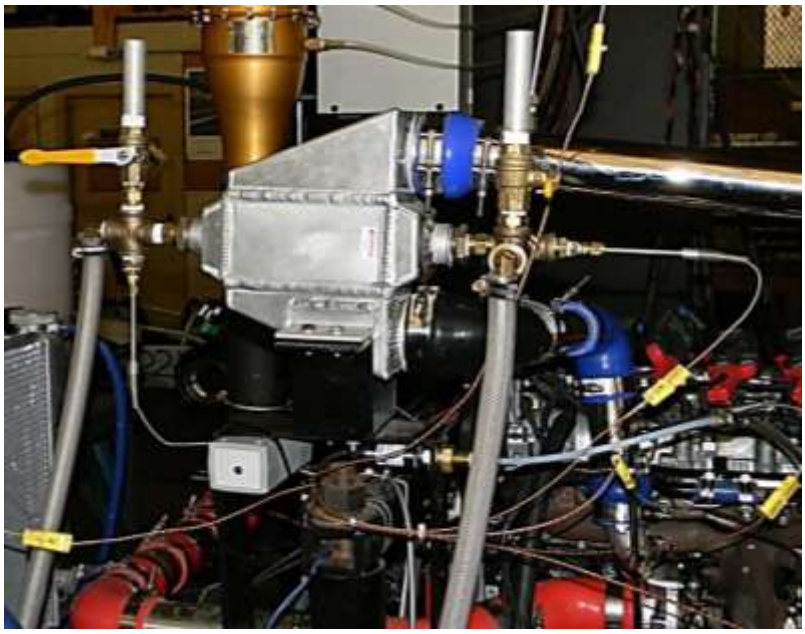

Figure 41 - Liquid-to-Air Intercooler used to cool the fresh air after it has been compressed in the turbocharger.

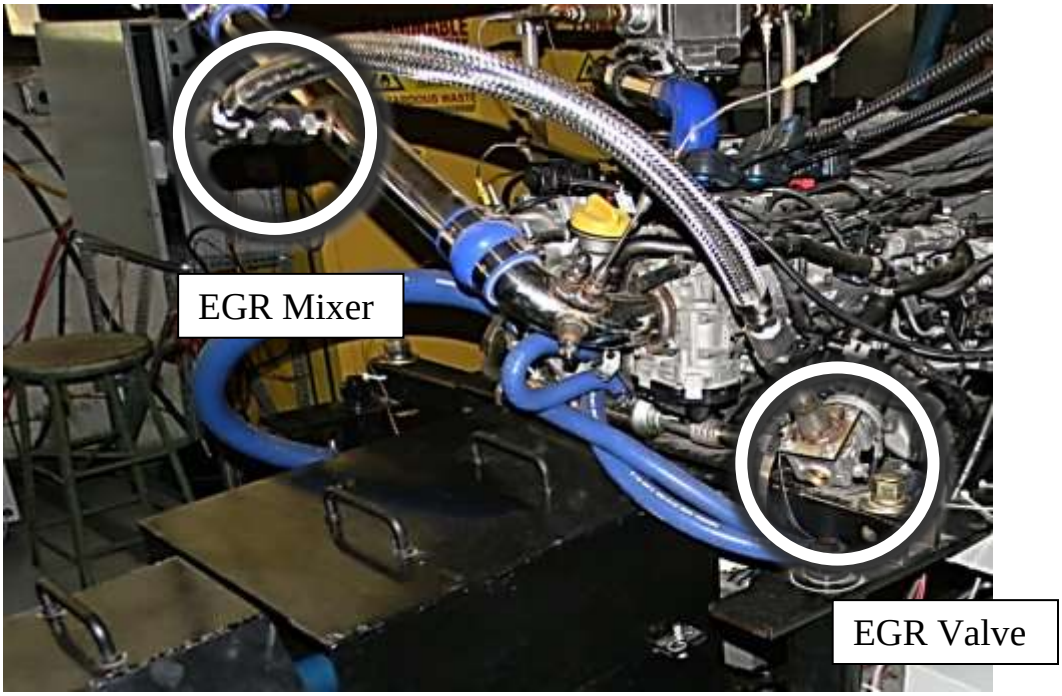

Figure 42 - Exhaust Gas Recirculation (EGR) addition relocation up stream of intake manifold.

8.1.3 Engine coolant and radiator configuration

The engine is cooled using standard 50/50 mixture of coolant and water as required. The radiator used is quite a bit oversized for the engine (300 kW Radiator compared to 110 kW engine). This design choice was made to allow the potential for a large range of operating coolant temperatures. The radiator fan has a speed controller implementation in the engine controller that allows for precise real-time PID control over the coolant temperature by modulating the fan speed. In order to enable this wide control range, the thermostat housing valve was removed so that coolant is always flowing through the engine. This may slightly increase the warm up time, but not detrimentally. A side effect of the oversized radiator is that the engine water pump was not able to provide enough pressure to circulate the coolant. Therefore a second pump was added in series that is run at only just enough power to start the flow of coolant as indicated by the flow sight visible in Figure 39. A graphical representation of the coolant flow path is shown in Figure 43 including the previously mentioned secondary pump and flow sight.

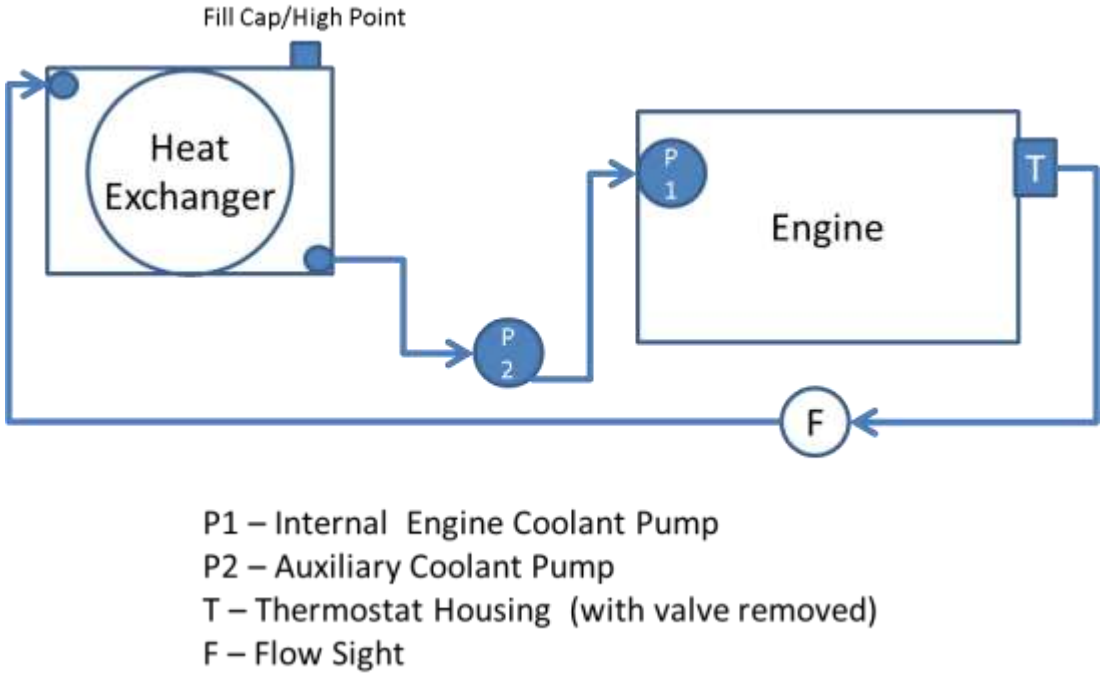

Figure 43 - Engine Coolant Flow Path Illustration

8.1.4 Fuel delivery and measurement system configuration

The measurement of fuel flow rate is one of the most important aspects of any experimental engine research. It is imperative that the measurement be accurate as many of the performance parameters are a function of the fuel delivery/consumption rate. In order to meet this high accuracy demand, the fuel flow rate measurement becomes a relatively complex system. The major components are illustrated by flow schematic in Figure 44 and final assembly pictured in Figure 45.

The fuel system has two loops, the supply tank loop and the engine loop, and connecting the two loops is the fuel metering system. The fuel metering system measures the amount of fuel being added to the engine loop – this is equal to the fuel

being consumed assuming there are no leaks. The two loops are differentiated in Figure 44 by solid (engine) and dashed (supply tank) lines. Circulating the fuel in each loop requires two separate fuel pumps each equipped with a potentiometer based pulse width modulator board that allow for the pumps to be operated at less than full power (which will extend their operational life). Finally, the different line colors in Figure 44 represent supply (red) and return (green) fuel lines.

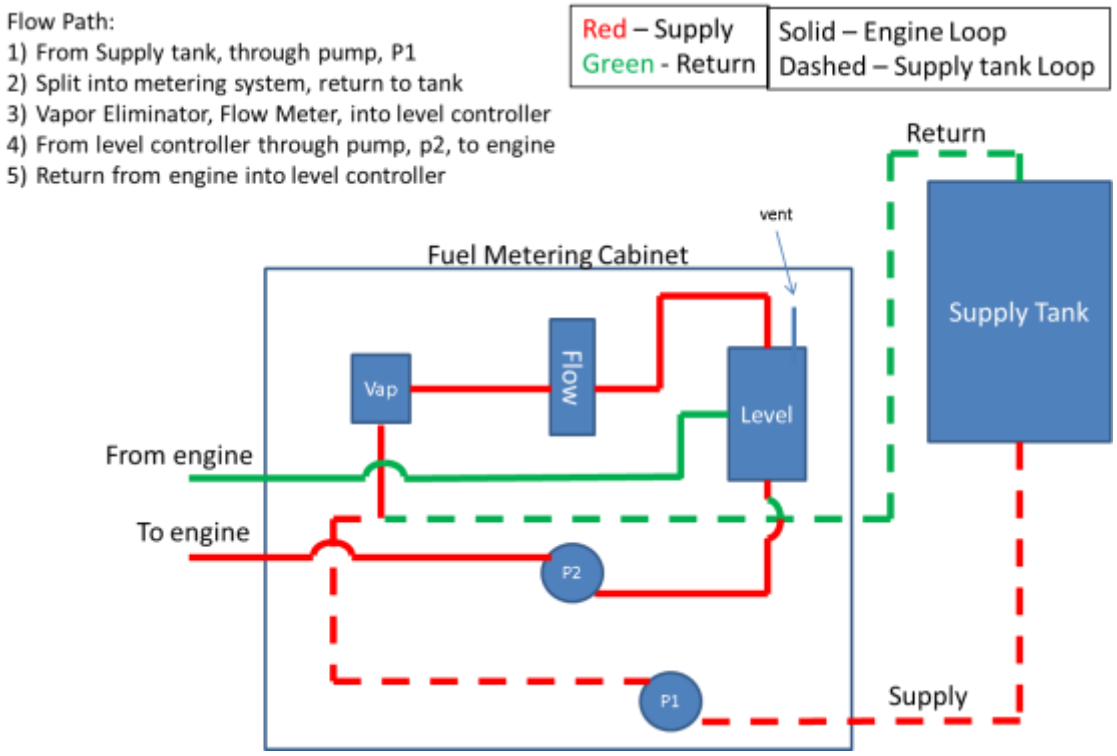

Figure 44 - Engine fuel delivery and measurement system flow path illustration

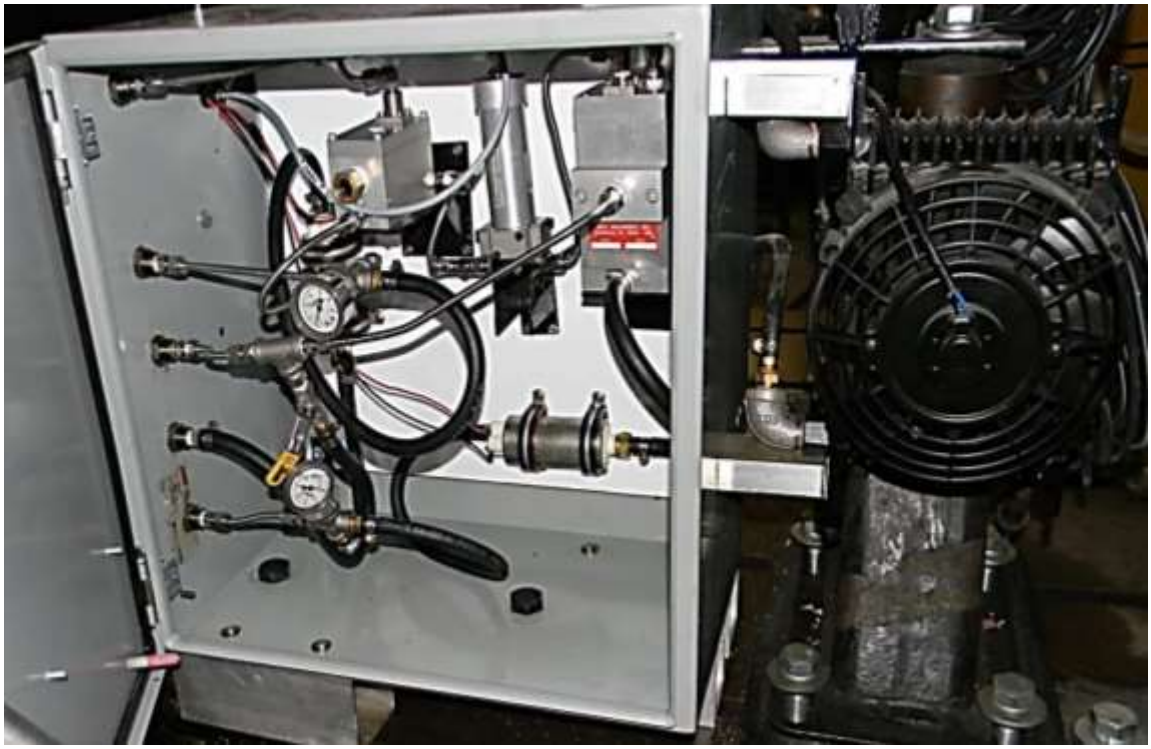

Figure 45 - Engine fuel measurement system final assembly picture.

The supply tank loop is gravity primed and filtered. The pump (P1) is set to maintain the required inlet pressure to the fuel metering system of 5-10 psig. As seen in Figure 44, the fuel then goes back to the supply tank through a ball valve that is adjusted to provide back pressure against the pump.

The fuel metering system consists of three devices: vapor eliminator, fuel flow meter, and level controller. The fuel from the supply loop at 5-10 psig is pushed through the vapor eliminator which has a check valve in the top to allow any vapor bubbles to escape and be vented. This is crucial for accurate flow rate measurement as the fuel flow meter is a positive displacement based measurement device. The now liquid only fuel is pushed through the fuel flow meter which operates based on a known pulses-per-cubic-

centimeter of flow. The pulses-per-flow is factory calibrated based on the size and number of small pistons inside the flow meter that act essentially as a pump taking in the fuel from the inlet and pushing it out the outlet. The data acquisition system then translates pulses-per-flow to pulses-per-second and then to a volumetric flow rate measurement. Finally, the measured fuel is then added to the level controller. The level controller has two inlets and one outlet. The outlet goes to the engine (through pump, P2 in Figure 44). One inlet comes from the fuel flow meter and the other is the return from the engine. The level controller has a float valve inside that only allows just enough fuel in from the fuel flow meter to make up for the difference between the fuel returning from, and going to, the engine – i.e. the fuel consumed. In this manner a very precise fuel flow measurement can be achieved.

The engine loop pulls fuel out of the level controller and provides the 40 psig inlet pressure required by the high pressure common rail fuel pump on the engine. The return from the engine is then passed through a small radiator to be cooled before returning to the level controller as mentioned above. The fuel heat exchanger can be seen on the right side of Figure 45.

8.1.5 Engine controller and data acquisition hardware

All of the stock engine actuators and sensors, as well as the additional measurement and control devices that were installed, are connected the engine controller or data acquisition hardware through an instrumentation boom. All of the hardware is contained in a single modular rack mount cabinet, pictured in Figure 46. The major components are highlighted and labeled.

The air flow rate is measured using a laminar flow element (LFE) which is attached to a differential pressure transducer that indicates the volumetric flow rate through the LFE. The differential pressure transducer is shown. Each major accessory device has an individual power switch. This includes the radiator fan, each fuel pump, intercooler pump, and others. The selector panel that houses each of these switches is shown. Instead of a battery and alternator the engine and the accessory devices are powered with two power supplies (13.5 V, 30 A each). This saves money and makes the power system less prone to problems. The power supplies are shown. The cylinder pressure transducers are connected to a signal conditioning charge amplifier. It is located right next to the data acquisition input boards as shown. Finally, the engine wiring harness must be interfaced with the custom engine controller. This is done in the wiring harness breakout drawer located in Figure 46.

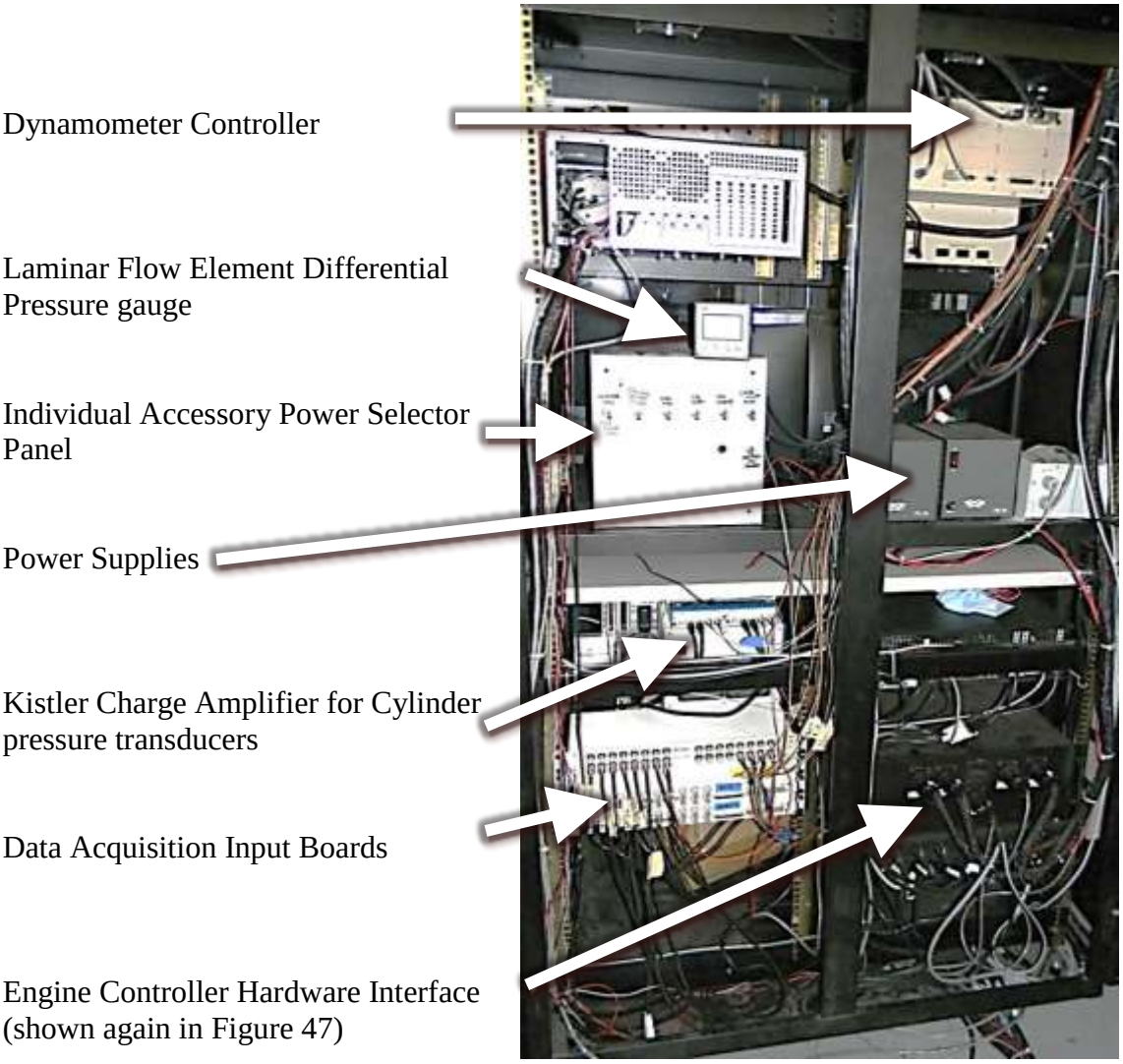

Figure 46 - Data acquisition, engine controller hardware interface, and dyno controller housing cabinet pictured as installed in the test cell.

The engine controller hardware interface breakout drawer is the link between the National Instruments hardware based engine controller and the stock engine wiring harness. A closer look at the drawer is shown in Figure 47. Each connector is linked to various modules in the controller. One connects the injectors to the injector driver

module. Another connects the various pulse width modulated (PWM) actuators to the PWM control module. Another connects the crank angle encoder and fuel flow meter to the digital input module. One connects the exhaust oxygen sensor to the required signal conditioning and control module. Finally, the various sensors on the engine are connected to the Analog-to-Digital converter module. The drawer also houses various power supply and control devices and distribution buses.

Figure 47 - Engine controller hardware to engine wiring harness interface breakout drawer. Front of the drawer with connectors to engine wiring harness (left), and the inside of the drawer with the wiring breakout to the engine controller hardware connections (right).

8.1.6 Engine test cell configuration summary

The previous sections include a detailed description and illustration of the major components of the test cell. Other aspects such as the emissions bench, the smoke meter, and the dynamometer are not described in detail as they are not new to the this setup and engine commissioning. Additionally, some of the software and hardware details of the

engine controller have been omitted in this section. They will be addressed as necessary in other sections – particularly the control ability and requirements for implementing the next cycle control routines that will be the focus of this study.

8.2 Baseline conventional combustion data

To finalize the initial commissioning of the new GM 1.9L engine a virtual pedal position sweep (primary input to controller) was performed at relatively low loads as that will be the target for LTC control mode in later work. Two different engine speeds were investigated (1500 and 1750 RPM) for pedal position from 10-30% in 5% steps. The dynamometer maintained the speed set point and a PID controlled radiator fan maintained the coolant temperature at 90°C. Some troubleshooting issues with the turbocharger actuator made using the boost set point feature inconsistent so it was disabled. Besides those constraints the engine operated based on static control map settings for each actuator based on the speed and pedal position inputs. Some data from this test will be presented now with descriptions as appropriate.

8.2.1 Engine load and fuel consumption

The first figures of interest are the effect of the pedal position on load and fuel consumption. As expected, the load (represented by the brake mean effective pressure, BMEP) is roughly a linear function of pedal position as seen in Figure 48. When considering that the low speed condition has the higher BMEP, recall that the boost control was not enabled and note that at 1750 RPM the boost set point is quite a bit higher than the 1500 RPM set point. Because the desired boost is not being delivered the

BMEP curve at that speed is shifted to the right for the 1750 RPM case relative to the 1500 RPM case.

The effect that not having the boost actuator has on the performance at the 1750 RPM condition is clear at low pedal position when looking at the brake specific fuel consumption (BSFC), shown in Figure 49. The factors influencing BSFC are torque, speed, and fuel flow rate. The fuel injection duration is assigned based on an expected boost level and the fuel flow rate is shown in Figure 50. Note that the fuel flow rates are almost the same for each speed at each pedal position, therefore the behavior of the BSFC at a given speed is primarily caused by the BMEP characteristics. When the boost isn't delivered as expected the BMEP at the low pedal position is lower than expected and subsequently the BSFC increases. The effect is most pronounced at the lowest pedal position because the difference in BMEP is almost 100%. For both conditions as the pedal position is increased the BSFC generally has a downward trend as is expected (i.e. engines operate the most thermally efficient at high loads under conventional combustion conditions).

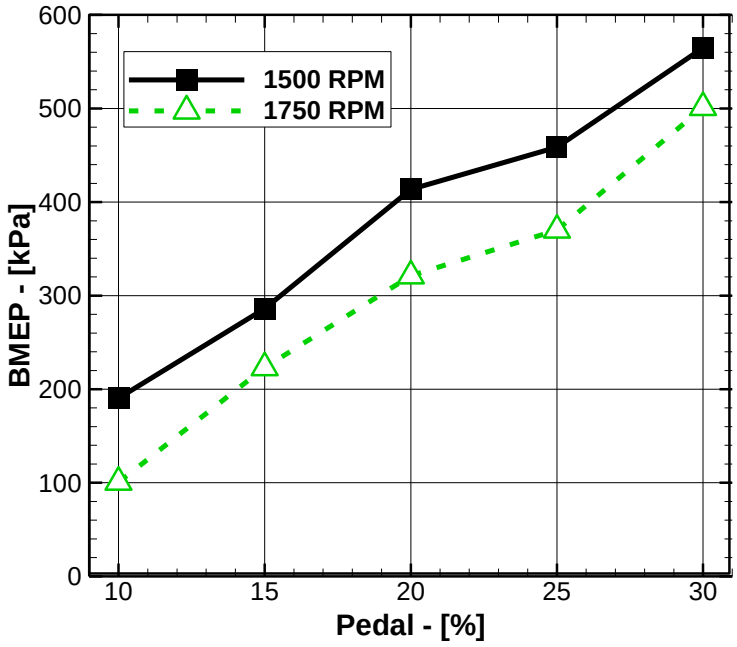

Figure 48 - Brake Mean Effective Pressure [kPa] as a function of pedal position at engine speeds of 1500 and 1750 RPM.

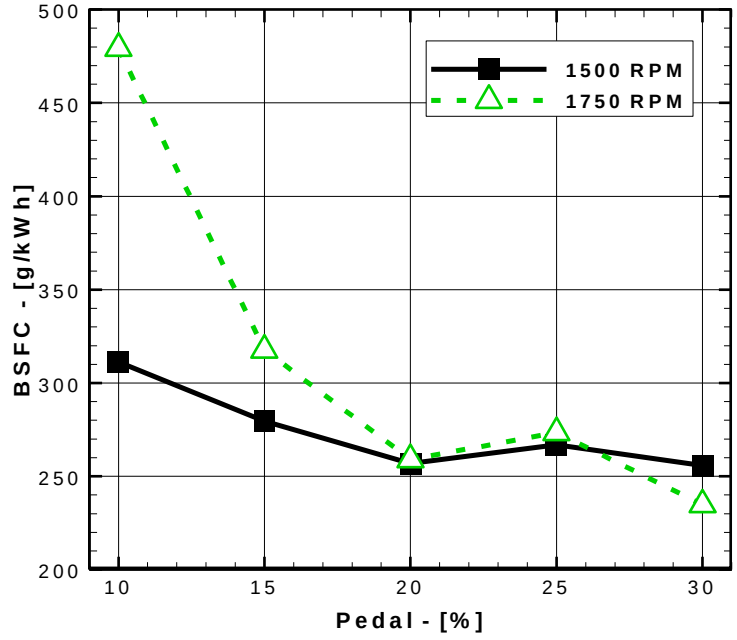

Figure 49 - Brake Specific Fuel Consumption [g/kWh] as a function of pedal position at engines speeds of 1500 and 1750 RPM.

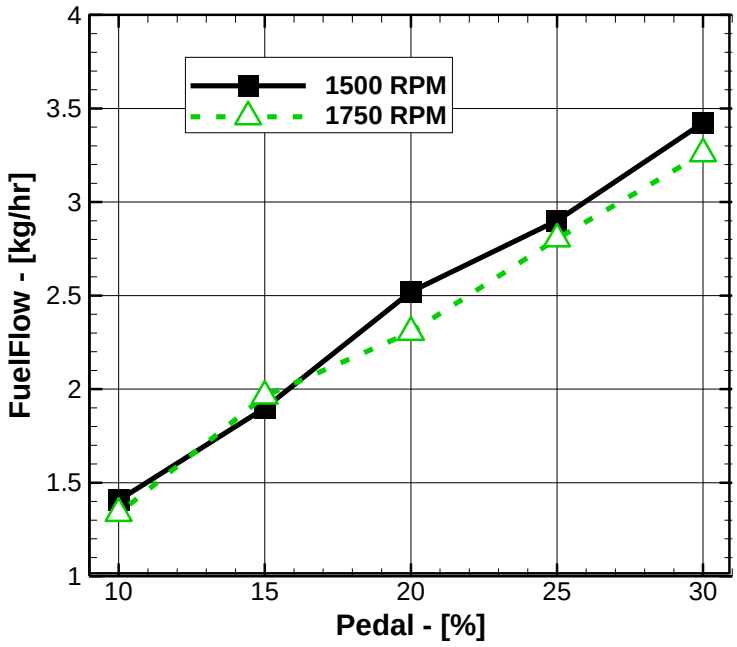

Figure 50 - Fuel Flow Rate [kg/hr] as a function of pedal position at engine speeds of 1500 and 1750 RPM.

8.2.2 Engine out emissions concentrations

The following figures present some of the exhaust emissions data for the test conditions. The vertical axis label shows the measurement units (either ppm on a wet or dry basis, or percent) and in some cases the range that the analyzer was calibrated over. For example, in Figure 51, the carbon monoxide (CO) is measured in an analyzer calibrated for 0-5000ppm and it is measured on a ppm dry basis (i.e. with the water condensed out of the sample).

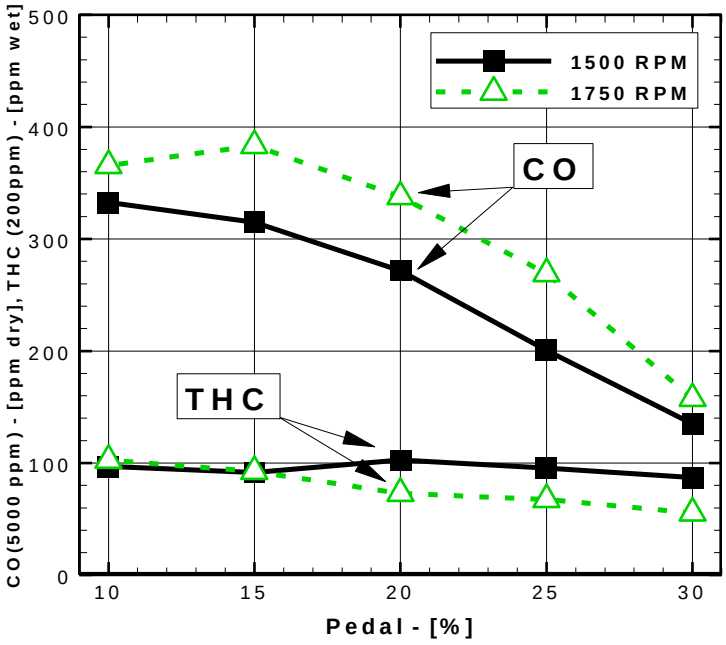

Figure 51 - Exhaust concentrations of Carbon Monoxide (CO) and Unburned Hydrocarbons (THC) as a function of pedal position at engine speeds of 1500 and 1750 RPM.

The higher load (increasing pedal position) is equated with higher cylinder pressures and temperatures and likely higher CO oxidation rates (more complete combustion) manifested as lower CO concentrations. The THC concentration remaining constant represents the offsetting of the increased fuel injection with the higher oxidation rates. There may also be a slight time effect present causing differences in the chemical kinetics behavior at each speed. This is mentioned for completeness, but not quantification can be made about the significance of this effect. The difference in CO and THC at the two speeds is more likely a result of random variations.

The behavior of the O2 and CO2 is shown in Figure 52. The rate of increase in CO2 (and decrease in O2) is initially relatively steep matching the trend of increased

fuel with pedal position. After about 25 % pedal position the slight change in the slopes (increase for CO2, and decrease for O2) is primarily due to the behavior of the global equivalence ratio. As will be shown below as the equivalence ratio stabilizes at higher pedal position, so does the exhaust concentrations of the CO2 and O2 based on the chemical equilibrium mechanisms. The effect on peak cylinder pressure and temperature as the pedal position is changed will also be shown a bit further down.

As the pedal position is increased the combined nitrogen oxides concentration (NO + NO2 = NOx) is also increased at both speed conditions as seen in Figure 53. In this case this is primarily a result of the changing EGR level (seen in Figure 54 and Figure 55). As the EGR level is decreased with increasing pedal position, the expected corresponding increase in NOx is observed. Note that though the injection timing is advanced with pedal position (discussed later) which advances combustion phasing toward higher temperatures (suggesting an increased NOx formation) the observed behavior of the NOx levels show that the EGR effect is dominant. The higher speed, 1750 RPM, case has a lower NOx concentration due to a slightly higher EGR rate and also the generally retarded combustion phasing due to injection timing set point (discussed later).

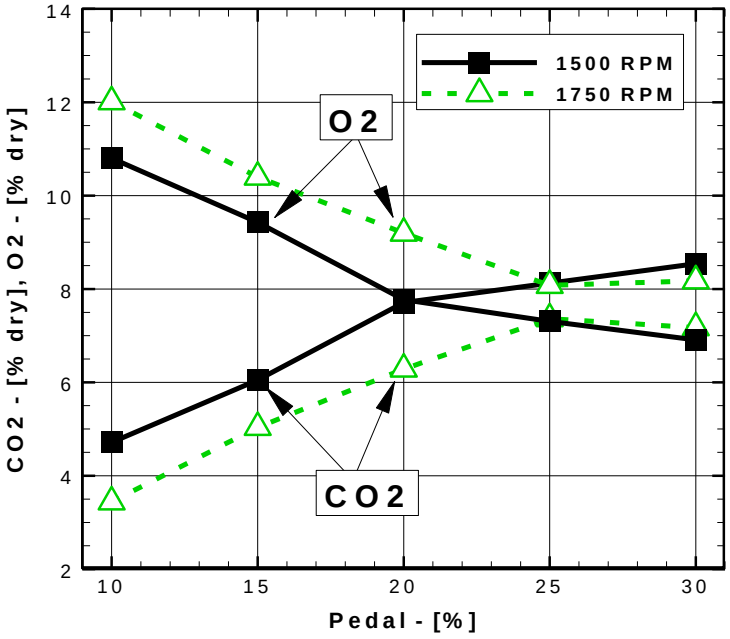

Figure 52 - Exhaust concentrations of Carbon Dioxide and Oxygen as a function of pedal position at engine speeds of 1500 and 1750 RPM.

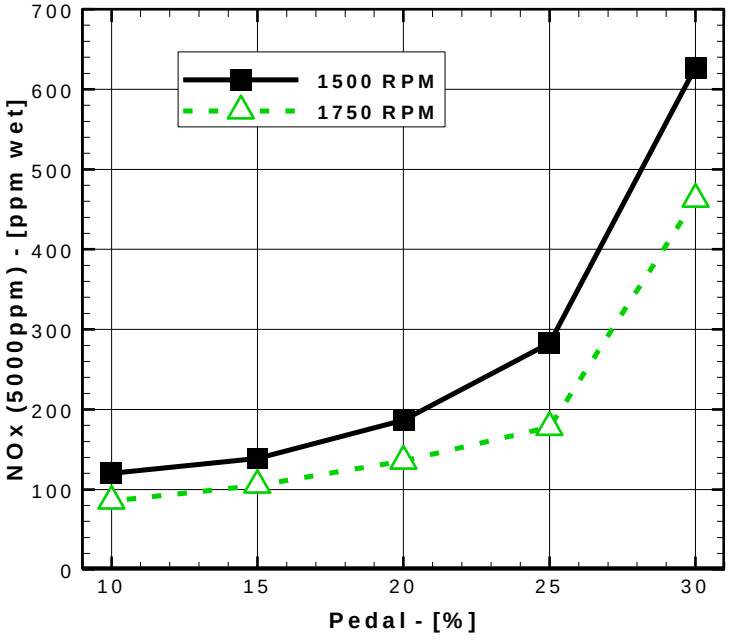

Figure 53 - Exhaust concentrations of Nitrogen Oxides (NO + NO2) as a function of pedal position at engine speeds of 1500 and 1750 RPM.

8.2.3 Global equivalence ratio calculation results

There are a number of methods available in the engine setup utilized here to calculate the global equivalence ratio of the engine. The results are shown in Figure 54 for 1500 RPM and Figure 55 for 1750 RPM. The calculation methods include the following: an exhaust emissions stoichiometry solution (Phi – Emissions), using the stock exhaust Lambda sensor (Phi- Lambda Sensor), or two methods that both utilize the same fuel flow rate measurement but that use either the stock mass air flow (MAF) sensor (Phi – MAF) or the laminar flow element (LFE) air flow measurement (Phi – LFE).

While the local equivalence ratio is the dominate factor in determining the exhaust emissions concentrations, the global value shown here can still give useful insight into the engine operating condition. In both speed cases the general trends among each method are the same, but there is quite a range of calculated equivalence ratio. A future task will be determining why they are different and which one to utilize in potential prediction routines. The effect on the global equivalence ratio as the EGR level is changes is quite clear. The engine speed is constant, so a change in EGR rate directly causes an opposite change in the fresh air flow rate and thus a change in the equivalence ratio as observed below.

One last thing to note regarding the equivalence ratio measurements is that based on others personal experience the reliability of the LFE is suspect at these relatively low flow rates [42]. Therefore if the LFE results are not included the agreement between the other calculation techniques is much better.

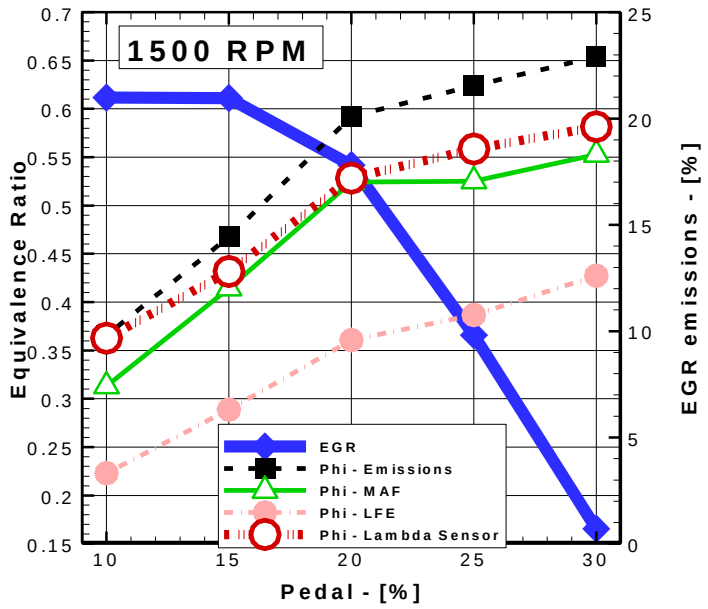

Figure 54 - Exhaust Gas Recirculation level (based on emissions bench measurements) and various method of calculating the global equivalence ratio as a function of pedal position at an engine speed of 1500 RPM.

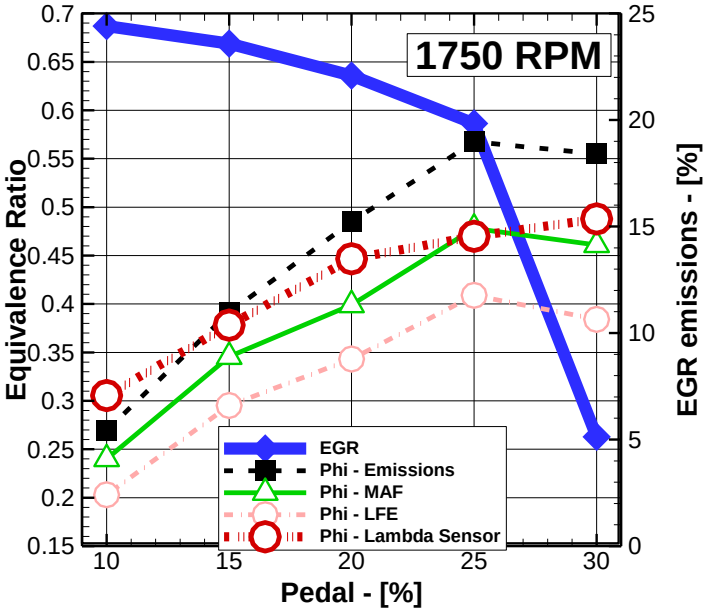

Figure 55- Exhaust Gas Recirculation level (based on emissions bench measurements) and various method of calculating the global equivalence ratio as a function of pedal position at an engine speed of 1750 RPM.

8.2.4 Cylinder pressure and heat release rate results

Cylinder pressure based diagnostics will be the foundation of the work done here, so understanding the behavior of this particular engine at the various speeds, loads, and combustion modes under study will be very important. For this section, the cylinder pressure and heat release rate will be shown for each speed at each pedal position (Figure 56 and Figure 57). Additionally for one representative pedal position the cylinder pressure for all four cylinders is shown to illustrate the cylinder-to-cylinder variation. The data shown is the ensemble average of 25 cycles and filtered with a low pass FIR with rollback and a cutoff frequency of 0.1% of sampling frequency. This filtering technique is based on a thorough investigation into digital signal processing techniques done by Payri et al. [43].

Figure 56 shows the data for the 1500 RPM condition. The observed effect of pedal position is as expected recalling that the BMEP increased with increasing pedal position. That is to say that with increasing pedal position (load) there is an advancing in injection timing (and thus ignition) clearly seen in both the pressure and heat release results. Additionally, there is a higher cycle pressure (and temperature) as discussed when describing the CO and CO2 emissions results above. With increasing load there is a transition from primarily premixed combustion mode to a mixing dominated combustion condition creating longer combustion durations and higher peak pressures.

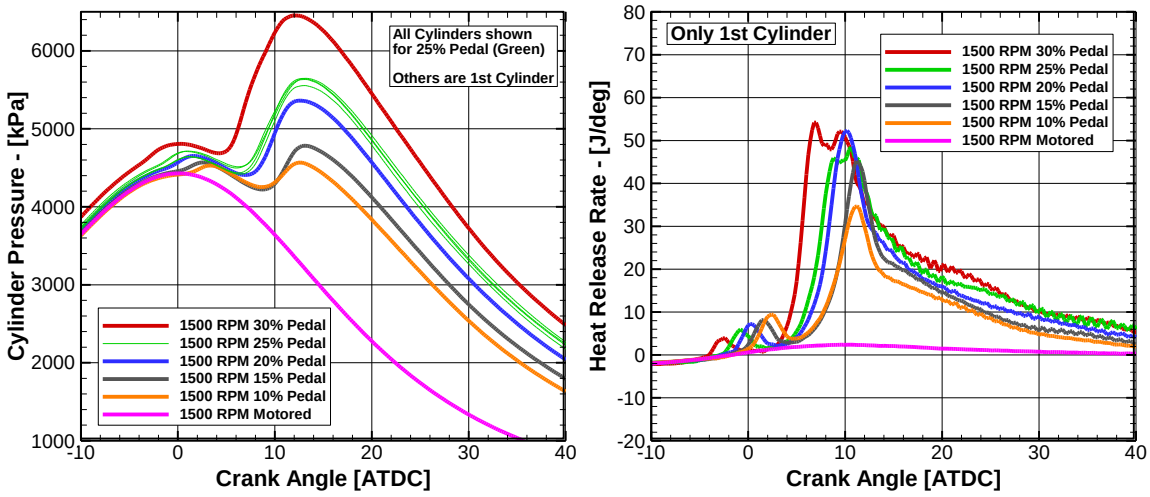

Figure 56- Cylinder pressure (left) and Heat Release Rate (right) for each pedal position at 1500 RPM. For the 25% pedal position (green) condition the cylinder pressure (left) for all four cylinders is shown, while for every other condition only the first cylinder is shown.

The cylinder-to-cylinder variation seen for the 25% pedal position is actually quite low and likely due to the higher fraction of mixing controlled combustion which is typically more consistent compared to premixed modes.

Figure 57 shows the data for the 1750 RPM condition. The same general trends with pedal position are seen at this speed as well. Advancing injection (and thus ignition), higher peak heat release rate due to better mixing as a result of a higher injection pressure (not shown). Interestingly, from 25% to 30% pedal position there is finally shift to mixing control dominated combustion as the ignition delay is decreased causing a reduction in the premixed burning fraction. This also causes a drop in peak heat release rate and a corresponding increase in combustion duration which manifests as a significant increase in cylinder pressure from 25% to 30% pedal position.

At this speed there is a much larger cylinder-to-cylinder variation at the 25% pedal position. This is primarily due to the high peak heat release rates (and thus high premixed fraction) being much more sensitive to slight cylinder variations in air, fuel, or EGR distribution.

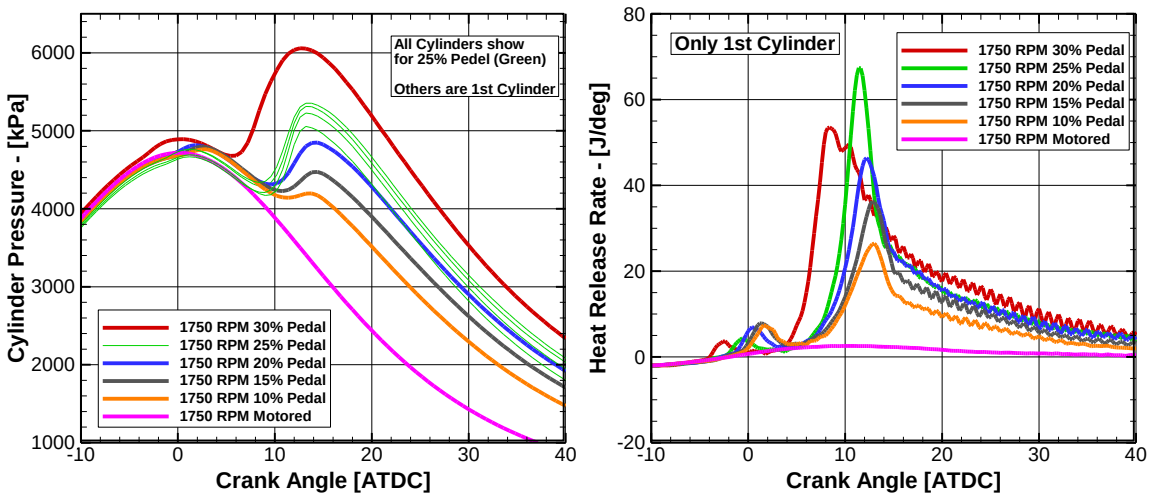

Figure 57 - Cylinder pressure (left) and Heat Release Rate (right) for each pedal position at 1750 RPM. For the 25% pedal position (green) condition the cylinder pressure (left) for all four cylinders is shown, while for every other condition only the first cylinder is shown.

8.2.5 Conventional combustion data summary

As demonstrated in this section, the data presented shows expected trends and indicates a successful commissioning of the engine. There are a few final troubleshooting issues to resolve, but nothing that would suggest the test cell is not ready for publication grade experimentation.